5.4 Evaporation Rates

As above, an important aspect of Cockburn Sound's dynamics, particularly in summer, is the effect of evaporation rates, which can lead to increased local salinity. This increased salinity in the Sound creates horizontal density gradients that drive vertical stratification across much of the deep basin. Evaporation rates calculated from the model simulations at the three locations in summer (January to March 2008) and winter (August to November 2008)) are shown in Figure 5-109. Very little variation can be seen across the stations, however there was considerable variation between seasons. Evaporation rates in summer were generally between 5 and 10 mm/day, whilst in winter they were generally below 3 mm/day. These values agree with expected evaporation rates, as discussed in D'Adamo (2002).

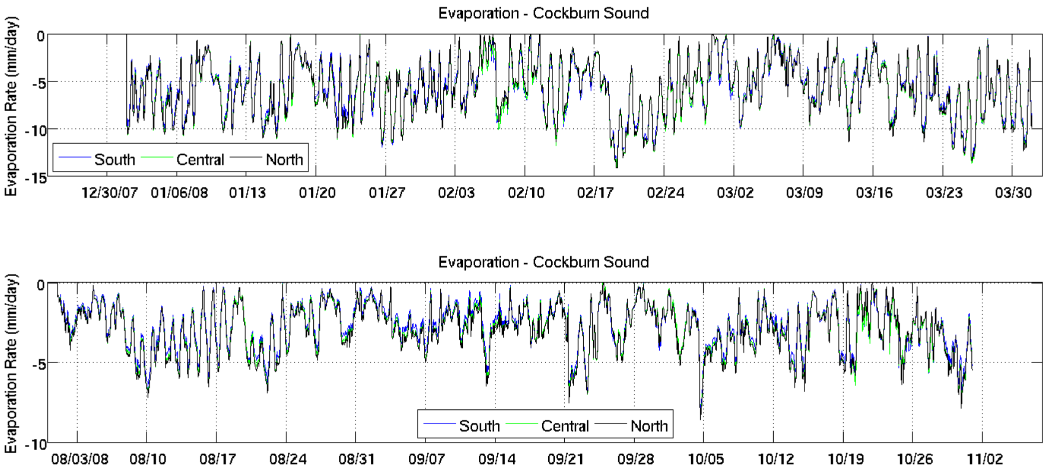

Figure 5-109 Evaporation rates, wind, and relative humidity in Cockburn Sound. The negative values indicate evaporation is a flux out of the model domain.

5.5 DO comparisons

DO data at the same three locations in the deep basin of Cockburn Sound (Figure 2-4) were used for model comparisons. RTMS DO data was deemed inaccurate due to persistent sensor drift, and as such was not used for model performance assessment. Data from MAFRL profiles (which were the same profile events as temperature and salinity presented above) were adopted for model comparisons.

5.5.1 Water quality model parameterisation

As discussed in Section 4.1, AED2 was parameterised for SOD and surface aeration. Surface aeration is computed within AED2 as per Wanninkhoff (1992). Benthic oxygen fluxes are computed as per the second term on the right-hand side in Figure 4-1, parameterised by maximum SOD ($F_{max}^{O_2}$), a half saturation constant, $K_{sed}^{O_2}$ to represent limitation based on the DO concentration in the bottom waters and an Arrhenius temperature multiplier, $\theta_{sed}^{O_2}$ to account for seasonal changes in SOD.

In the transition from summer to autumn 2008, the measured DO data (Figure 2-12) suggest that SOD, parameterised as $F_{max}^{O_2}$ was spatially variable with higher rates at the northern entrance of the

Sound (i.e. lower DO concentrations). As such a spatially variable $F_{max}^{O_2}$ was specified as per the distribution shown in Figure 5-110. Values of $F_{max}^{O_2}$ were selected based on measured fluxes (Read and Oldham 2005), literature values (Smith et al. 2010) and calibrated to account for observed DO depletion.

In the transition from winter to spring, DO measurements suggest that SOD is considerably reduced throughout the model domain when compared to summer observations (Figure 2-12). The Arrhenius multiplier was therefore set at 1.13 to account for these seasonal differences. A $K_{sed}^{O_2}$ value of 156.25 mmol/m3 (5 mg/L) was used, consistent with measured DO limitations on SOD (Read and Oldham 2005; Hipsey et al. 2014).

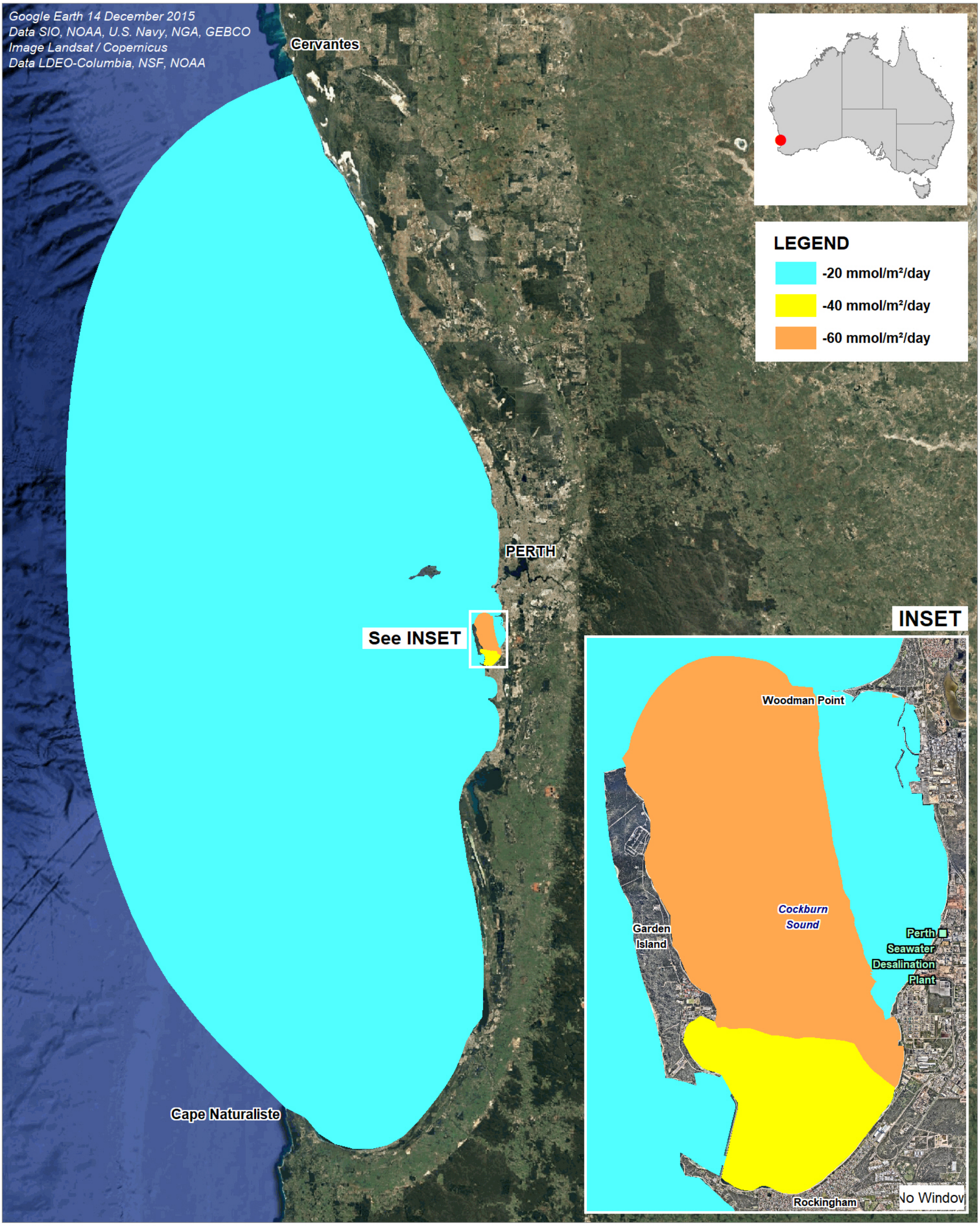

Title:

Spatial Distribution of *FmaxO2*

Figure: 5-110

Rev: A

N

0 40 80km
Scale - Main Map

0 3 6km
Scale - Inset

BMT
www.bmt.org

Filepath: I:\B22253.I.meb.CockburnSound\DRG\CAR_007_170929_Spatial Distribution of FmaxO2.wor

5.5.2 Summer to early autumn 2008

DO comparisons are shown for each of the summer profiles at the North, Central and South Buoy stations in Figure 5-111 to Figure 5-113, respectively. The model results demonstrated that the DO dynamics over the period were correctly simulated. In particular, the model reproduced the DO reduction near the bed associated with the development of stratification in the overlying water, both due to temperature (January and early February, at South Buoy), and salinity (early March, at North and Central Buoy).

It is important to note that the lowest DO concentrations occurred early in March in association with the overflow dynamics described in Section 5.3.2.1 and 5.3.2.2. This characteristic was successfully reproduced by the model. The role of the overflows (from the ocean) was to cap the bottom layer and therefore preclude surface reaeration, allowing the DO demand at the bottom to deplete oxygen concentrations below the pycnocline levels. This relationship between DO depletion and density stratification is illustrated in Figure 5-114 to Figure 5-116. The figures demonstrate that the higher the pycnocline resides in the water column, the thicker the low DO layer beneath it becomes, and the more gradually the observed and modelled DO reductions evolve (Figure 5-111 to Figure 5-113).

Contrastingly, the events at the end of March did not present significant DO reductions (measurements available at North Buoy only), despite the signature of overflows. The model slightly overestimated the magnitude of DO reduction during this time, likely influenced by the shape and position of the halocline predicted by the model in comparison to the measurements (Figure 5-41).

It is to be noted that the model did not predict the DO reductions observed for some of the lowest DO concentrations in March at North Buoy (see profiles on 06 March in Figure 5-111). These low concentrations were associated with a sharp temperature and salinity stratification at approximately 18.0 m depth that was not sufficiently well reproduced by the model (see Section 5.3.2.1). Further, these results indicated how sensitive DO (and also model results) were in relation to fine transient details of the water column stratification (see shape of the salinity profile in Figure 5-41). The model replicated the depth and magnitude of recorded DO reductions at the Central Buoy location well across the entire model simulation period.

At the South Buoy, the model simulated slightly higher DO concentrations near the bed throughout January. Later in the simulation, the profiles indicated that the model was better replicating the stratification (e.g. profiles on 5 February and 29 February in Figure 5-113). Sensitivity testing (not presented) indicated that increasing the $F_{max}^{O_2}$ values throughout the summer simulation could provide a better match between simulated and recorded DO concentrations near the bed under these deep stratification events. This would be, however, at the expense of excessive DO consumption in the winter-spring simulation period. The adopted values were therefore chosen in such a way that both winter and summer simulations could be forced with the same $F_{max}^{O_2}$ values that would be fit for the purposes of the modelling assessment.

Across the March period at South Buoy, the model simulated slightly lower DO concentrations than observations near the bed. In this case, any underprediction was largely affected by small mismatches in the salinity stratification.

The development of low DO associated with stratification is further illustrated with an animation showing temperature, salinity and DO curtains along Cockburn Sound from north to south (see link for animation in Appendix H). Particularly noticeable in these animations is the sporadic development of lower DO further south of South Buoy, near the southern end of Mangles Bay. Notably, despite the considerably lower DO demands in comparison to North Buoy, DO depletion in Mangles Bay led to similar and occasionally lower bottom DO concentrations in comparison to water further north in the Sound, partially due to the higher temperatures but also due to the limited flushing of the area (consistent with DEP 1996). The lower DO concentrations in Mangles Bay are generally associated with sustained winds from the south and are in line with observations of low DO events in Mangles Bay (D'Adamo 2002). These episodes are further illustrated in Figure 5-117 with snapshots of the animations listed in Appendix H.

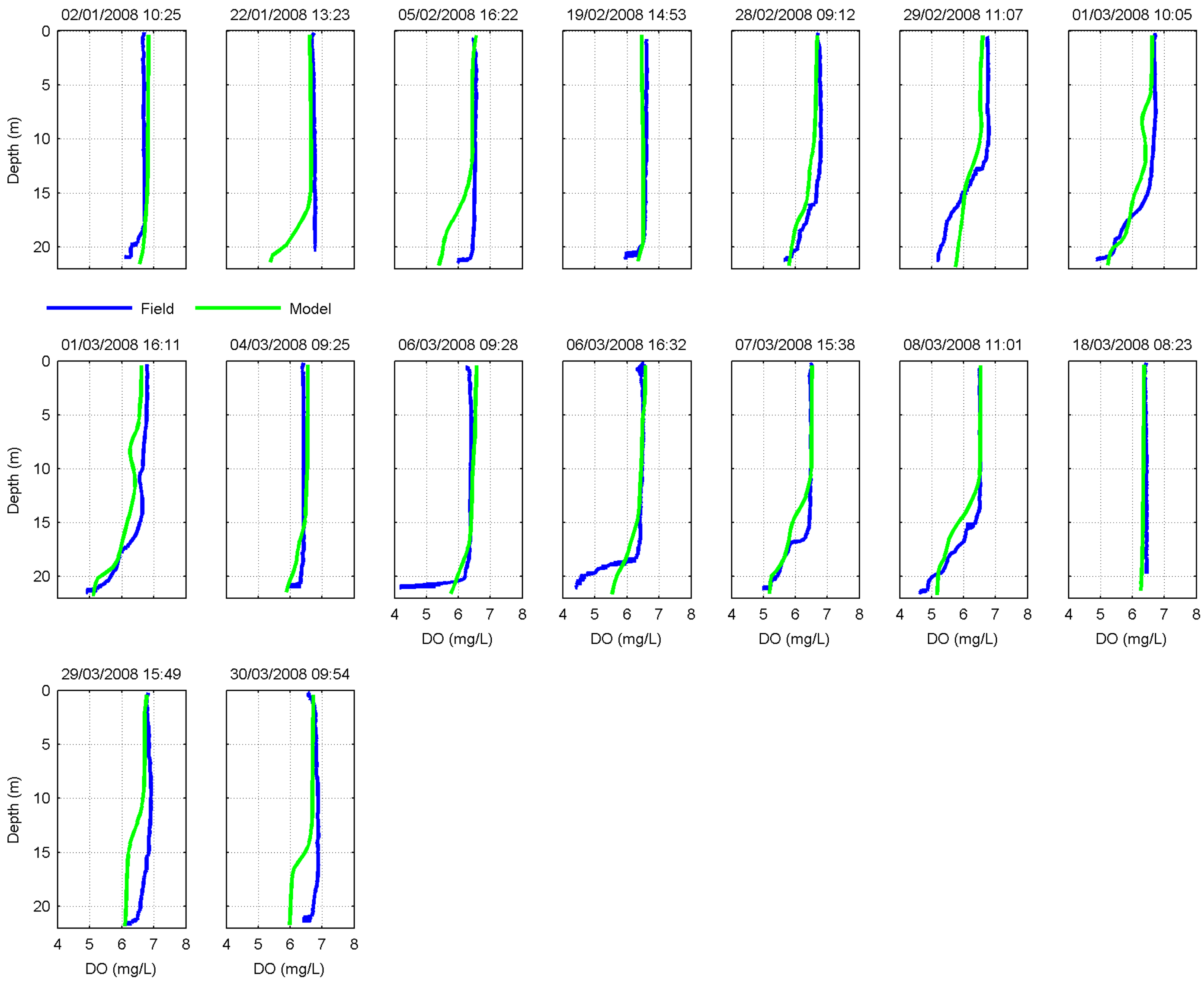

Figure 5-111 Comparisons between simulated DO and profile measurements at North Buoy in the transition between summer and autumn 2008

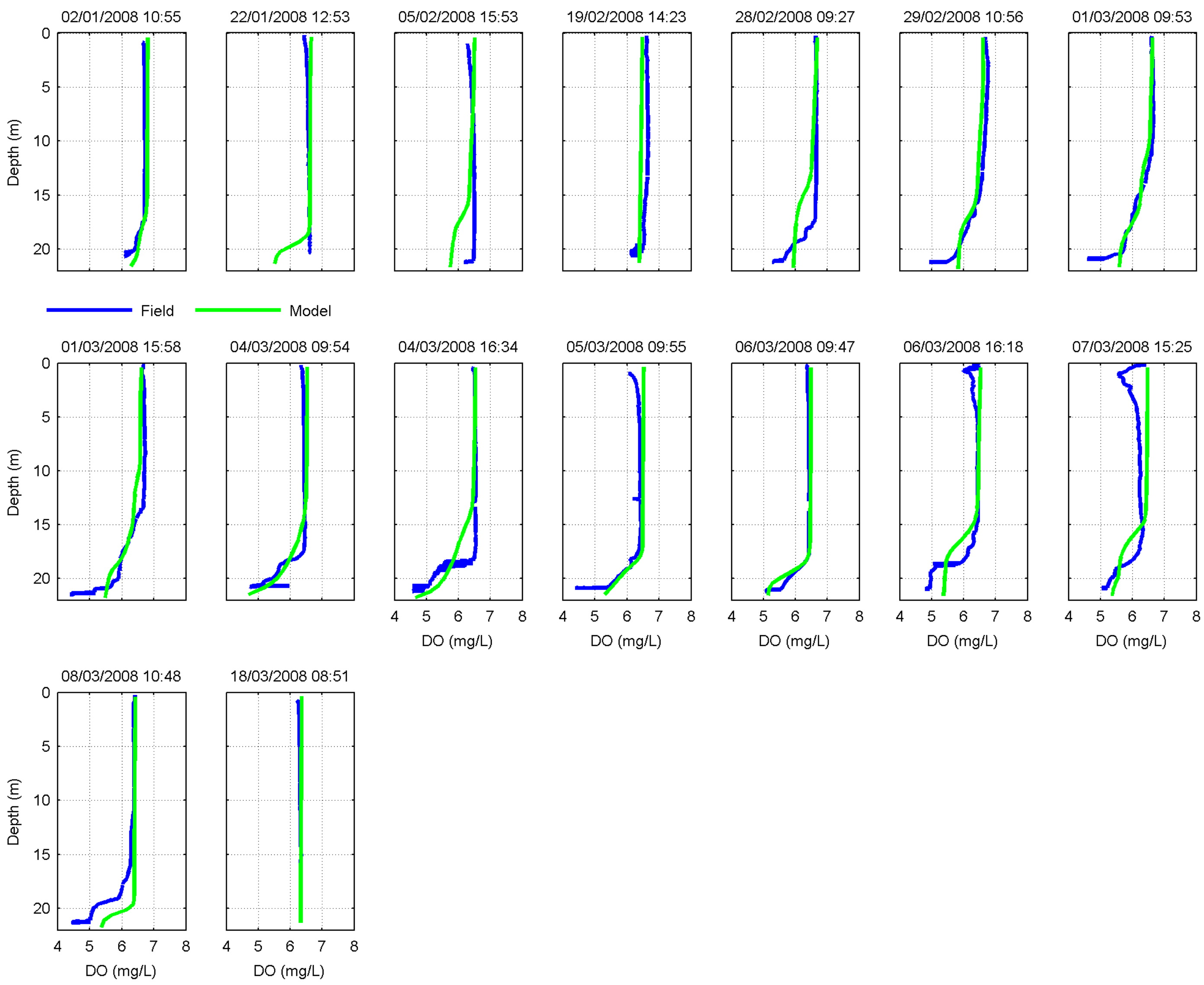

Figure 5-112 Comparisons between simulated DO and profile measurements at Central Buoy in the transition between summer and autumn 2008

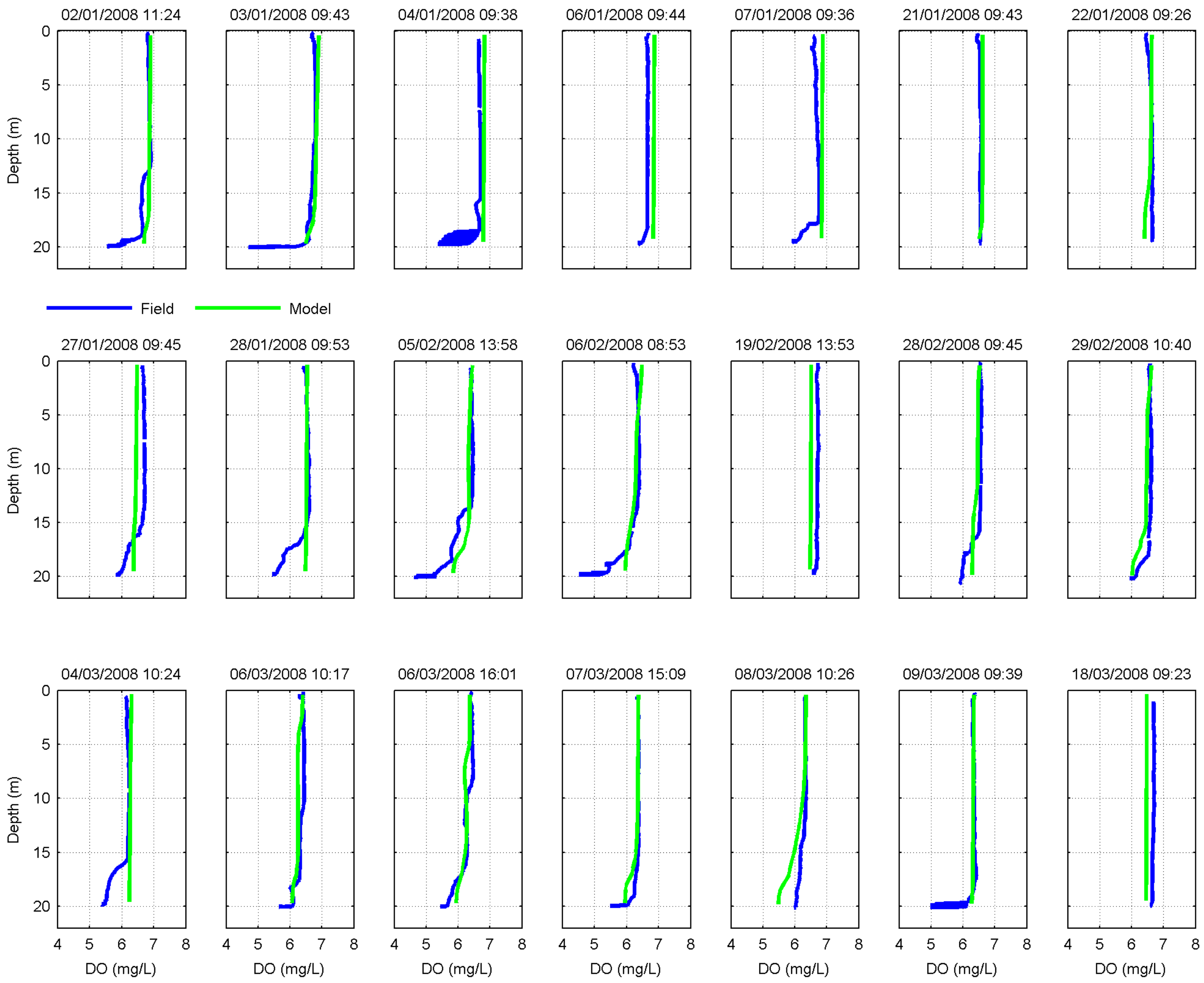

Figure 5-113 Comparisons between simulated DO and profile measurements at South Buoy in the transition between summer and autumn 2008

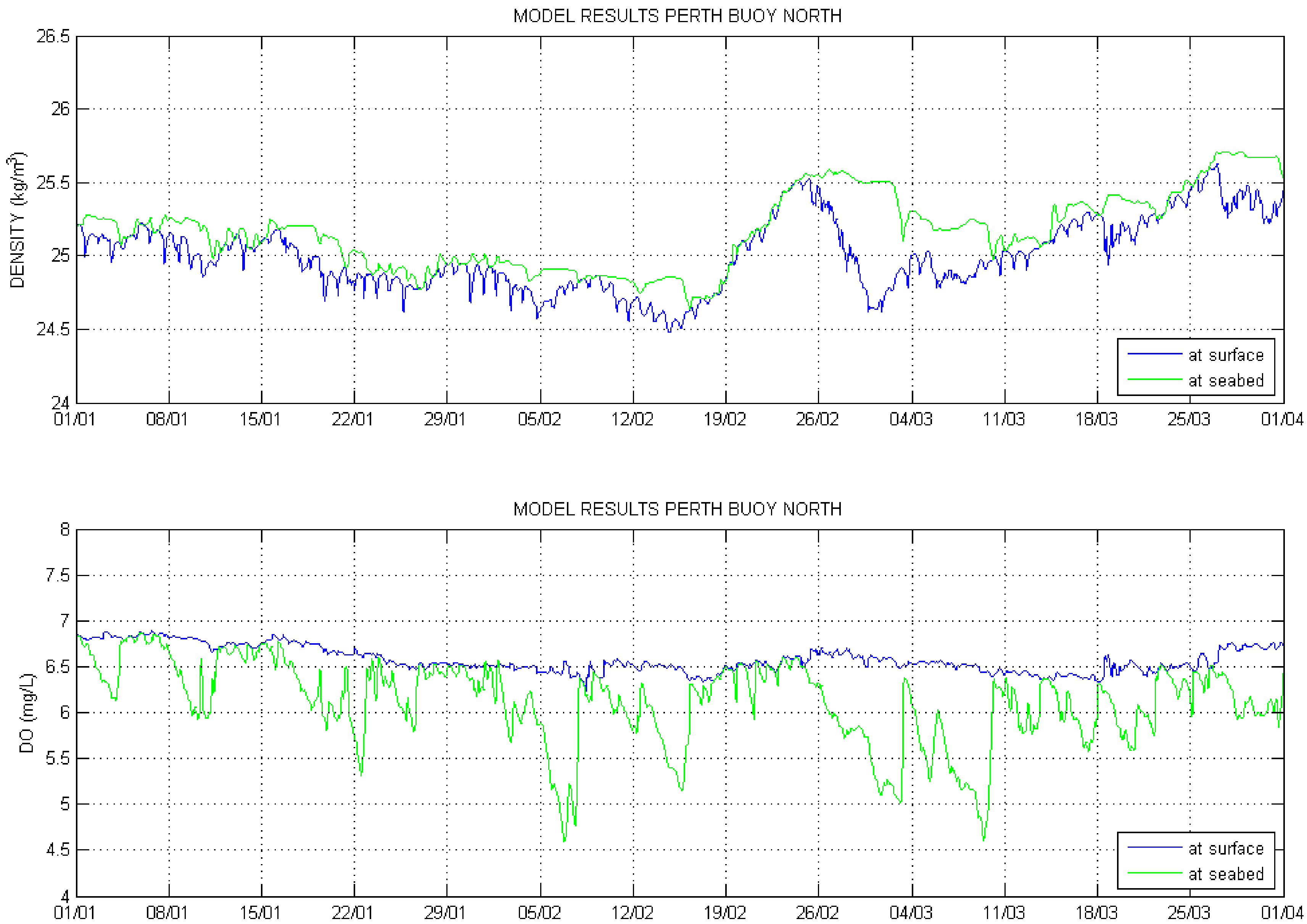

Figure 5-114 Simulated DO and density stratification at North Buoy in the transition between summer and autumn 2008.

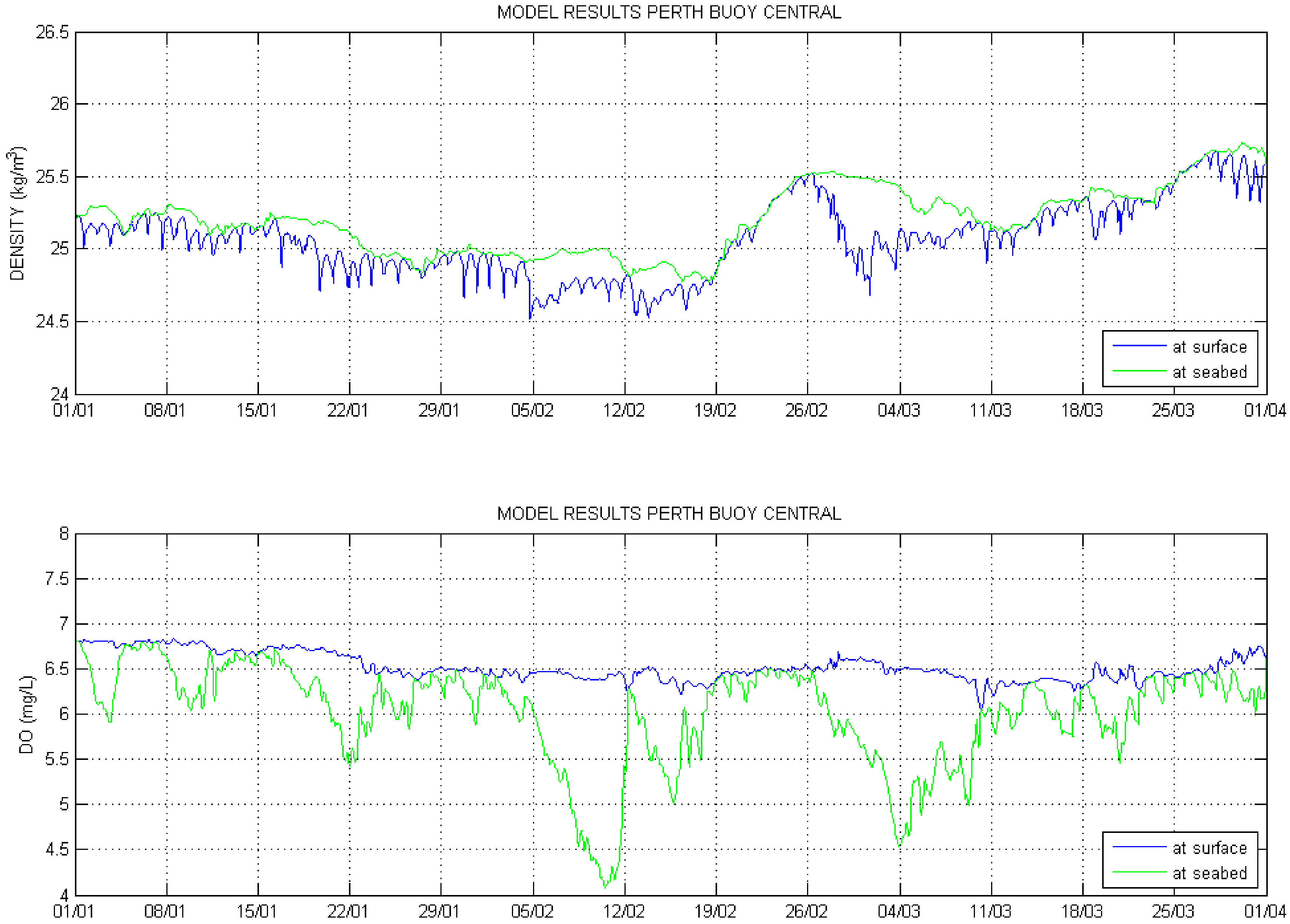

Figure 5-115 Simulated DO and density stratification at Central Buoy in the transition between summer and autumn 2008.

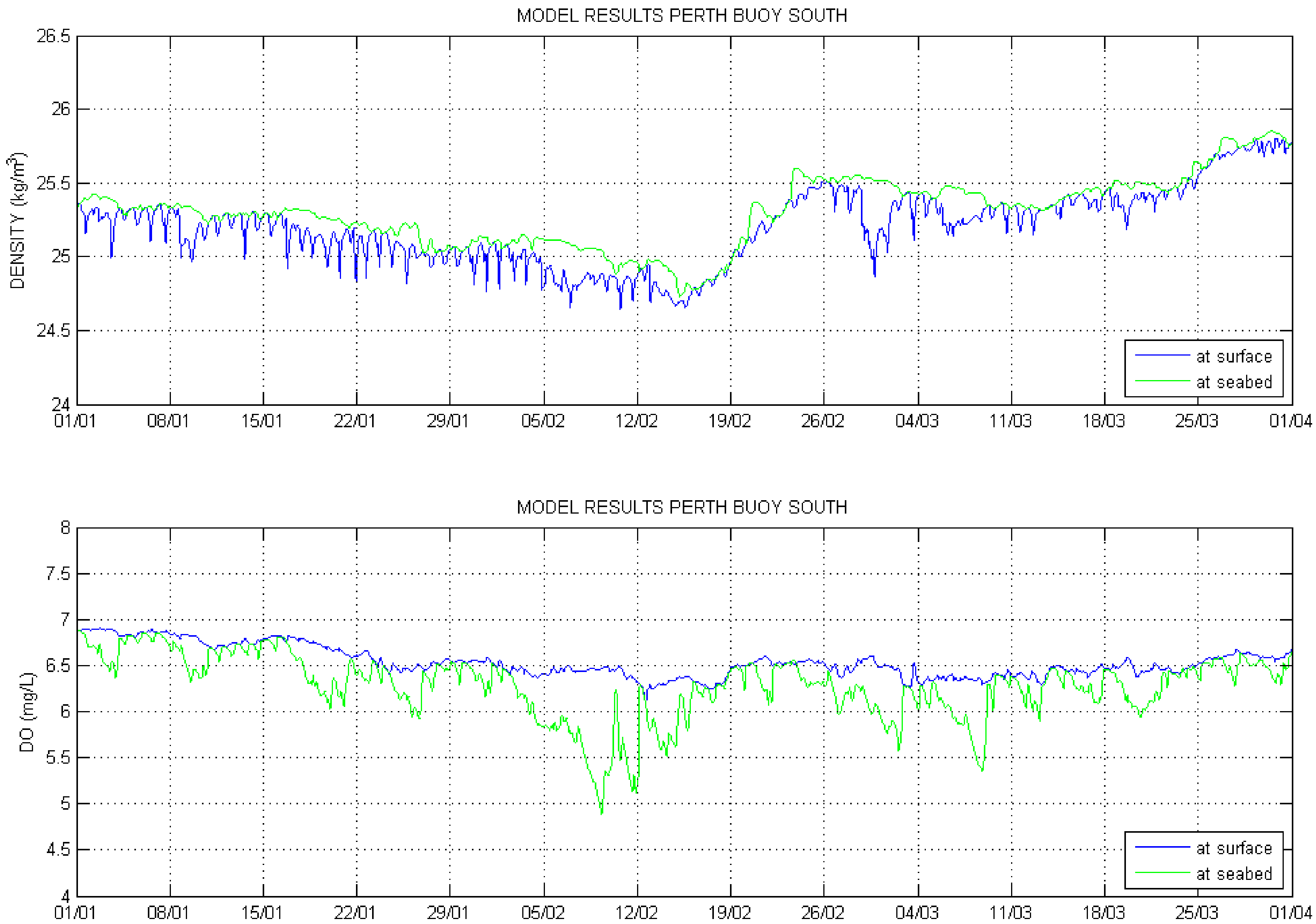

Figure 5-116 Simulated DO and density stratification at South Buoy in the transition between summer and autumn 2008.

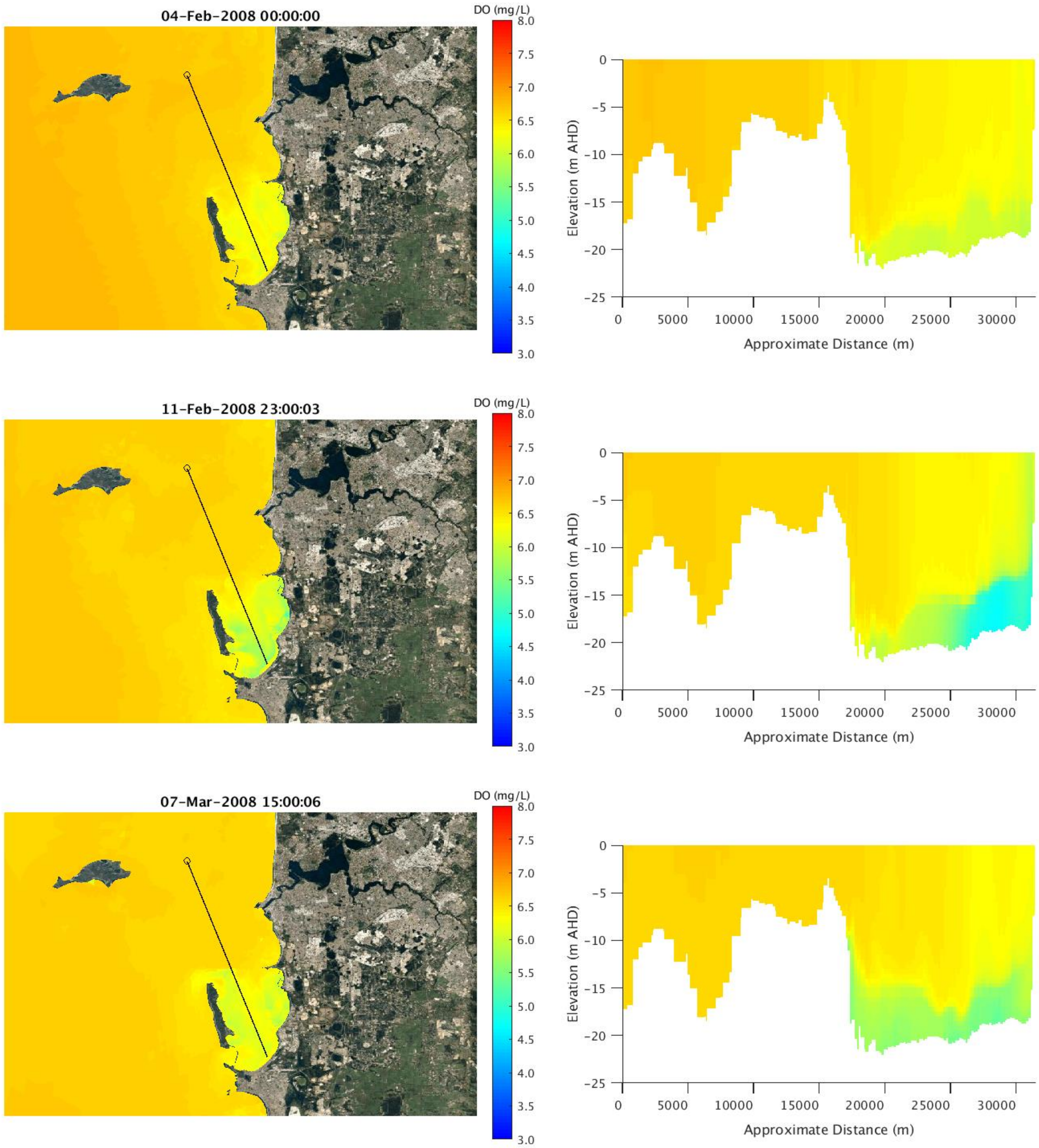

Figure 5-117 Simulated DO concentrations in Cockburn Sound illustrating near bed DO depletion in Mangles Bay. The black line in the left-hand column panes shows the plan transect of the profile presented in the right hand panes. The profiles run from northwest (left hand side) to southeast (right hand side)

5.5.2.1 Sediment oxygen demand

Whilst the AED2 model sediment oxygen demand is parametrised using $F_{max}^{O_2}$ (see Section 5.5.1), this quantity is not the actual simulated DO demand from the sediments. The adopted SOD model is also dependent on the water column temperature (through the Arrhenius coefficient), and near-bed DO concentration (through the Michaelis-Menten formulation) (see Section 4.1).

The simulated (actual) SOD demand in the transition from summer to autumn of 2008 at each of the three locations is presented in Figure 5-118. SOD flux magnitudes across all stations displayed an increasing trend towards the middle of the period (i.e. mid-February) and returned to approximately initial values by the end of the simulation (Figure 5-118). This trend followed the increased temperatures across the summer months and cooling into the transition to autumn, as expected.

The SOD fluxes at Central and North Buoy stations generally followed each other closely at typically between -1.3 and -2.0 g O_2/m^2/day (negative fluxes indicating DO is removed from the water column, Figure 5-118). The correspondence between locations was expected noting the similar flux parameterisation at both locations. The SOD fluxes magnitudes at South Buoy were lower (from -0.9 and -1.3 g O_2/m^2/day, Figure 5-118), and approximately proportional to the applied differences in $F_{max}^{O_2}$ between this station and North and South Buoys. These fluxes are within the same order of maximum values measured in the Sound -0.82 g O_2/m^2/day (DAL; 2005 referenced in CWR; 2006 – note CWR; 2006 quotes this in g O/m^2/day, so here BMT applied double the value in the reference.)

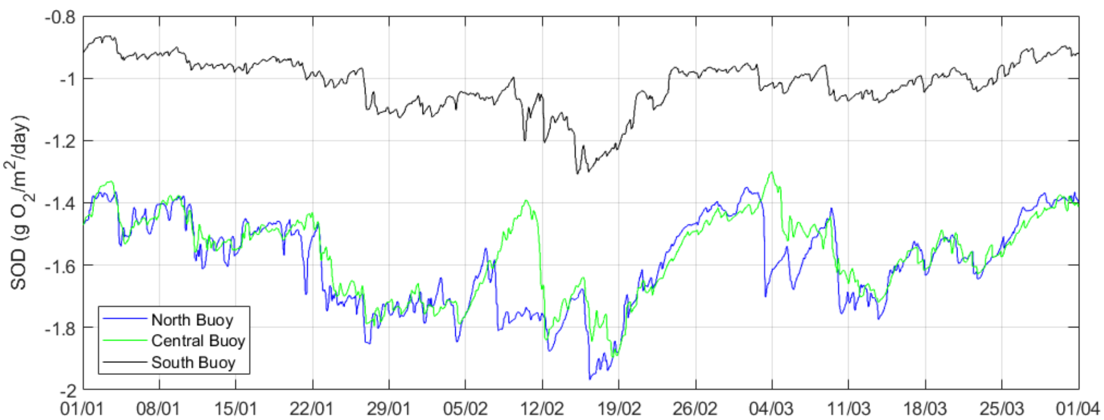

Figure 5-118 Actual simulated sediment oxygen demand in the transition from summer to autumn 2008

5.5.3 Winter to spring 2008

DO comparisons are shown respectively for each of the winter profiles at the North, Central and South Buoy stations in Figure 5-119 to Figure 5-121. Relative to summer, DO concentrations were generally higher (between 7.0 and 8.0 mg/L) and uniform across all stations, as expected. Also, the vertical structure of the profiles was more uniform, with only few instances of (slightly) reduced DO levels near the seabed. This trend was well replicated by the model across all stations. Again, the reductions of the simulated DO concentrations followed the density stratification patterns across the Sound (Figure 5-122 to Figure 5-124).

In particular, the model reproduced the near bed DO reductions associated with the temperature stratification in October, at all locations. The model also reproduced the slight DO reduction associated with the stratification induced by the Swan River flows early in August. This result further confirms that, despite the simplifications of the assumptions adopted for the Swan River flows, the model represents their influence on the DO in Cockburn Sound.

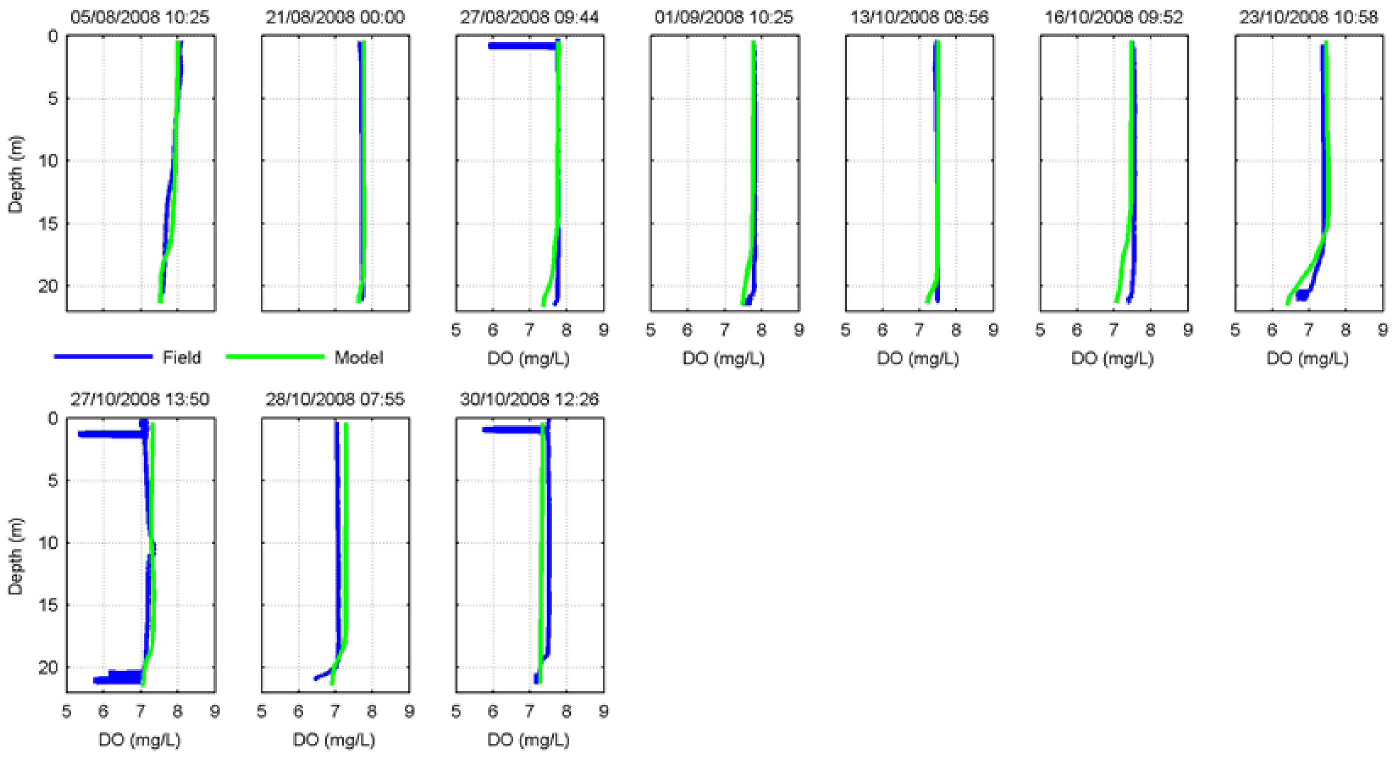

Figure 5-119 Comparisons between simulated DO and profile measurements at North Buoy in the transition from winter to spring 2008

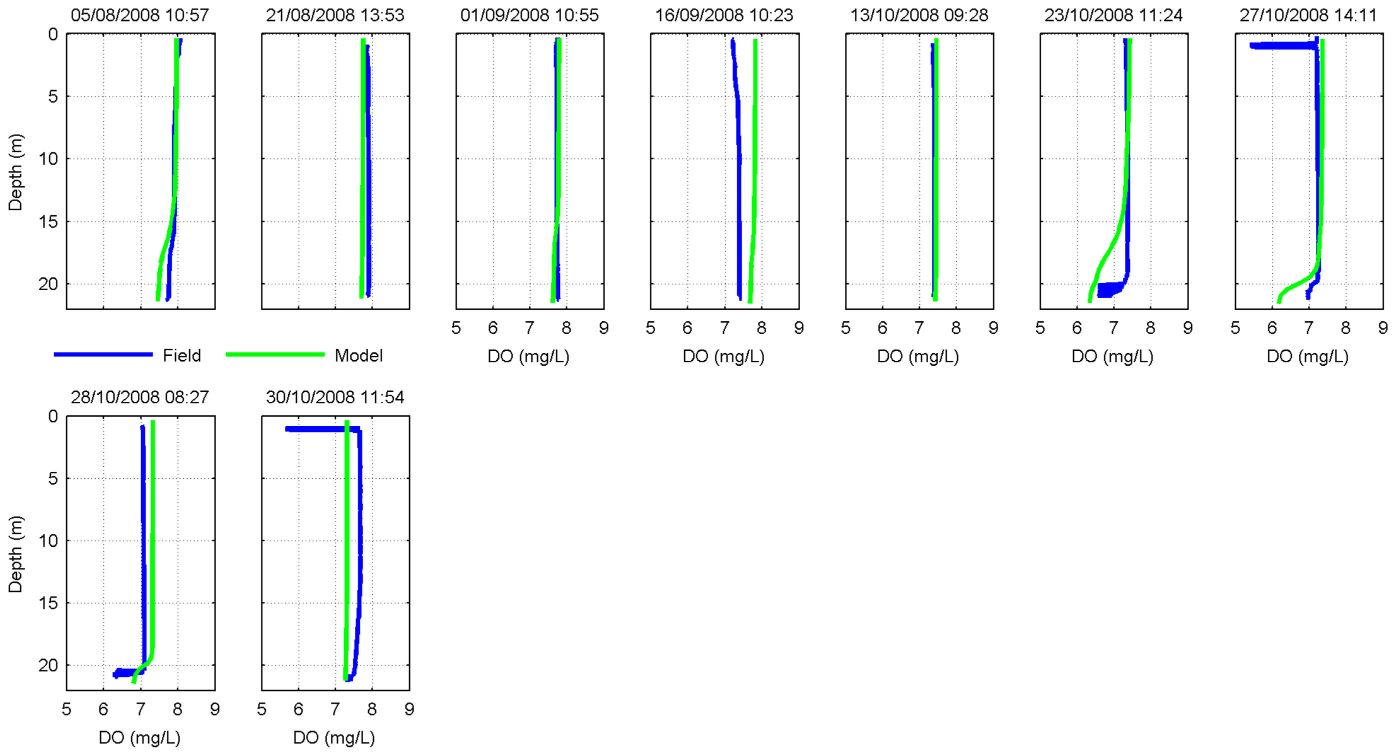

Figure 5-120 Comparisons between simulated DO and profile measurements at Central Buoy in the transition from winter to spring 2008

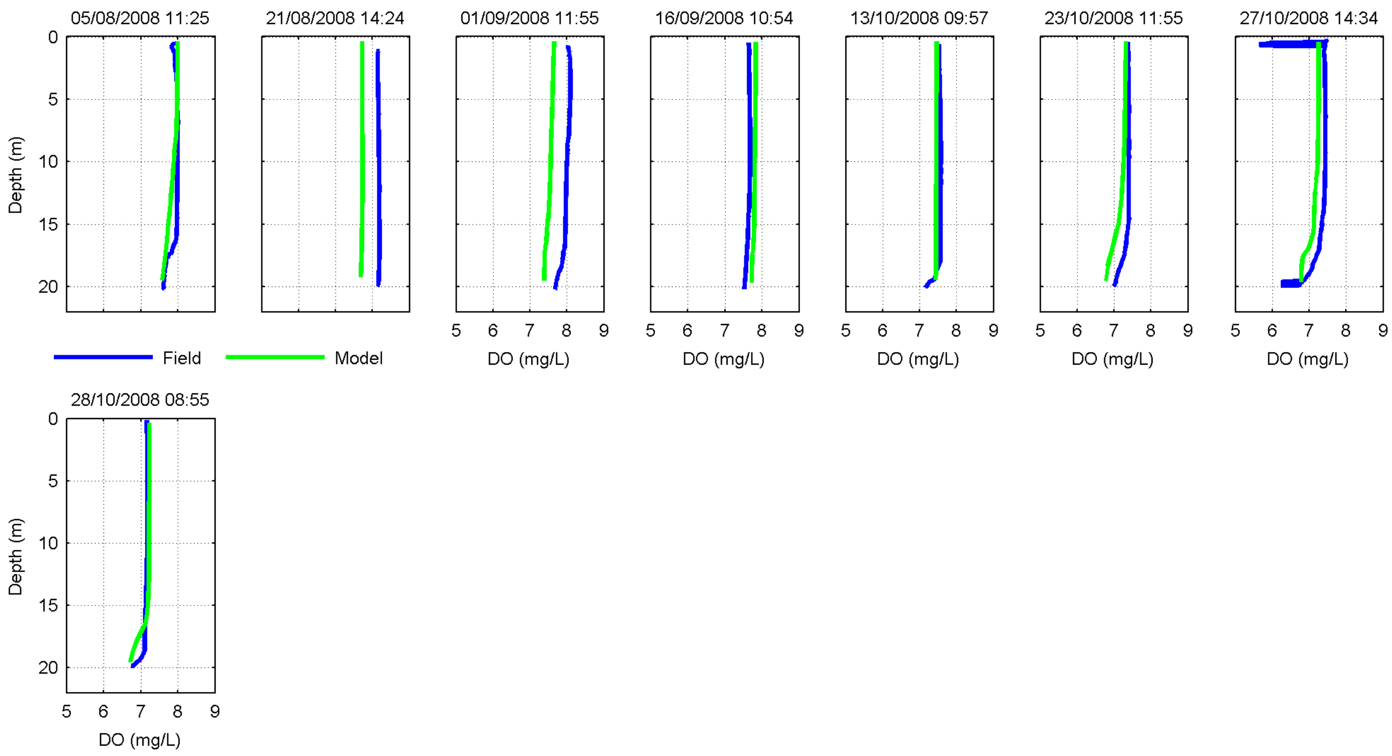

Figure 5-121 Comparisons between simulated DO and profile measurements at South Buoy in the transition from winter to spring 2008

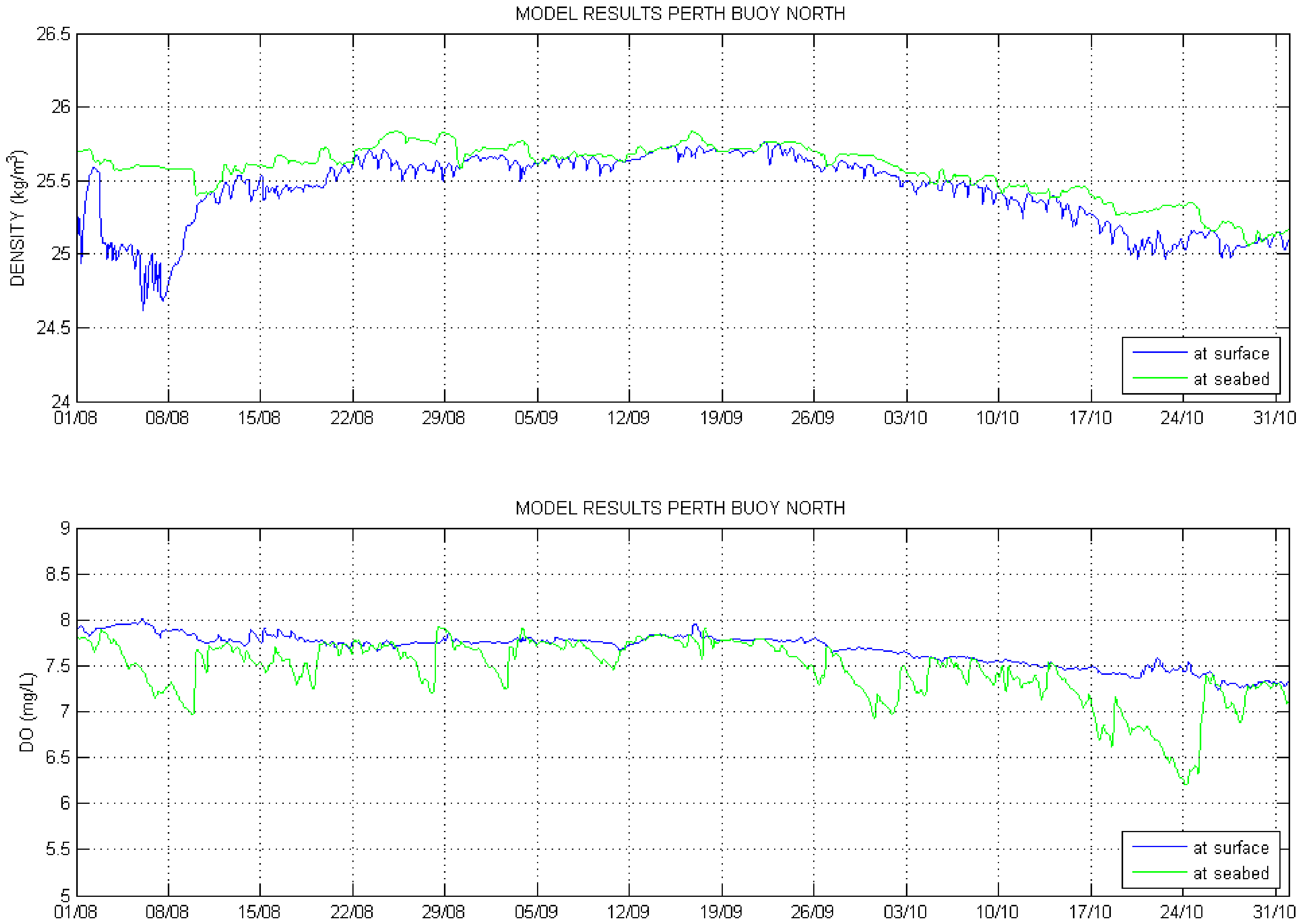

Figure 5-122 Simulated DO and density stratification at North Buoy in the transition from winter to spring 2008.

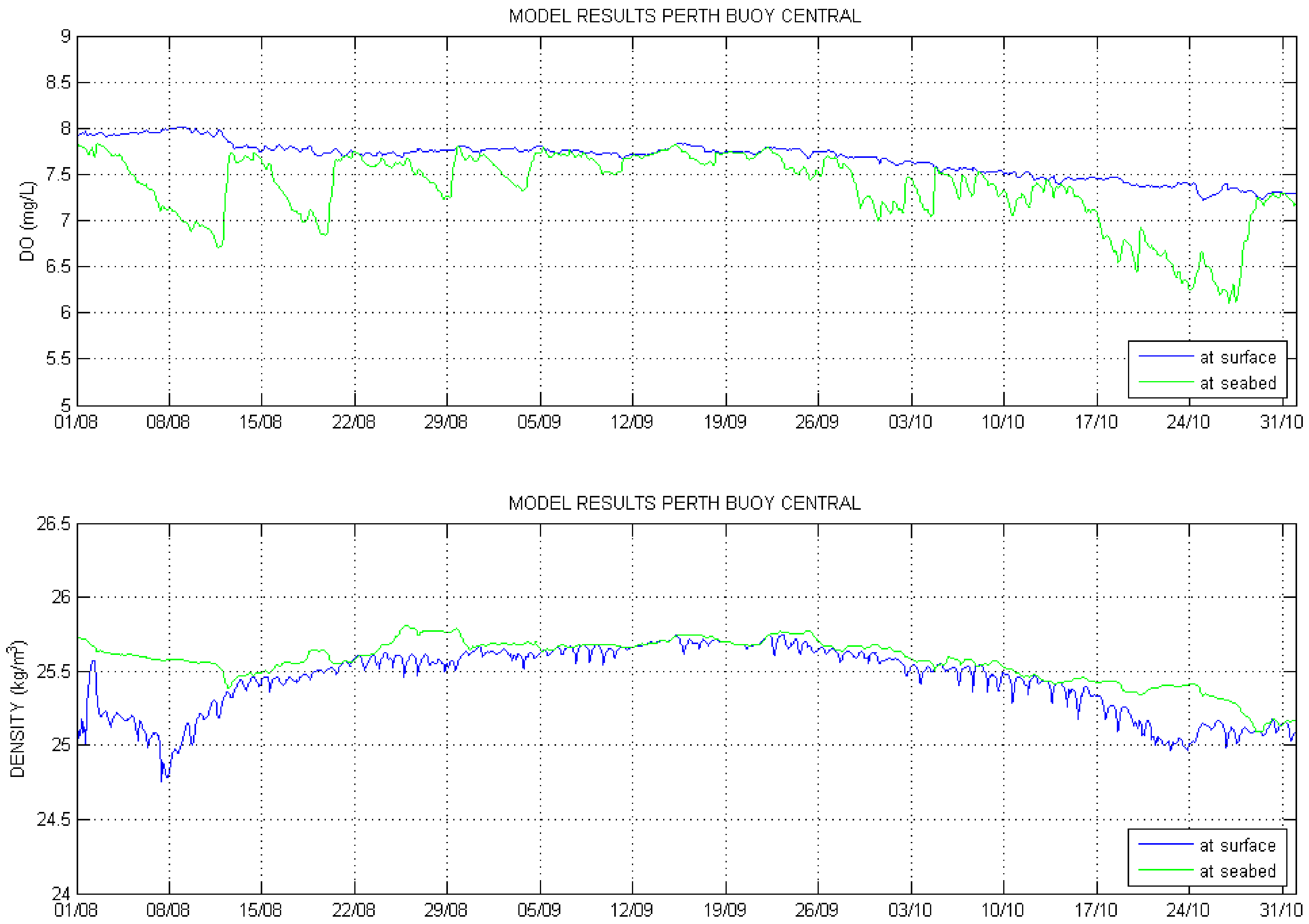

Figure 5-123 Simulated DO and density stratification at Central Buoy in the transition from winter to spring 2008.

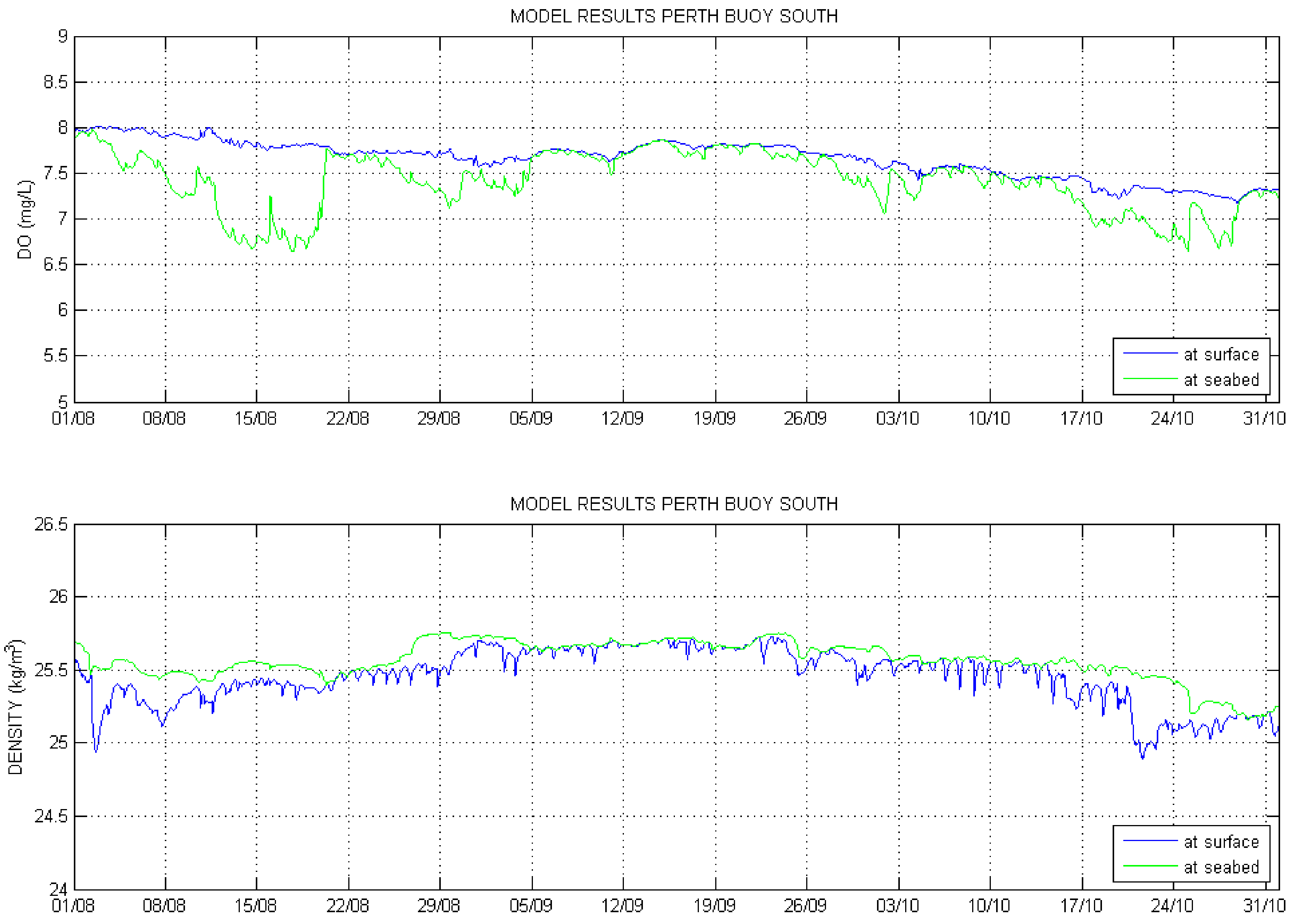

Figure 5-124 Simulated DO and density stratification at South Buoy in the transition from winter to spring 2008.

5.5.3.1 Sediment oxygen demand

The simulated SOD demand in the transition from winter to spring of 2008 at each of the three locations is presented in Figure 5-125. Over the period, SOD fluxes magnitudes increased in tandem with warming, particularly towards the end of the spring period. They were generally lower in magnitude when compared to the summer fluxes (Figure 5-118).

Again, the SOD fluxes at North and Central Buoys followed each other closely and were between -0.6 and -1.1 g O_2/m^2/day (Figure 5-125). The SOD fluxes magnitudes at South Buoy were lower (from -0.4 and -0.7 g O_2/m^2/day, Figure 5-125) and once more, approximately proportional to the applied differences in $F_{max}^{O_2}$ between this station and North and South Buoys. By the end of the period the SOD fluxes were similar to the starting period in summer 2008 (c.f. Figure 5-118 and Figure 5-125). Values are again consistent with literature and previous studies.

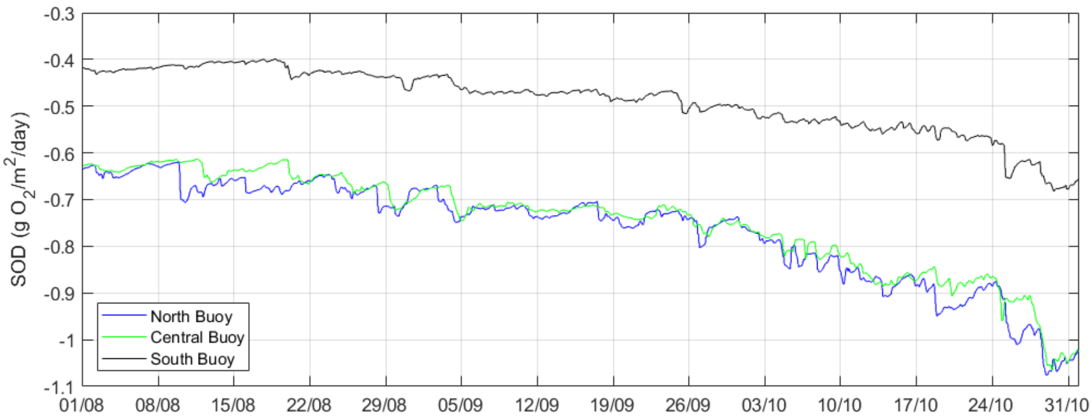

Figure 5-125 Actual simulated sediment oxygen demand in the transition from winter to spring 2008

5.5.4 Model error

The model predictive skill for DO was also tested statistically with calculations of the Coefficient of Determination (R^2), Mean Absolute Error (MAE), and Root Mean Square Error (RMSE) as defined in Appendix D. At project inception, the following calibration targets were agreed as indicators of satisfactory model validation (Table 5-10):

Table 5-14 Calibration goals for DO

Variable	R^2	MAE (mg/L)	RMSE (mg/L)
DO (profiles only)	0.8	≤ 0.5	≤ 1.0

The statistical evaluation of the DO profiles is shown in Figure 5-126 to Figure 5-128. The values from surface and bottom from both summer and winter simulations were aggregated, as per the salinity and temperature comparisons. Whilst DO model error performance was not quantified in other modelling investigations adopting similar data sets (e.g. CWR 2007c), the statistical indicators show excellent model correlation with observations (R^2 ≥ 0.85) MAE and RMSE within those agreed at project inception (Table 5-14). As described above, model error was generally consistent across the three measurement locations, where MAE was less than 0.21 mg/L and RMSE was less than 0.28 mg/L.

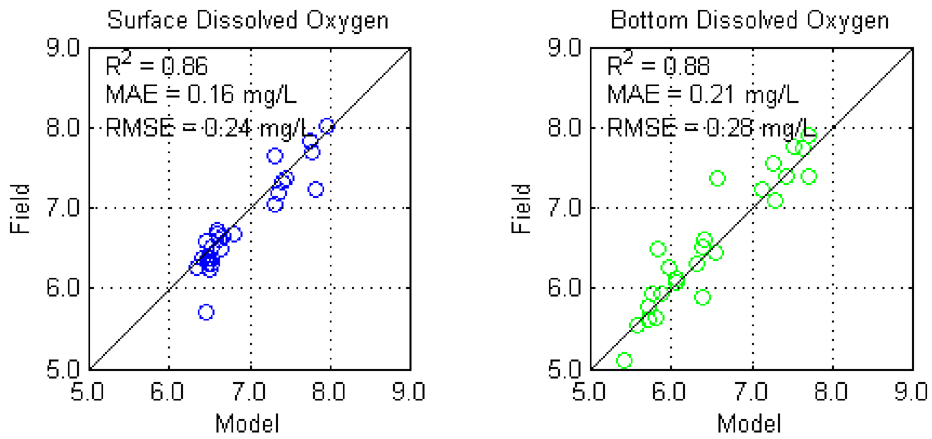

Figure 5-126 Model predictive skill statistics for DO profiles at North Buoy (top and bottom values)

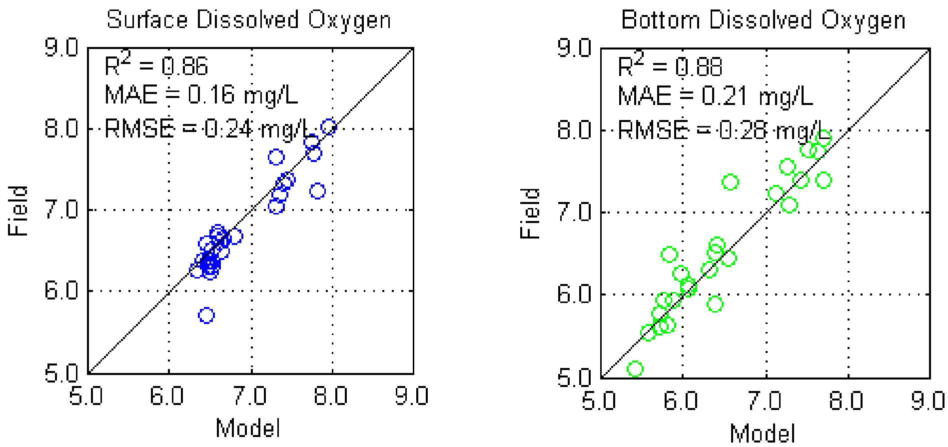

Figure 5-127 Model predictive skill statistics for DO profiles at Central Buoy (top and bottom values)

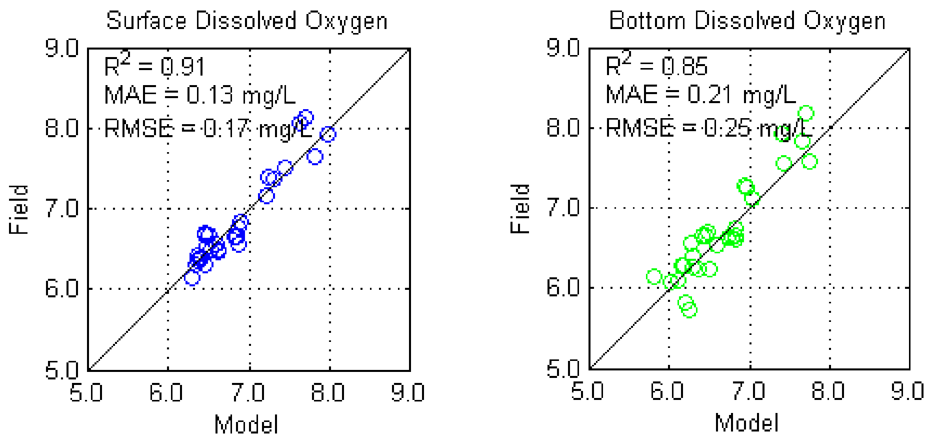

Figure 5-128 Model predictive skill statistics for DO profiles at South Buoy (top and bottom values)

5.5.5 Summer to early autumn 2013

Similarly to the temperature and salinity measurements, DO data were also collected as part of the MMMP in 2013. Again, these data allowed for model comparisons not only in the deep basin, but also in the transition to between the shallow eastern basin and the deep basin of Cockburn Sound. Further, the data allowed investigation of sediment flux demands in the shallow areas of Cockburn Sound through the model calibration process. The DO model comparisons are shown below.

5.5.5.1 DO profiles in the deep basin

Comparisons of DO profile data in the deep basin indicate the model correctly simulated the change from stratified conditions to well mixed conditions in the deep basin stations (Figure 5-129 and Figure 5-130). In both measured and simulated data, the position of the DO chemoclines coincided with the position of the haloclines (c.f. Figure 5-129 and Figure 5-130 with Figure 5-78 and Figure 5-80). As discussed in relation to salinity and temperature profiles in Section 5.3.4, variations in bottom salinities were associated with an ingress of less saline water on the surface layer into the Sound. As the salinity (and density) stratification developed, DO depletion near the bed intensified (see Section 2.3).

It can be seen that the model results at Central Buoy showed good agreement with the measurements, particularly with regards to the progressive reduction of DO concentrations up until 24 April and then subsequent return to well mixed conditions and high DO concentrations on 30 April (Figure 5-129). At South Buoy, the model generally over-predicted the DO concentrations near the bed and under-predicted concentrations towards the surface, particularly from 22 April to 28 April (Figure 5-130). As discussed earlier, the model inaccuracy stemmed from the inability, on this occasion, to determine the source of less saline water south of the Sound that led to the observed salinity and density stratification patterns (see Section 5.3.4). As a result, the DO demand calculated in the model was communicated over the entire water column, hence the under (over) prediction near the seabed (surface). The model did however reproduce the DO levels on 30 April (Figure 5-130), when both measurements and simulated results show well mixed conditions (see e.g. Figure 5-80).

5.5.5.2 DO profiles in the transition to the deep basin

The temperature, salinity and DO profiles collected in the transition between the shallow and deep basins of Cockburn Sound are presented in Figure 5-131 to Figure 5-140. Again, and similarly to the temperature and salinity plots, each of the figures in this section show a day of measurements, with each panel presenting a different location. Predictions from a companion simulation without the inclusion of the PSDP discharge is also presented in Figure 5-131 to Figure 5-140 as a dashed line.

The model replicated fundamental aspects of the PSDP discharge in this transition zone between the shallow and deep basins of Cockburn Sound. For example, the shape of the profiles within Stirling Channel (S2 and S3) was generally reproduced well in terms of shape, location of chemocline and DO concentration near the bed (Figure 5-131, Figure 5-132, Figure 5-133, Figure 5-135, Figure 5-139 and Figure 5-140). There were some exceptions, however, such as the profiles collected on 20, 23, 24 and 26 April (Figure 5-134, Figure 5-136, Figure 5-137 and Figure 5-138). For the profiles on the 20 and 23 April (Figure 5-134 and Figure 5-136), the lack of reproducibility by the model most likely resulted from the transient nature of the cooling water discharges around the PSDP discharge and the PSDP discharge itself, all of which were insufficiently well known so as to only allow specification of single average (or best estimate) flow rates and qualities in the model. It is likely that model predictions would improve with specification of transient flows in these discharges. On 24 and 26 April (Figure 5-137 and Figure 5-138), the ingress of the less saline layer from the south of the Sound likely resulted in changes to the profiles.

The model also predicted well the transition from stratified DO profiles in the inner radii (stations R2, A and B) before 22 April into subsequently more well mixed conditions. These profiles, in particular, were largely influenced by the transient nature of the discharge, particularly noticing the measured temperature and salinity instabilities between 16 and 20 April (see Figure 5-131 to Figure 5-134 for DO and Figure 5-83 to Figure 5-90 for temperature and salinity). Given the steady flow and salinity assumptions applied by necessity in the discharge boundary condition specifications (as a direct result of data paucity), the model was unable to replicate these unstable temperature and salinity profiles, and as such, their signature in some of the subtleties of the DO profiles (e.g. a bulge indicating reduction and increase of DO at depth).

In the outer radii (stations C and D), the influence of the brine discharge on the profiles was much less marked, such that the profiles' characteristics in both model and measured data resembled those of offshore stations (i.e. CT7 and CT3, South and Central; Figure 5-131 to Figure 5-140).

The lowest DO levels predicted by the model in the outer radii stations, and in most instances the thickness of the low near-bed DO layer, were in agreement with measurements (Figure 5-131 to Figure 5-140). However, for the instances where the model did not replicate the salinity stratification (due to the appearance of southern fresh water discussed above), the model was less accurate in its prediction of DO (e.g. the south-most stations between 22 and 28 April; Figure 5-135 to Figure 5-139).

In addition to the impacts on salinity, the PSDP discharge was also shown to influence DO concentrations (c.f. green solid and dashed lines in Figure 5-131 to Figure 5-140). Similarly to salinity, and as expected, the DO results from simulations with and without the discharge showed greatest impacts in Stirling Channel, and to a lesser extent at the inner radii sites (particularly stations R2 and A; Figure 5-131 to Figure 5-140).

In relation to the simulation without the inclusion of the PSDP discharge, the DO from the simulations including the discharge showed little (if any) change in the deep basin locations. Any differences are in the scope of model noise. Sometimes increased DO concentrations in Stirling Channel and some inner radii locations are present (Figure 5-131 to Figure 5-140). The increase of DO at depth in the simulations was generally associated with the (against constant) assumption of DO saturation in the discharge. Measurement of such data would improve model predictive capability.

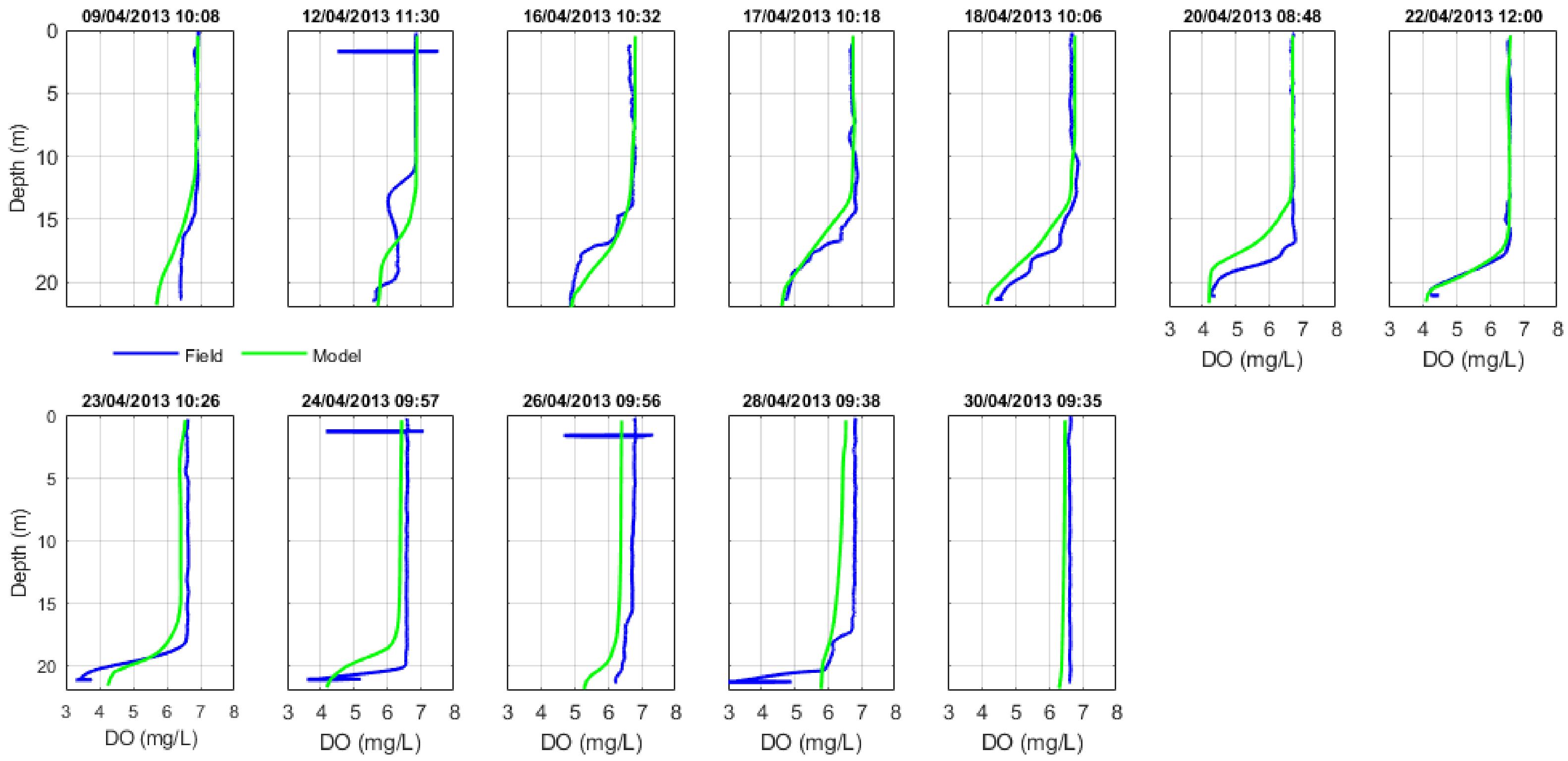

Figure 5-129 Comparisons between simulated DO and profile measurements at Central Buoy in the transition between summer and autumn 2013

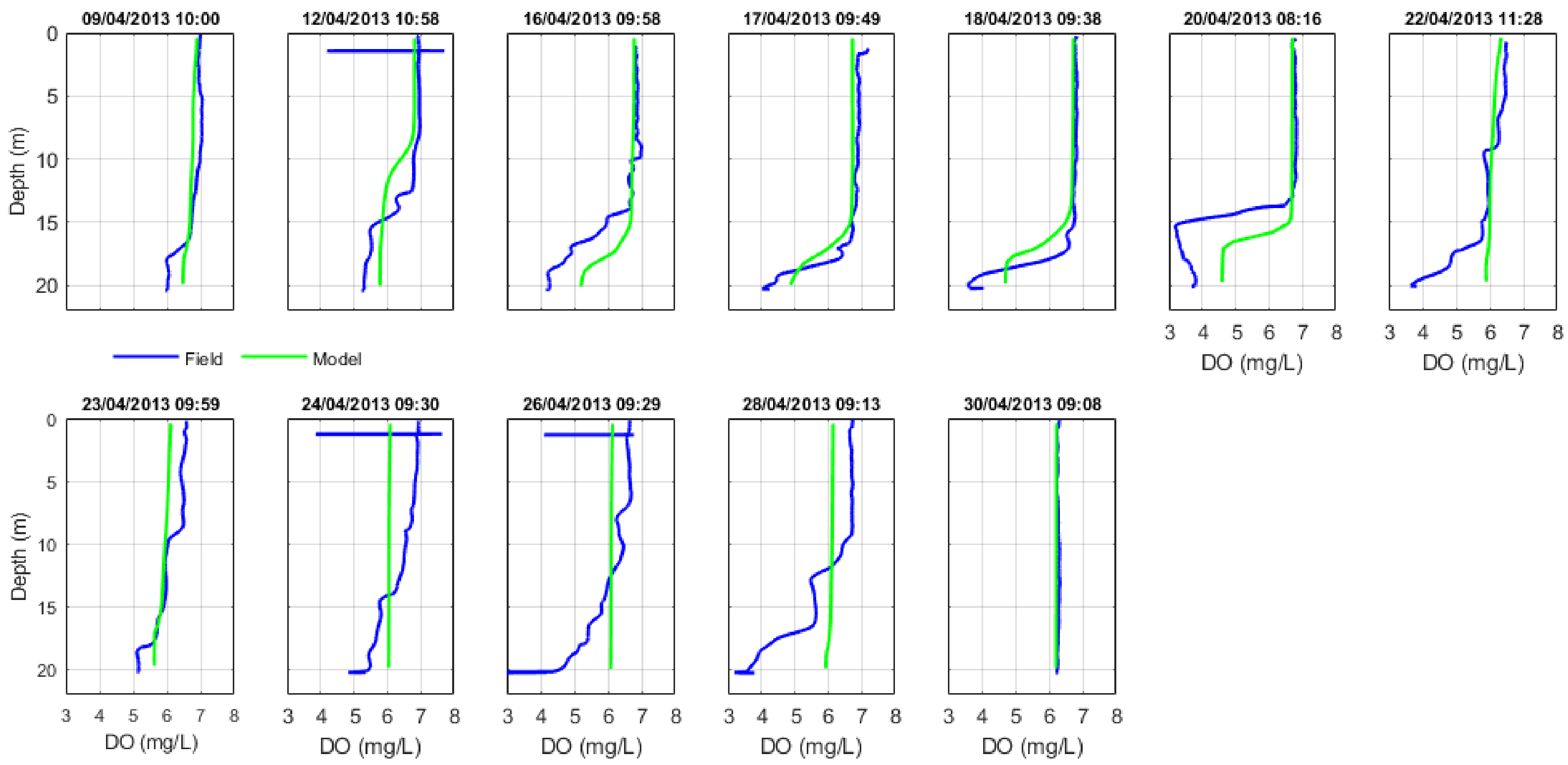

Figure 5-130 Comparisons between simulated DO and profile measurements at South Buoy in the transition between summer and autumn 2008

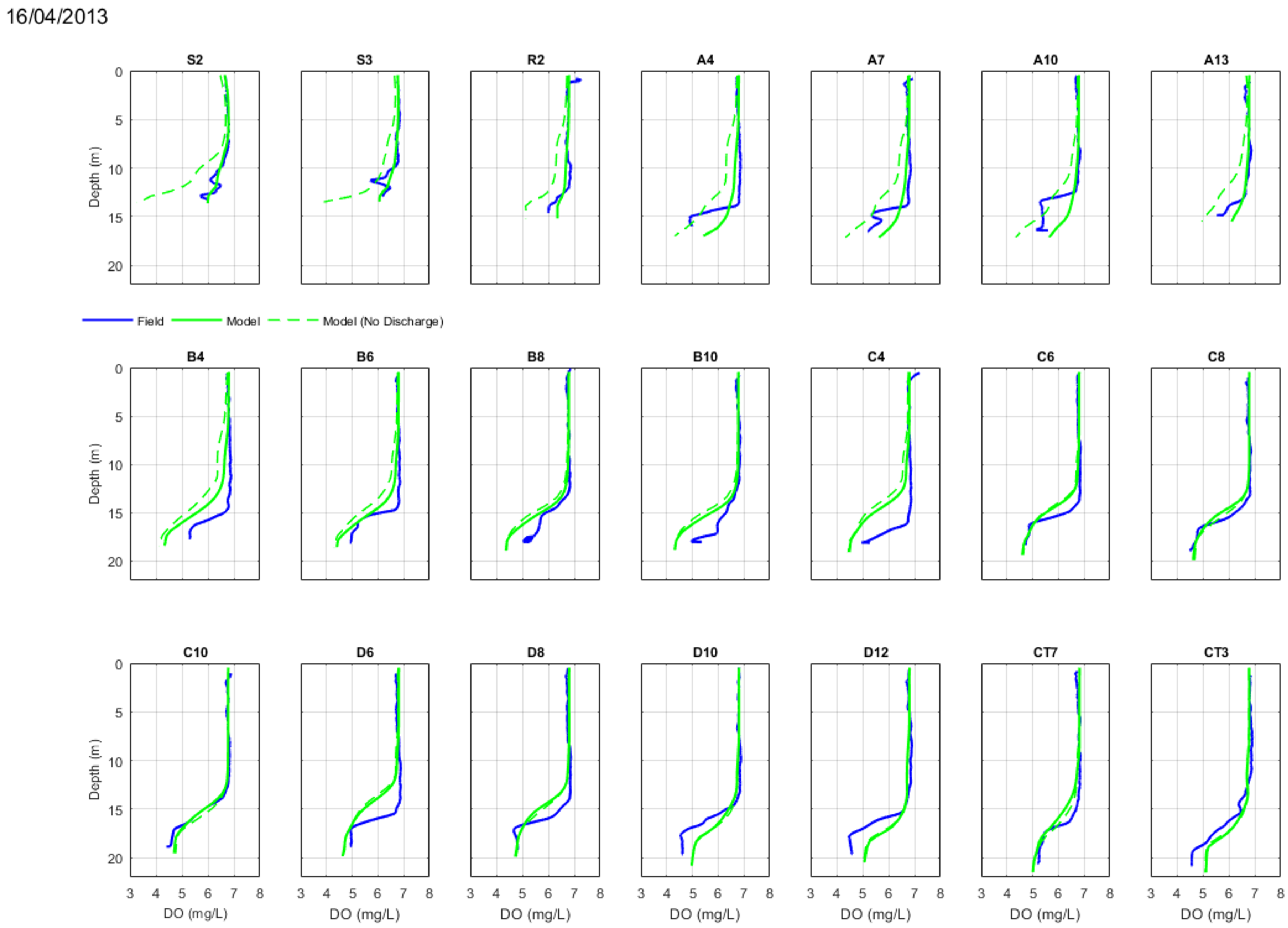

Figure 5-131 Comparison of simulated and measured DO profiles at a subset of the MMMP stations on 16 April 2013

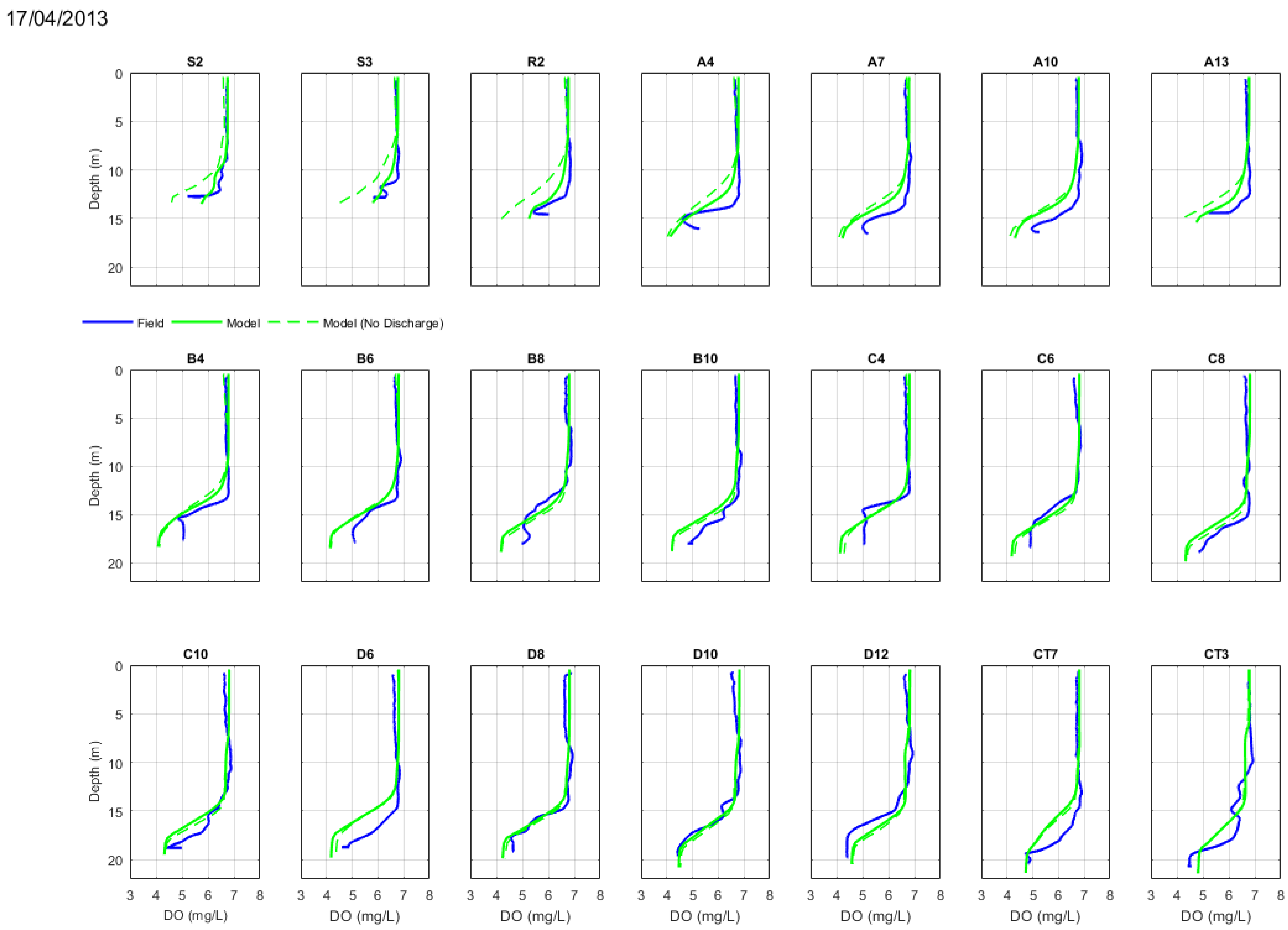

Figure 5-132 Comparison of simulated and measured DO profiles at a subset of the MMMP stations on 17 April 2013

18/04/2013

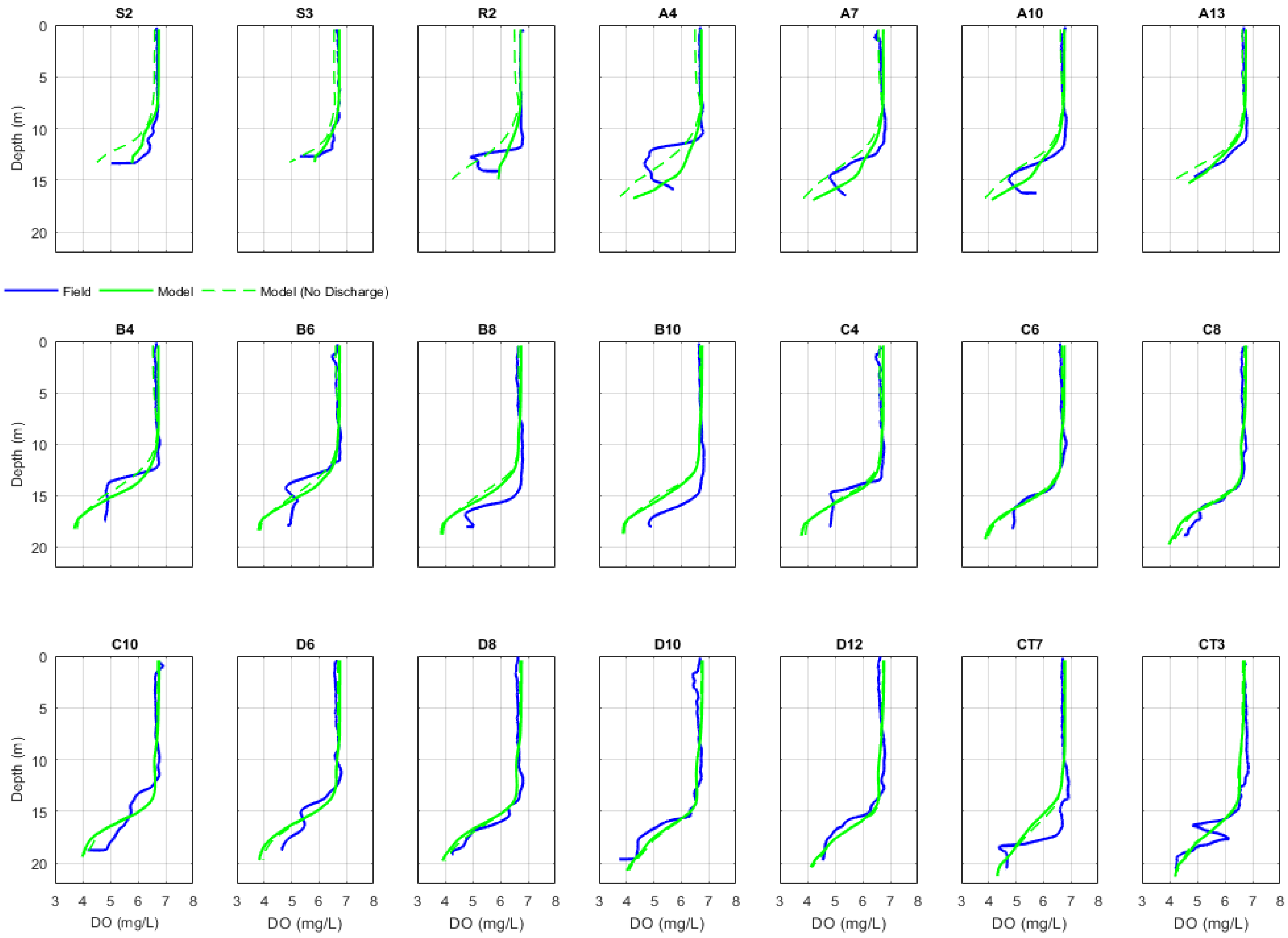

Figure 5-133 Comparison of simulated and measured DO profiles at a subset of the MMMP stations on 18 April 2013

20/04/2013

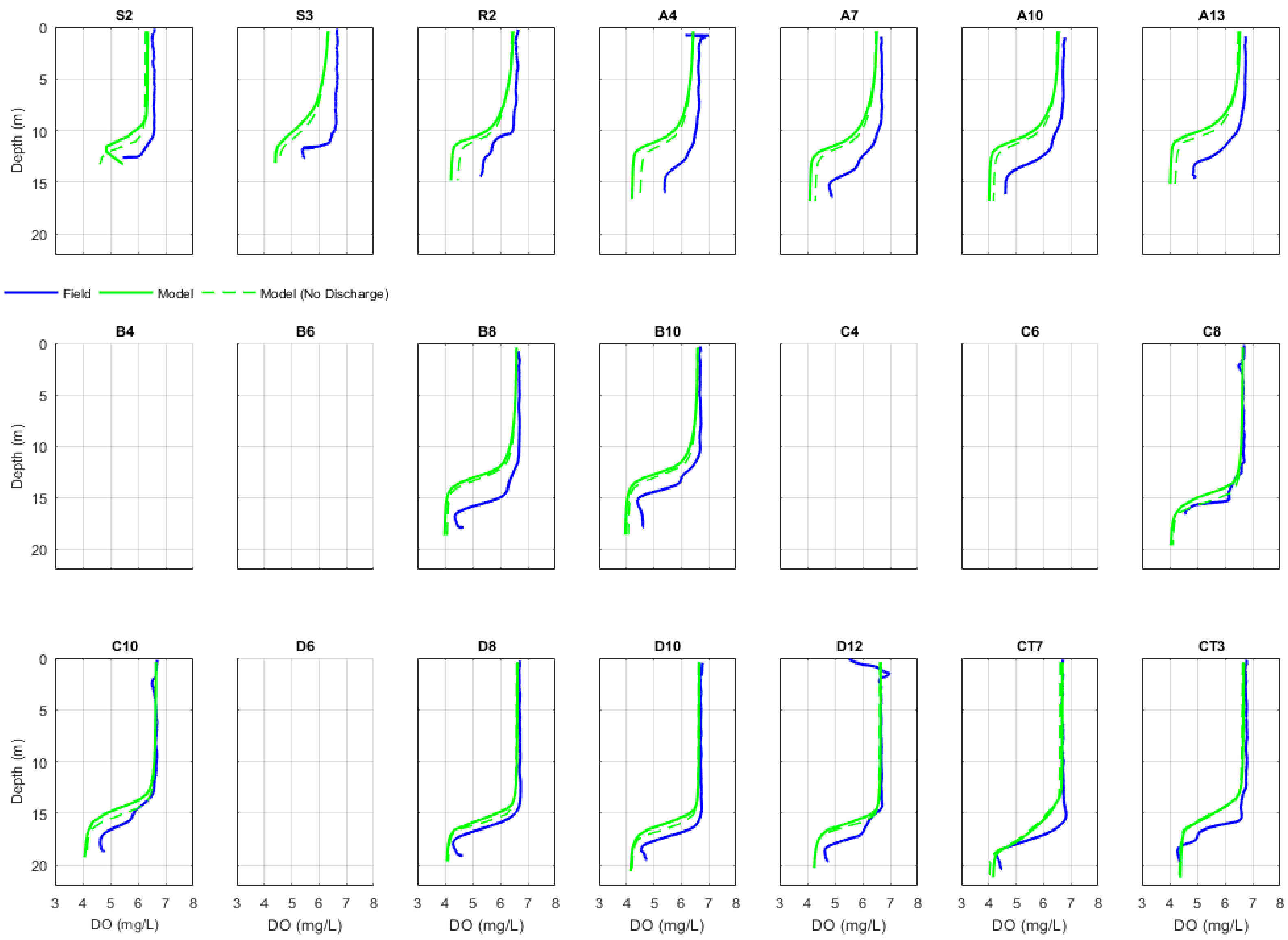

Figure 5-134 Comparison of simulated and measured DO profiles at a subset of the MMMP stations on 20 April 2013

22/04/2013

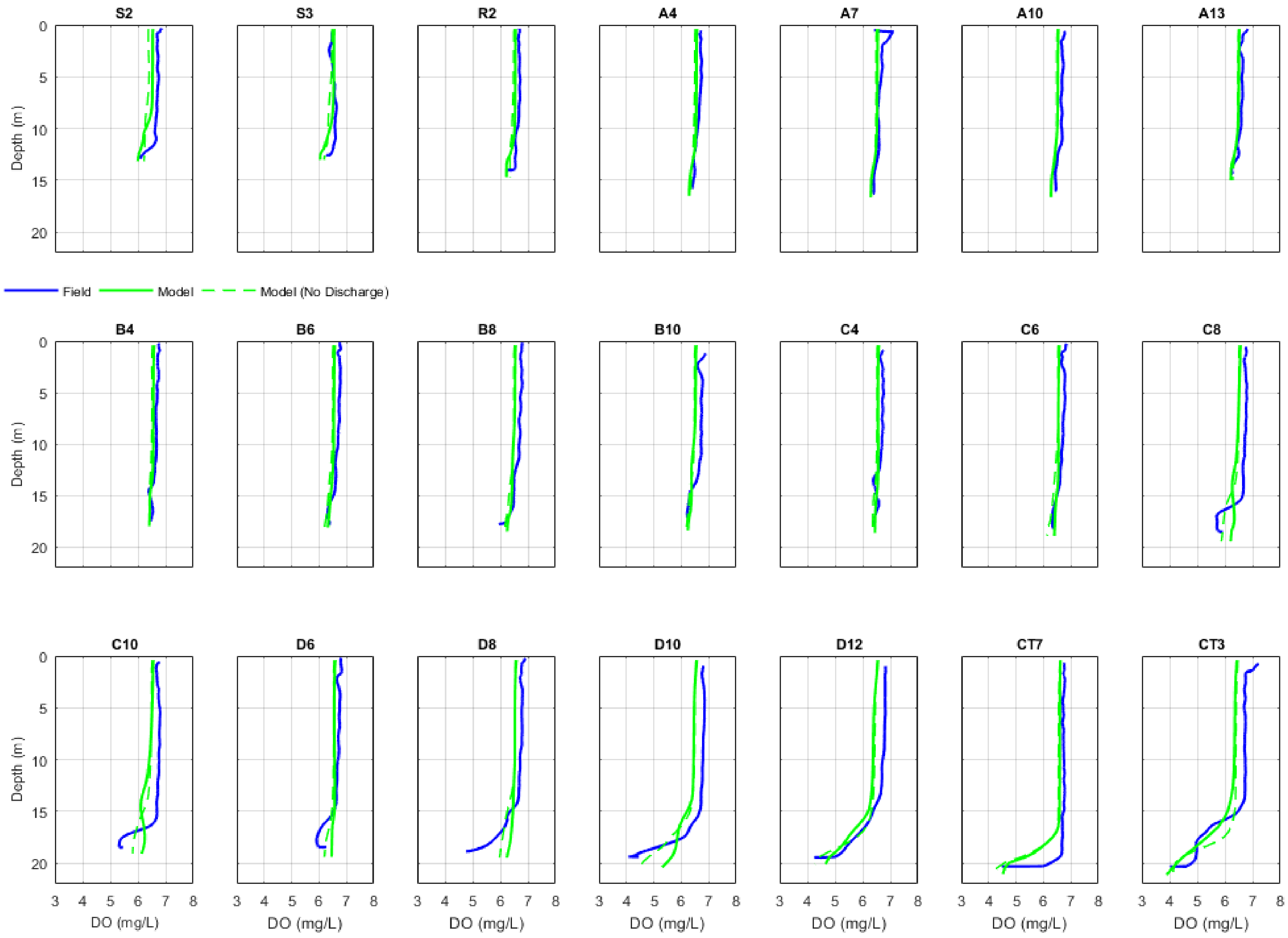

Figure 5-135 Comparison of simulated and measured DO profiles at a subset of the MMMP stations on 22 April 2013

23/04/2013

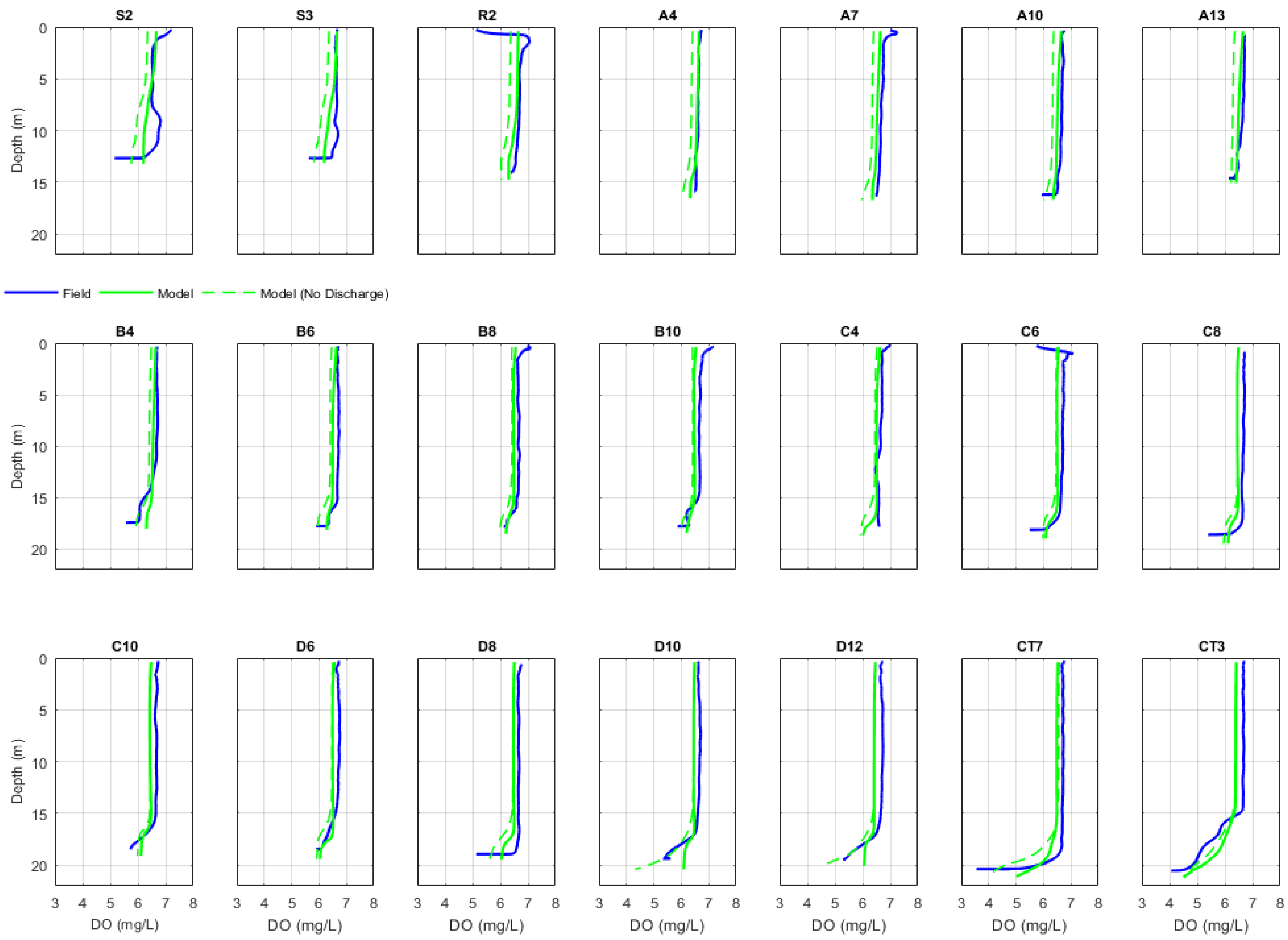

Figure 5-136 Comparison of simulated and measured DO profiles at a subset of the MMMP stations on 23 April 2013

24/04/2013

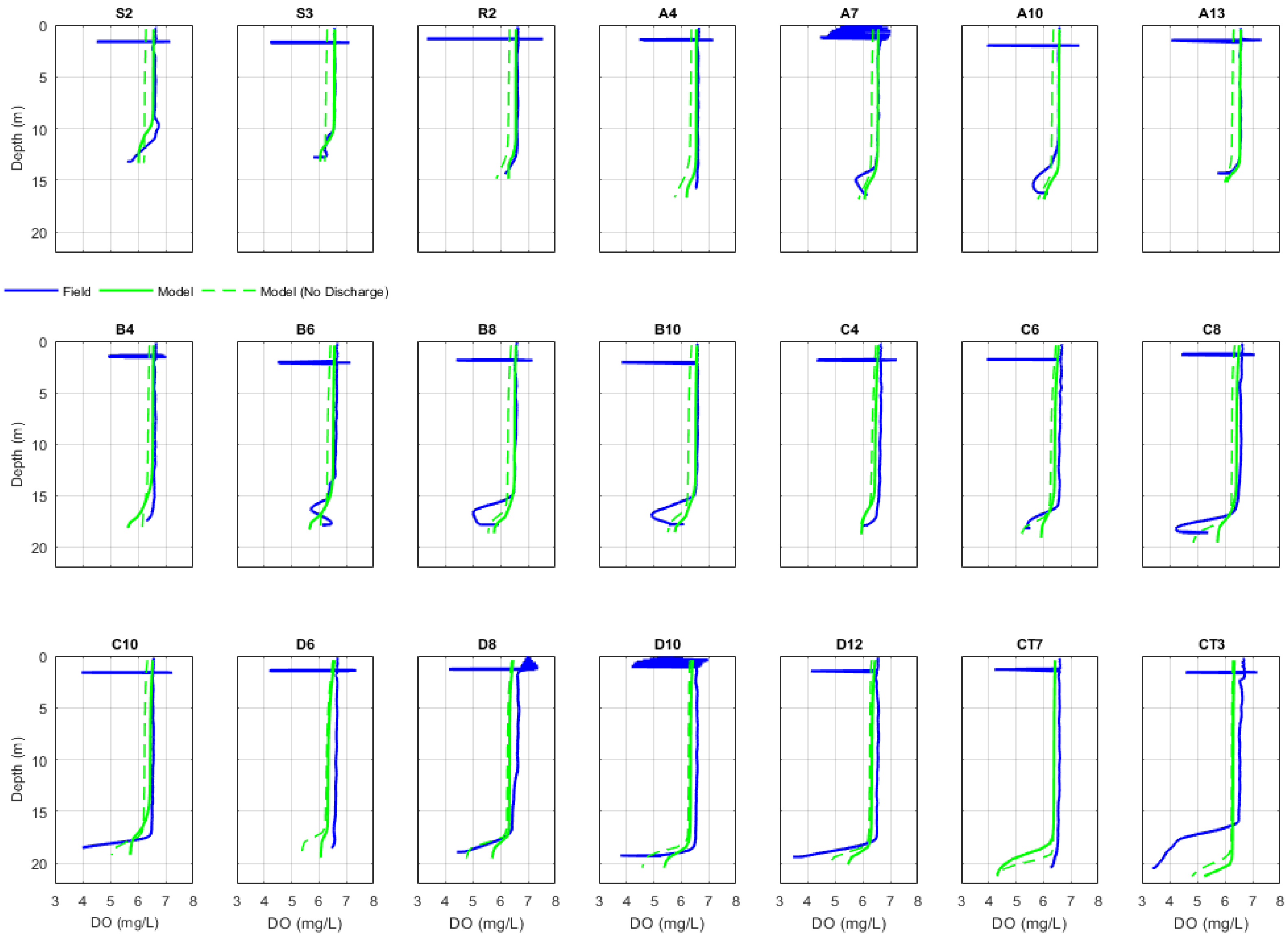

Figure 5-137 Comparison of simulated and measured DO profiles at a subset of the MMMP stations on 24 April 2013

26/04/2013

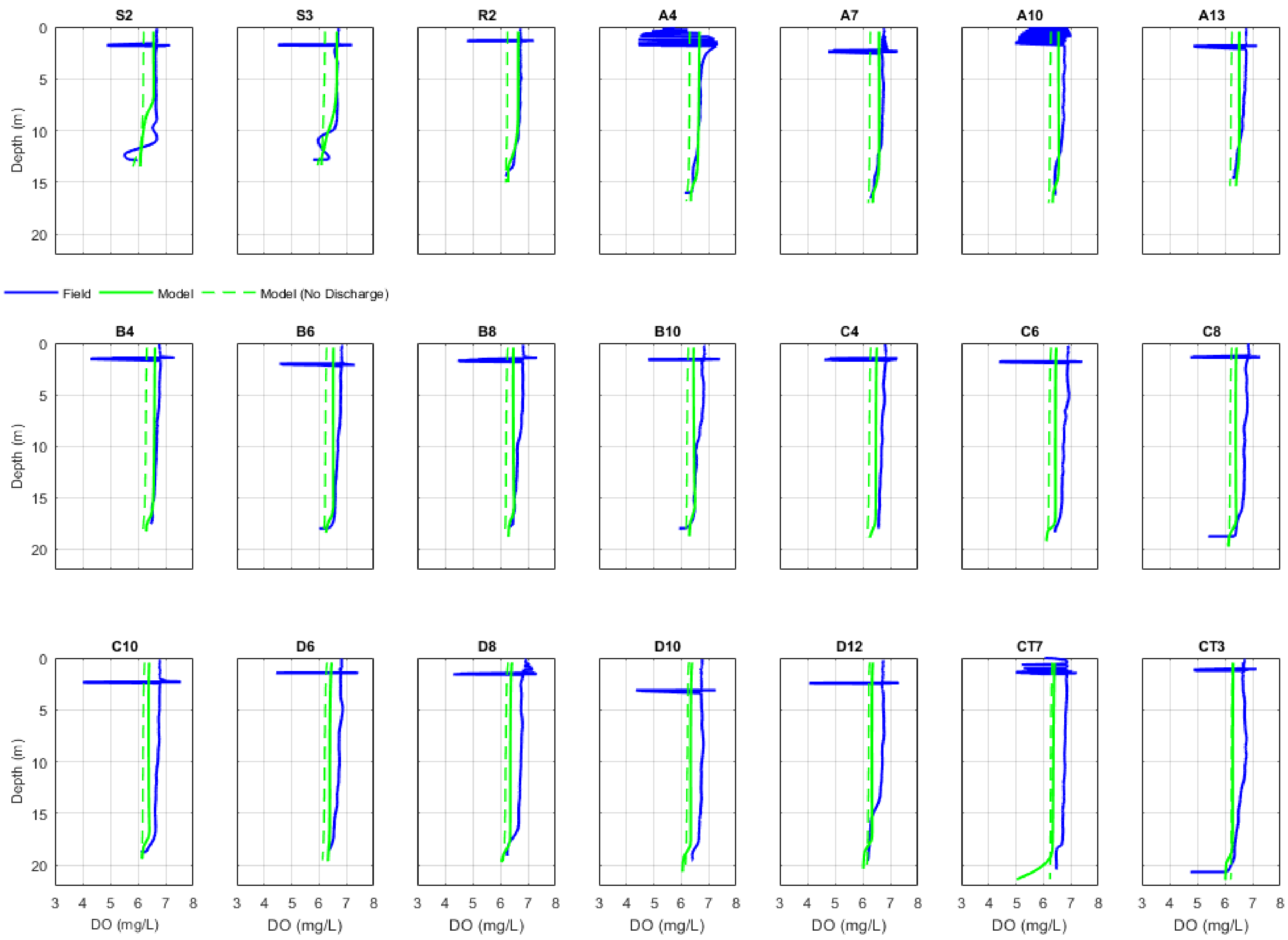

Figure 5-138 Comparison of simulated and measured DO profiles at a subset of the MMMP stations on 26 April 2013

28/04/2013

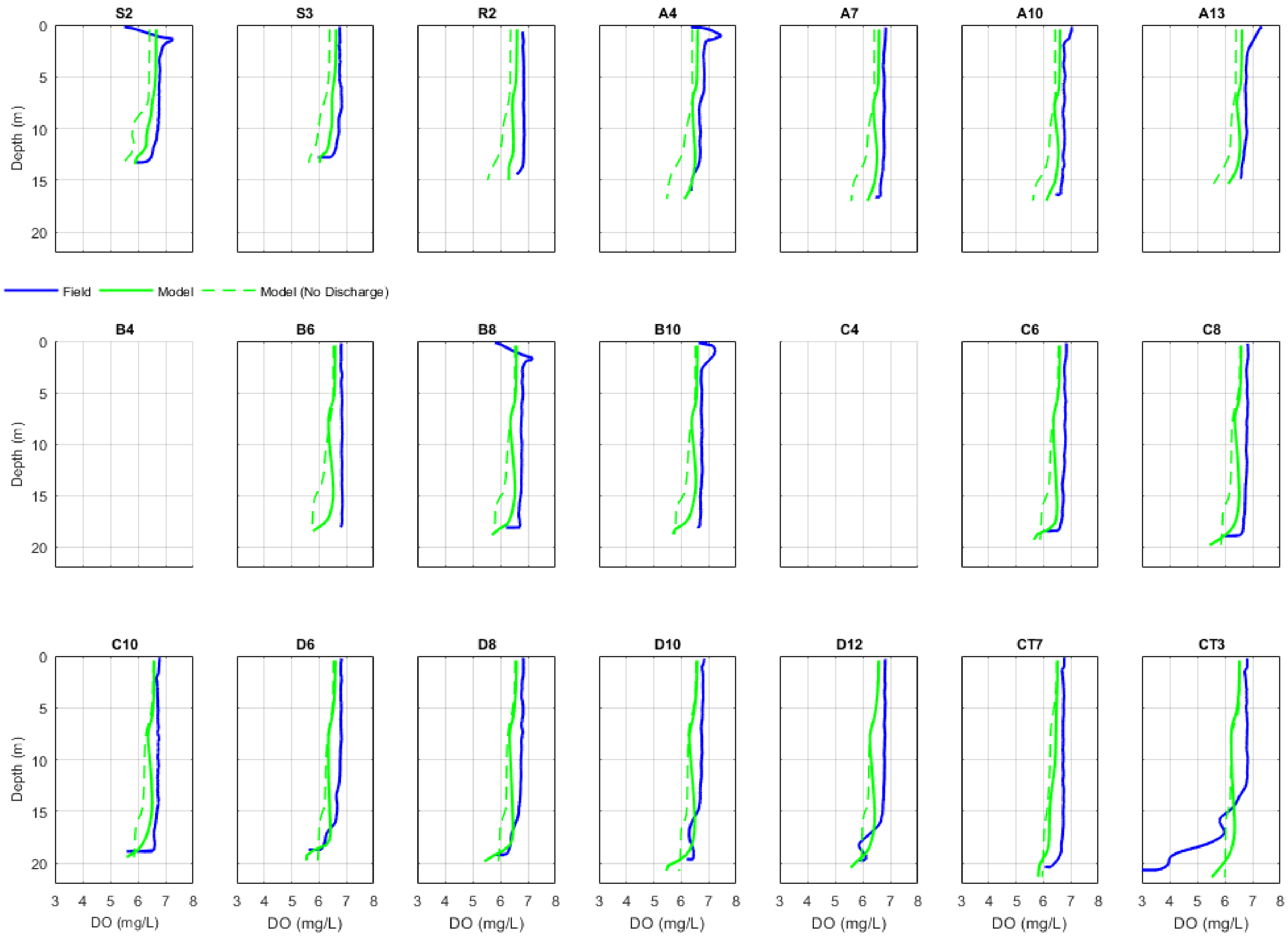

Figure 5-139 Comparison of simulated and measured DO profiles at a subset of the MMMP stations on 28 April 2013

30/04/2013

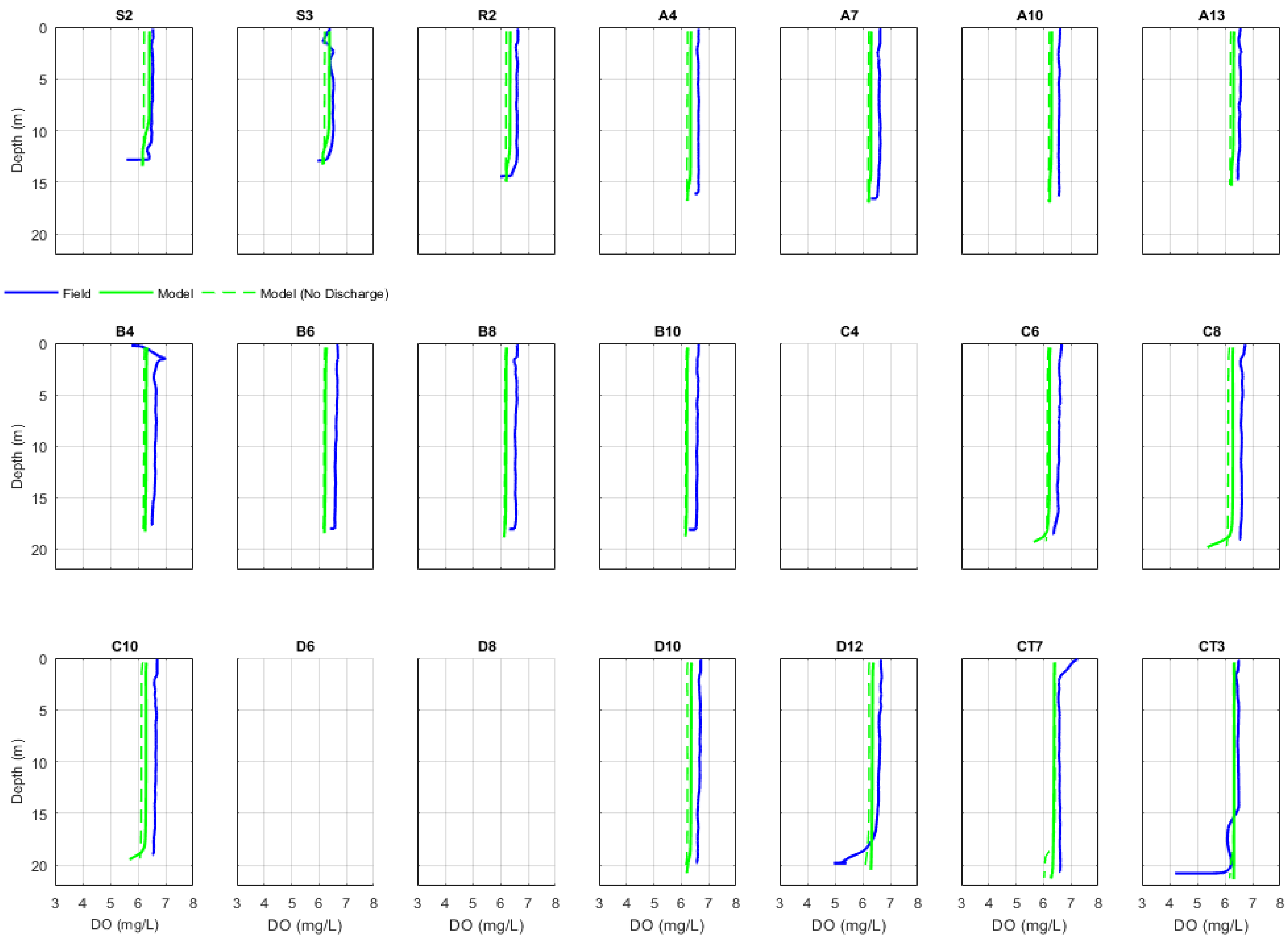

Figure 5-140 Comparison of simulated and measured DO profiles at a subset of the MMMP stations on 30 April 2013

5.5.5.3 Data mapping

To demonstrate the ability of the model to reproduce features of the discharge plume as it moves from point of discharge to extent of intrusion, a series of vertical curtain contour plots were prepared that compare modelled to observed data over April 2013. To the best of BMT's knowledge, preparation of these contours is the first time the MMMP data has been presented in this manner. Doing so offers a unique insight into the plume dynamics and makes full use of these extensive field data sets.

A series of colour contour figures follow, with each figure presenting both measured and modelled data for a single quantity (i.e. temperature, salinity or DO) for a given day in April 2013. Each figure includes three complementary panes for comparison, and from left to right are colour contours of measurements (temperature, salinity or DO), corresponding model predictions and (always) modelled tracer concentrations. The latter pane was included so as to clearly indicate plume morphology (the simulations attached a tracer to the PSDP discharge and assigned a value of zero elsewhere, thereby facilitating visualisation of the fate and transport of the modelled plume). In turn, each of the three panes within a figure comprises five colour contours. The upper four contours follow the concentric circles of observed data (rings A to D, see Figure 2-16 for the plan distribution of these rings). The lower curtain follows the general line of discharge intrusion from Calista and Stirling Channels (left hand side), to the outer ring (ring D), then diverts south. This long section therefore intersects curtains A to D after it leaves the channels, in an approximately perpendicular fashion.

The chainages of curtains corresponding to rings A to D were anchored to the northern most station (left hand side of each colour contour) and then progressed to the southern-most station (right hand side) around the curve of the ring. This orientation is denoted by an N (left hand side) and S (right hand side) on each colour contour. This style of presentation obviously therefore flattens rings into rectangular two-dimensional contours as presented, but with no loss of information.

The long section curtain chainage is anchored to station S2 (left hand side), closest to the point of discharge. Note that to preserve scale in the curtain series, station south could not be presented as it is located outside the chainage limits at a chainage of 7350 m from station S2. It was nonetheless still used to interpolate the data as presented.

For each of temperature, salinity and DO, a comparison was made between observed, model and tracer in each figure. For example, a figure presenting temperature contours on a particular day shows measured temperature (left hand pane), modelled temperature (central pane) and modelled tracer (right hand pane, with modelled tracer contours being repeated across temperature, salinity and DO figures). Colour scales are always the same so as to allow easy ocular inspection. Contours of field data are blanked where data were bad or missing.

Figure 5-141 presents an annotated example of a contour pane (which would be one of three within a figure) in the series of figures that follows. The series are presented in order of temperature, salinity and DO. In all contours, the uppermost MMMP surface measurements are deeper than those of the model, and on occasion this manifests itself as an apparent overprediction of surface temperature in the model. This is however, simply an artefact of the difference in surface depths.

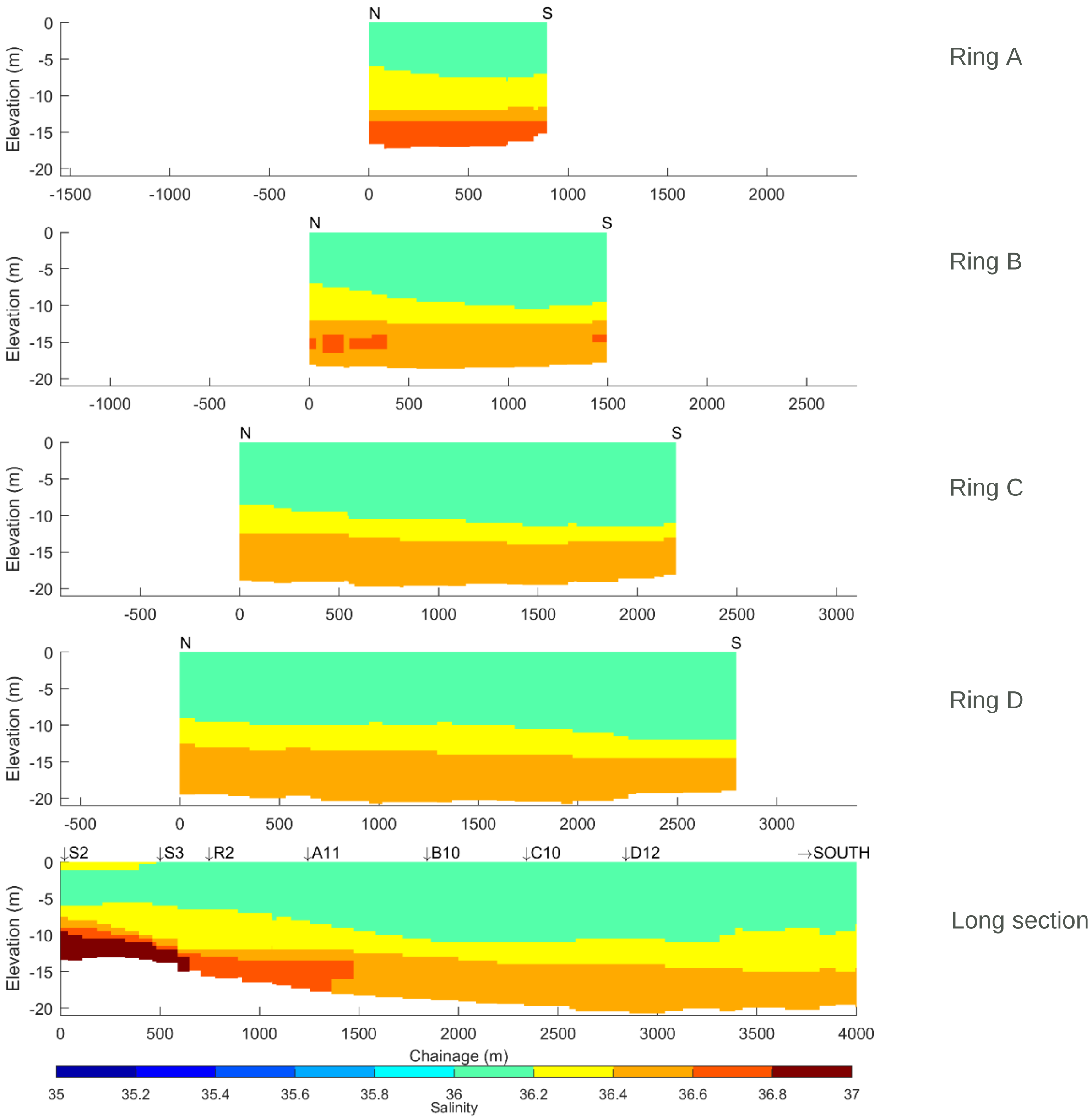

Figure 5-141 Example colour contour pane. It presents modelled salinity so would be the centre pane in the corresponding figure

5.5.5.3.1 Temperature results

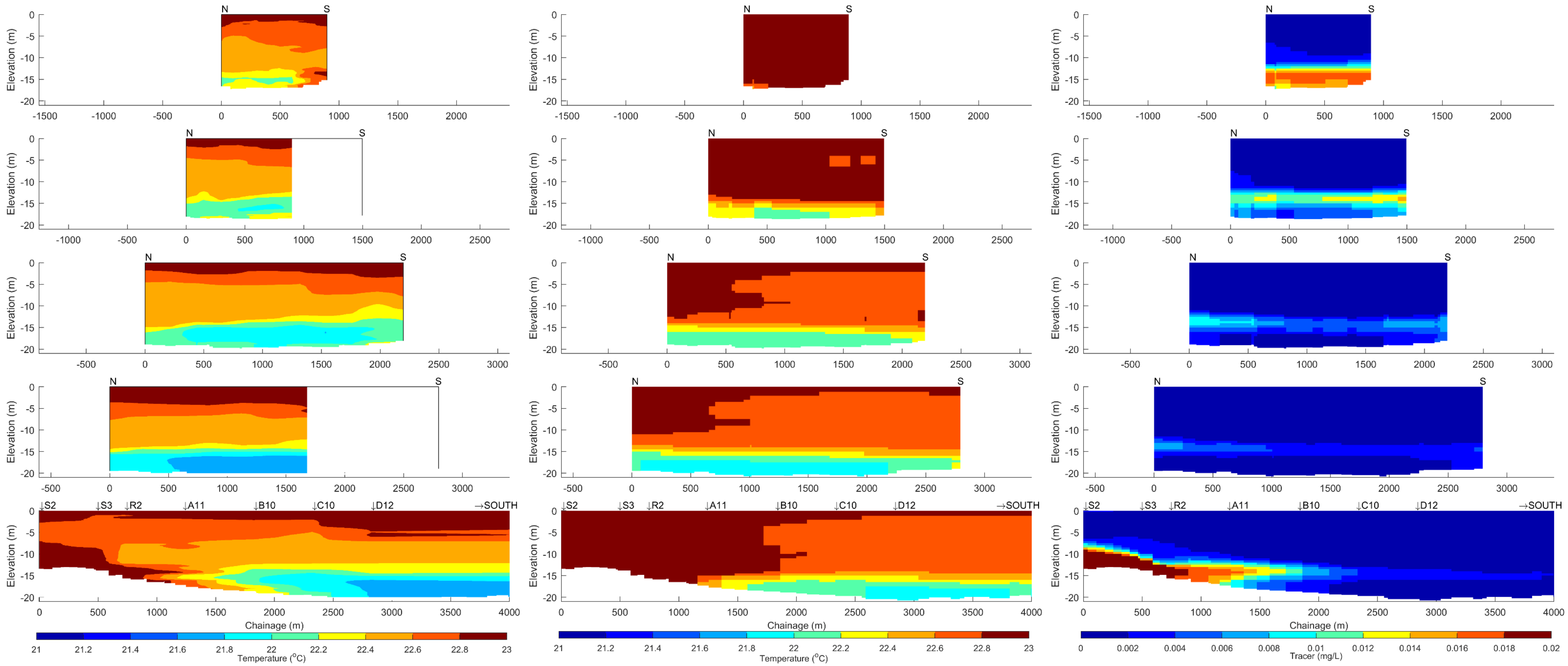

Figure 5-142 Temperature results – 16 April 2013 (field, model, tracer)

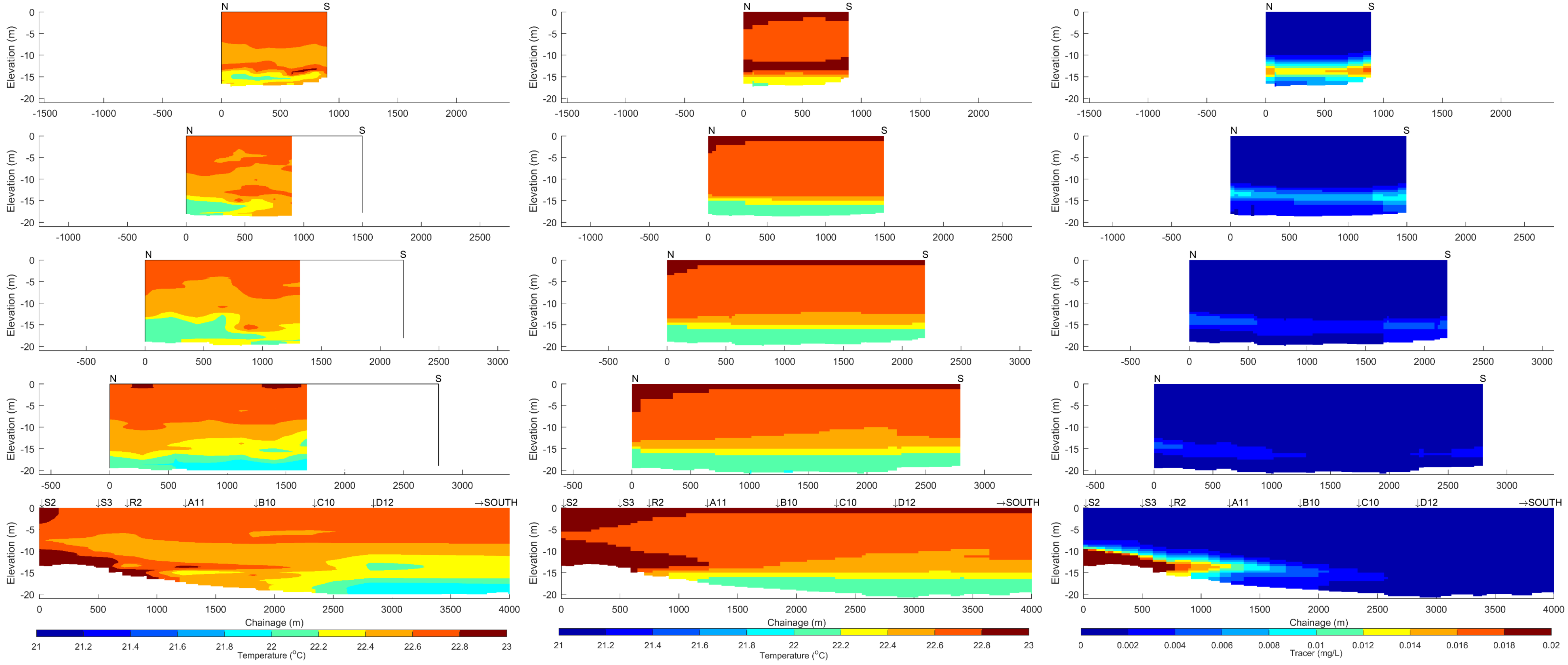

Figure 5-143 Temperature results – 17 April 2013 (field, model, tracer)

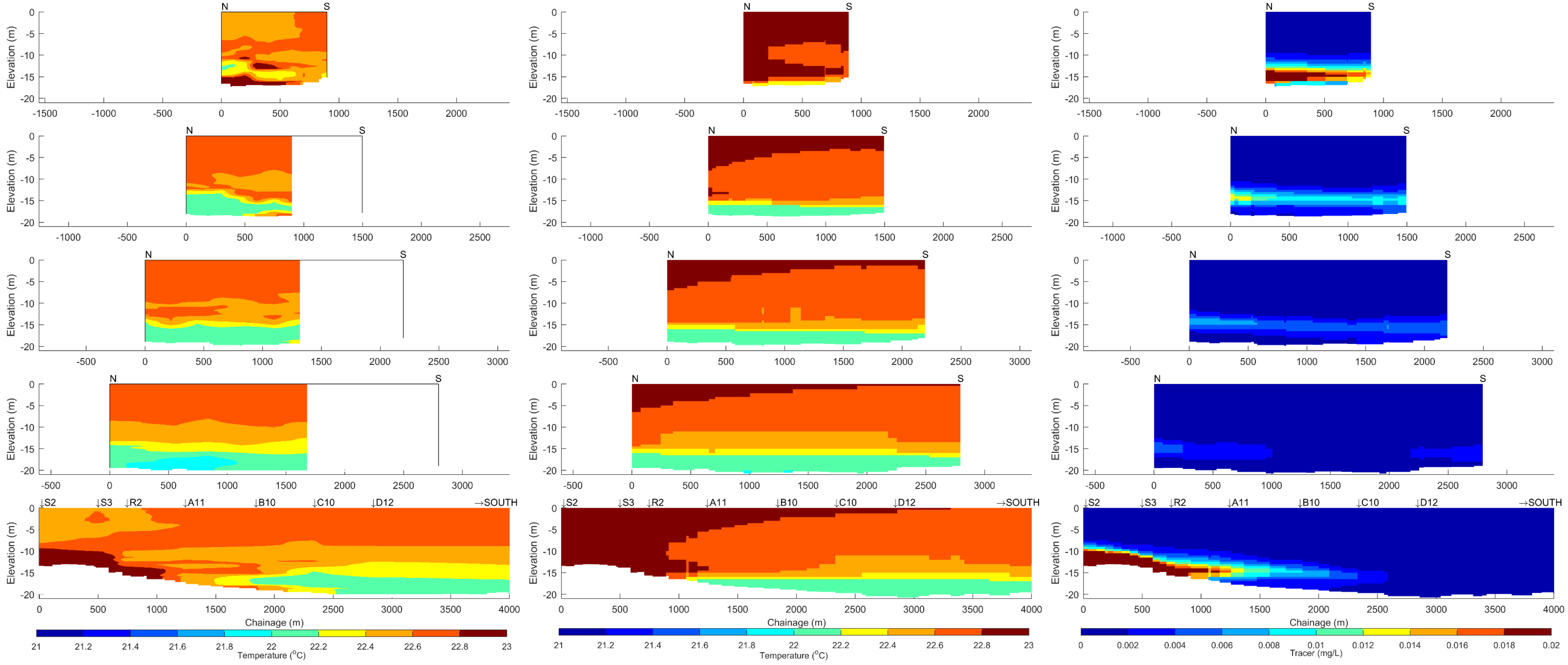

Figure 5-144 Temperature results – 18 April 2013 (field, model, tracer)

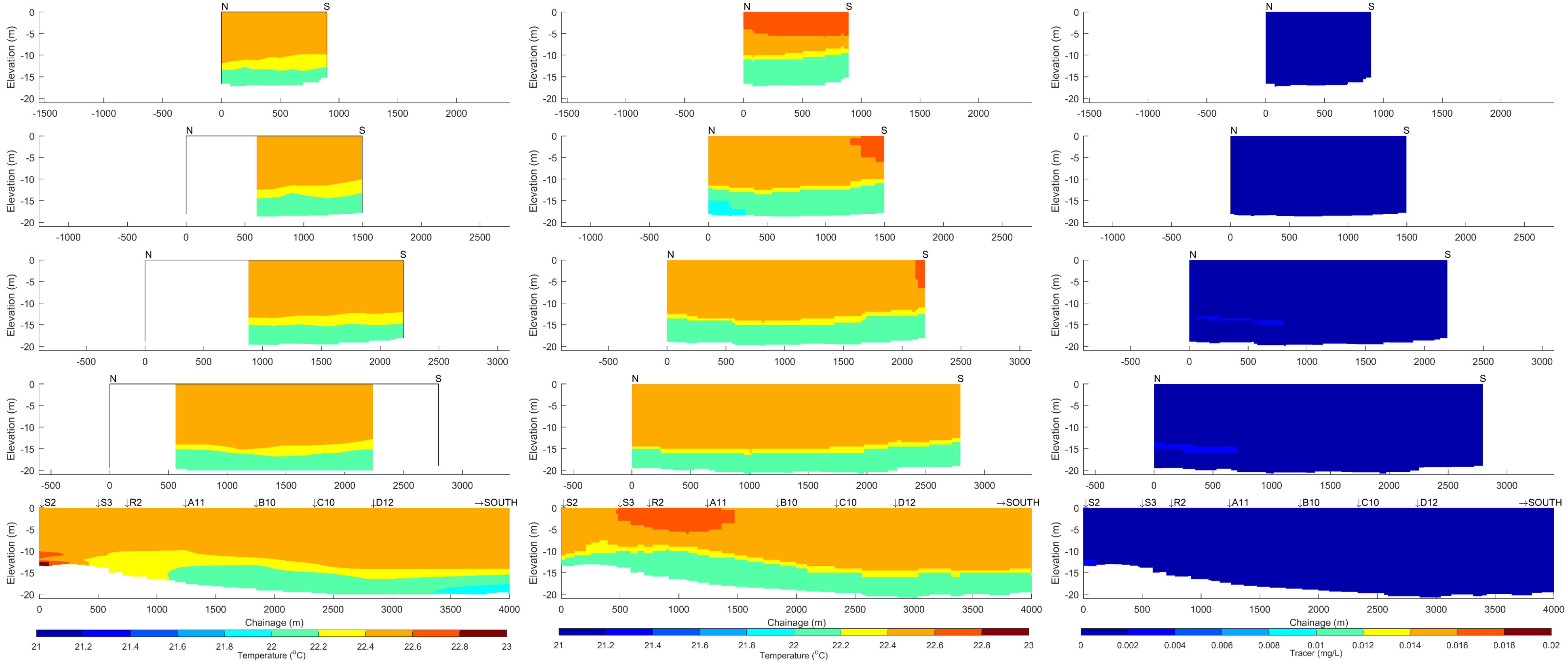

Figure 5-145 Temperature results – 20 April 2013 (field, model, tracer)

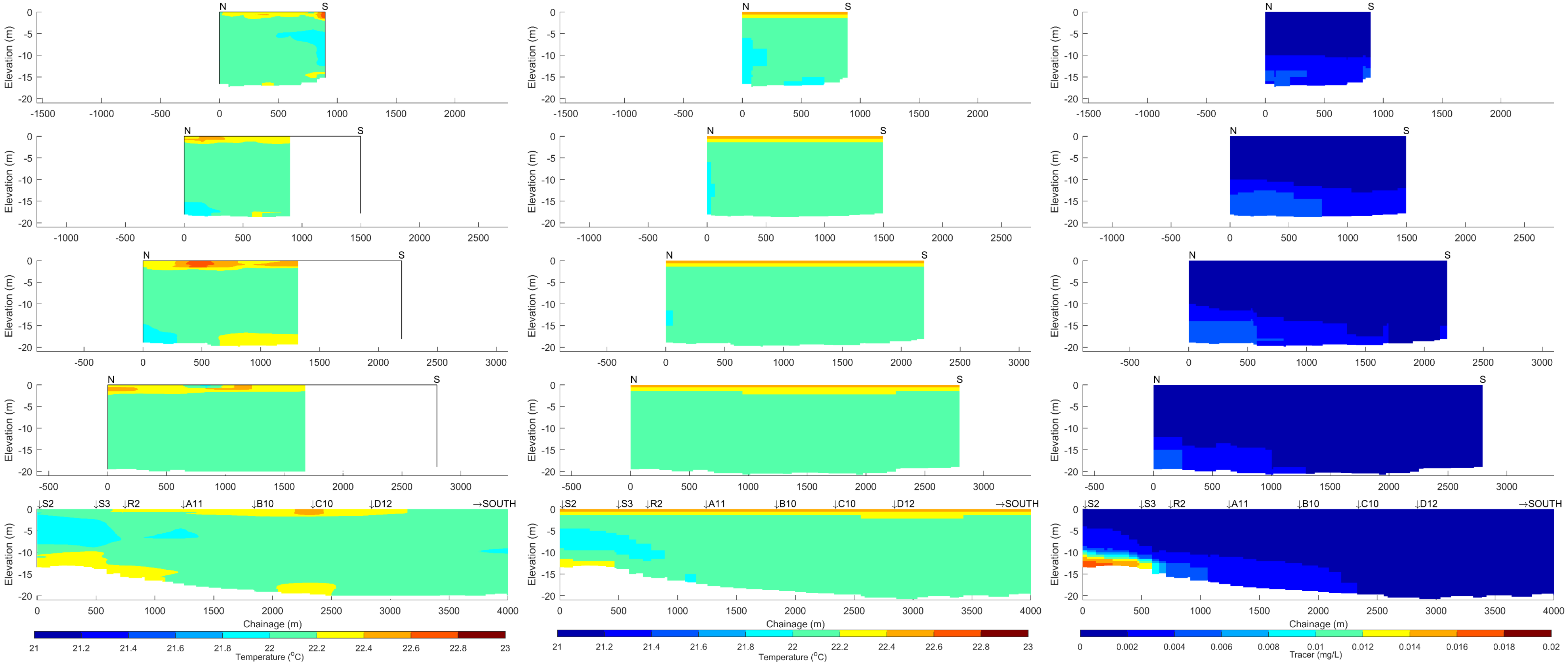

Figure 5-146 Temperature results – 22 April 2013 (field, model, tracer)

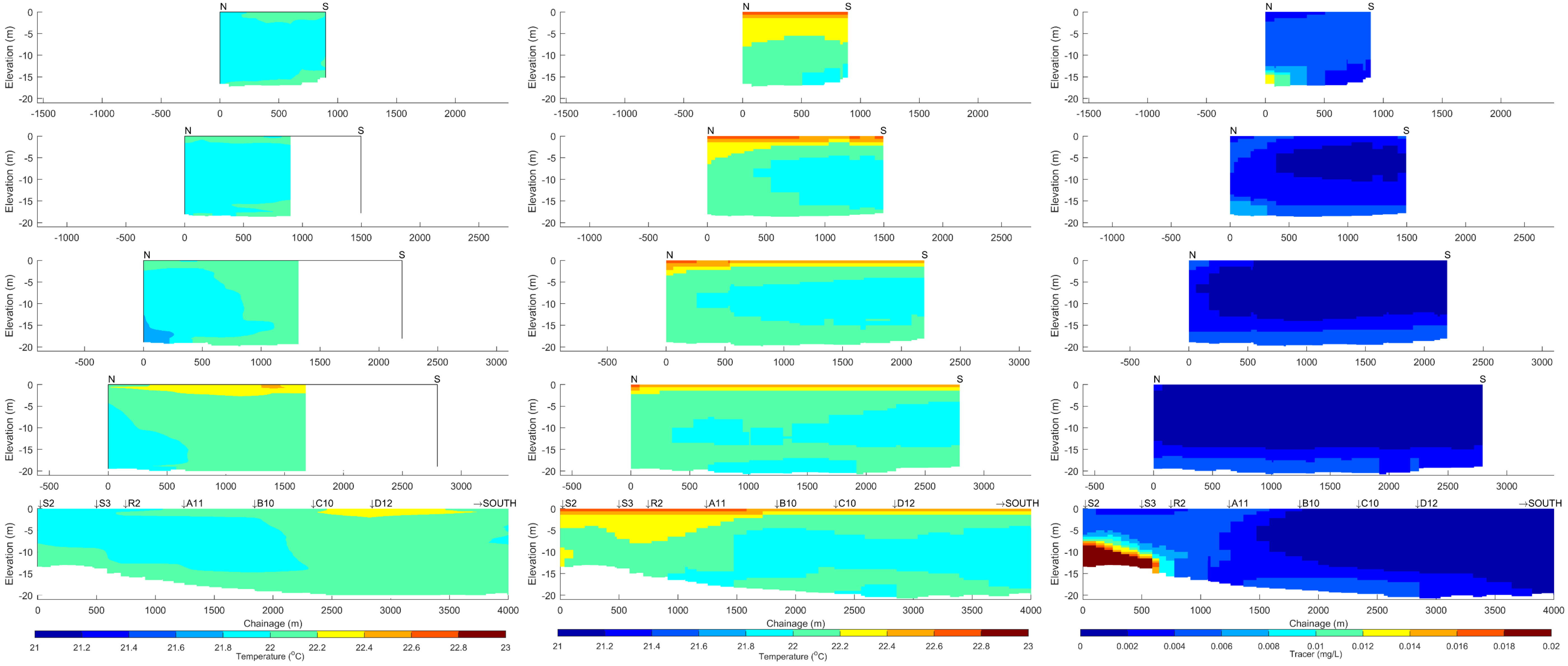

Figure 5-147 Temperature results – 23 April 2013 (field, model, tracer)

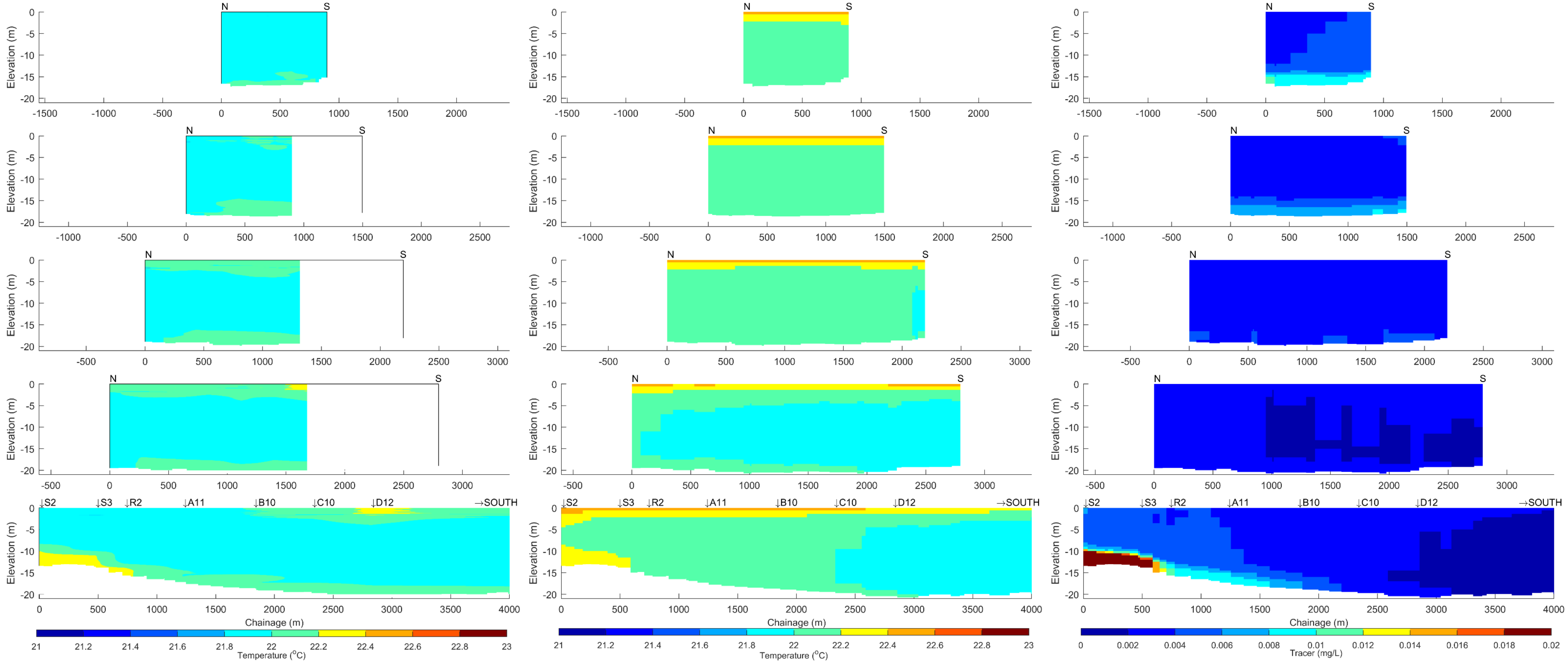

Figure 5-148 Temperature results – 24 April 2013 (field, model, tracer)

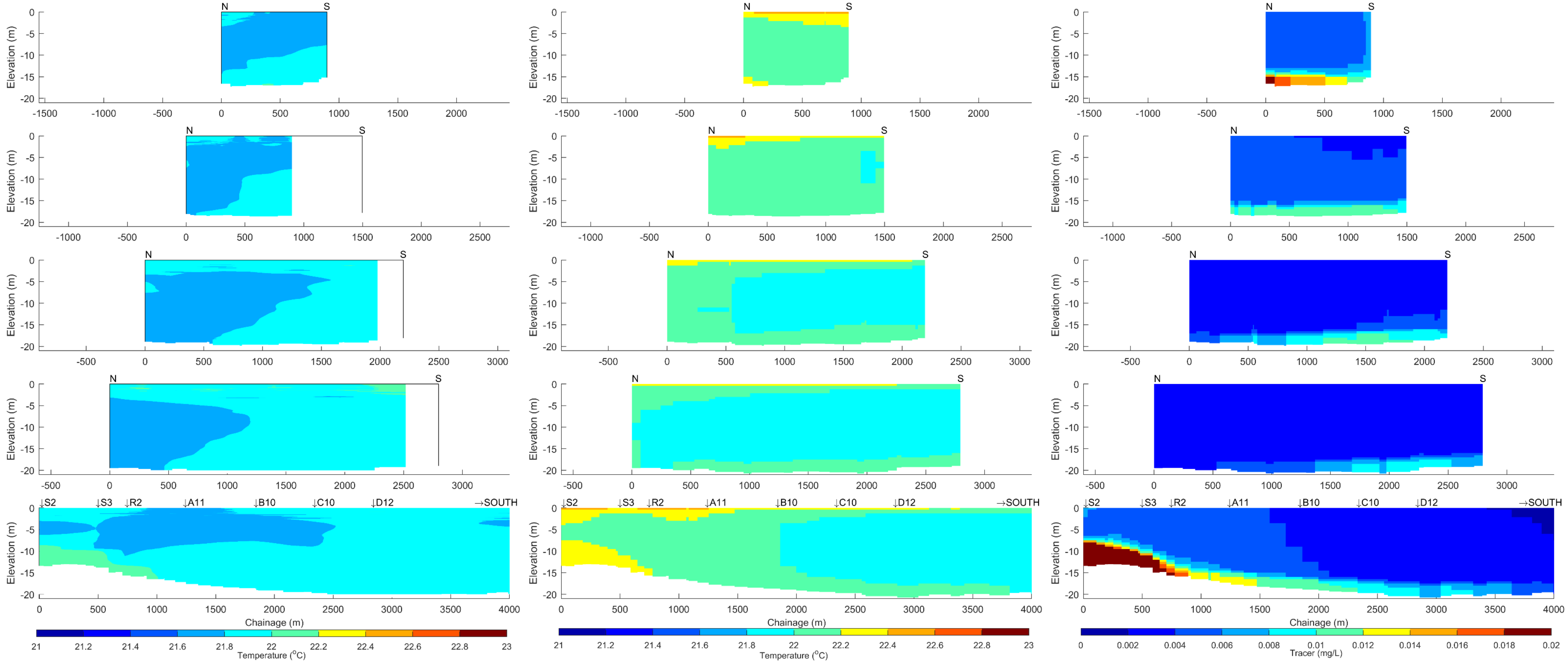

Figure 5-149 Temperature results – 26 April 2013 (field, model, tracer)

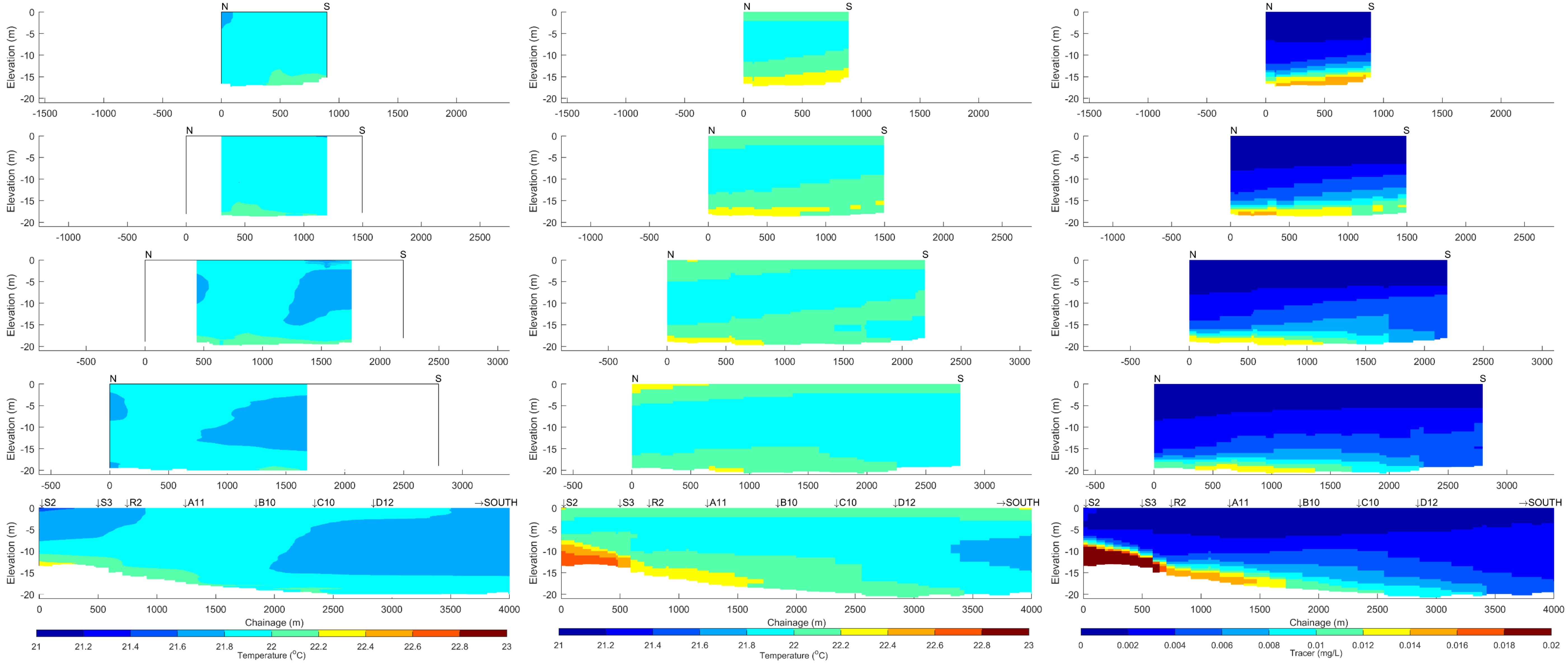

Figure 5-150 Temperature results – 28 April 2013 (field, model, tracer)

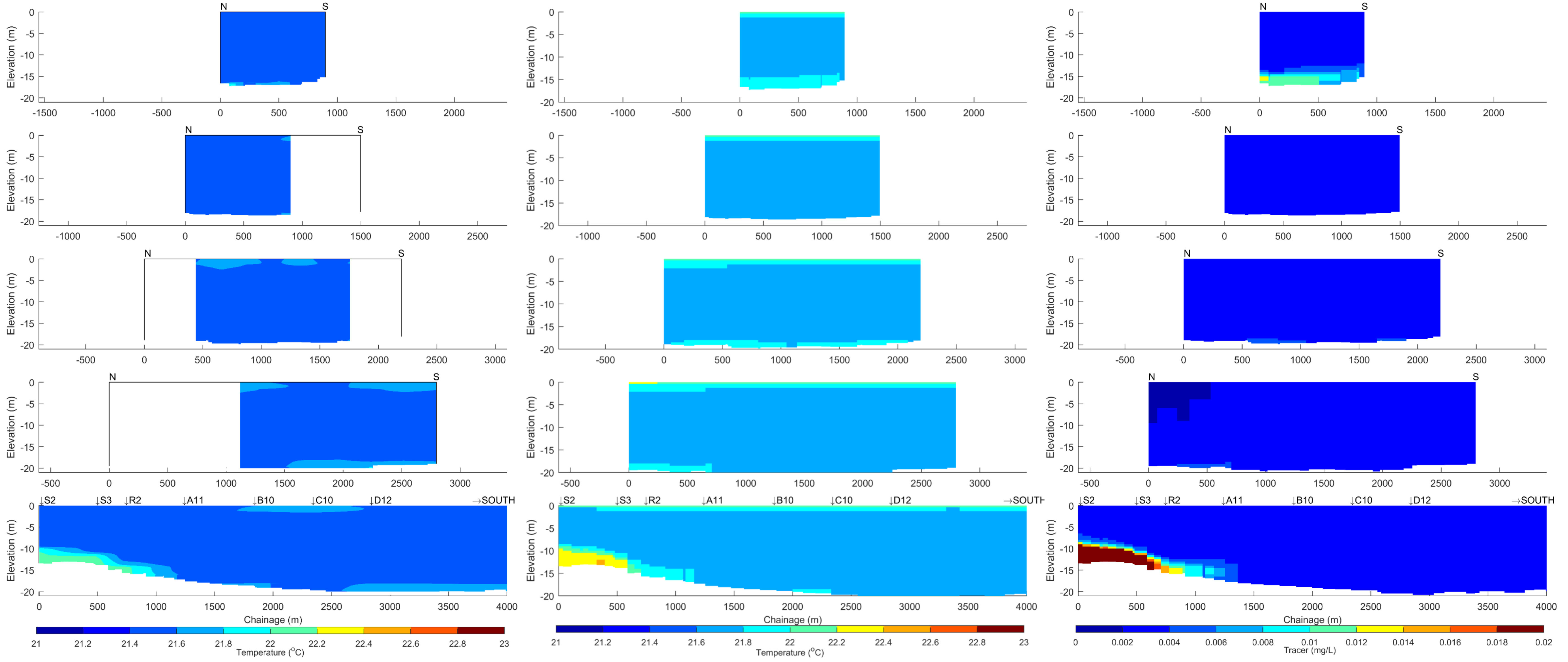

Figure 5-151 Temperature results – 30 April 2013 (field, model, tracer)

5.5.5.3.2 Salinity results

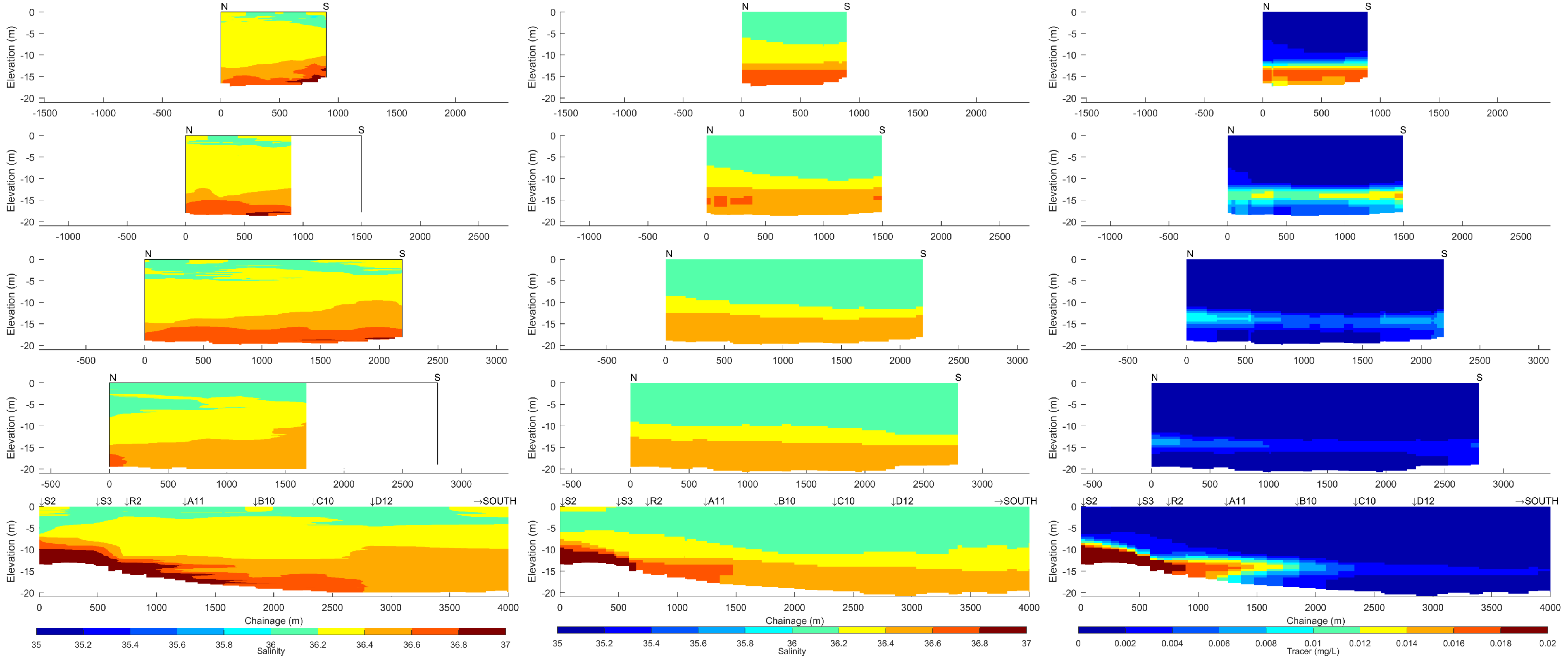

Figure 5-152 Salinity results – 16 April 2013 (field, model, tracer)

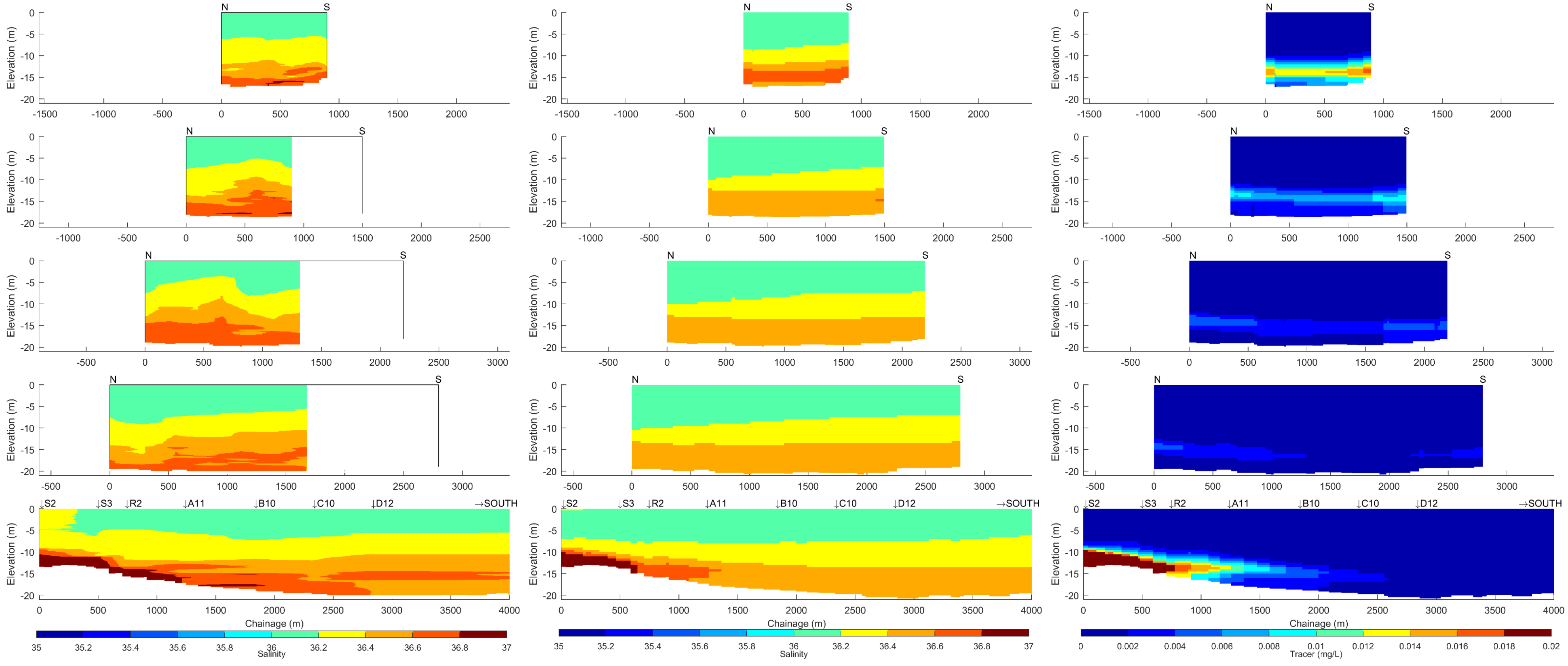

Figure 5-153 Salinity results – 17 April 2013 (field, model, tracer)

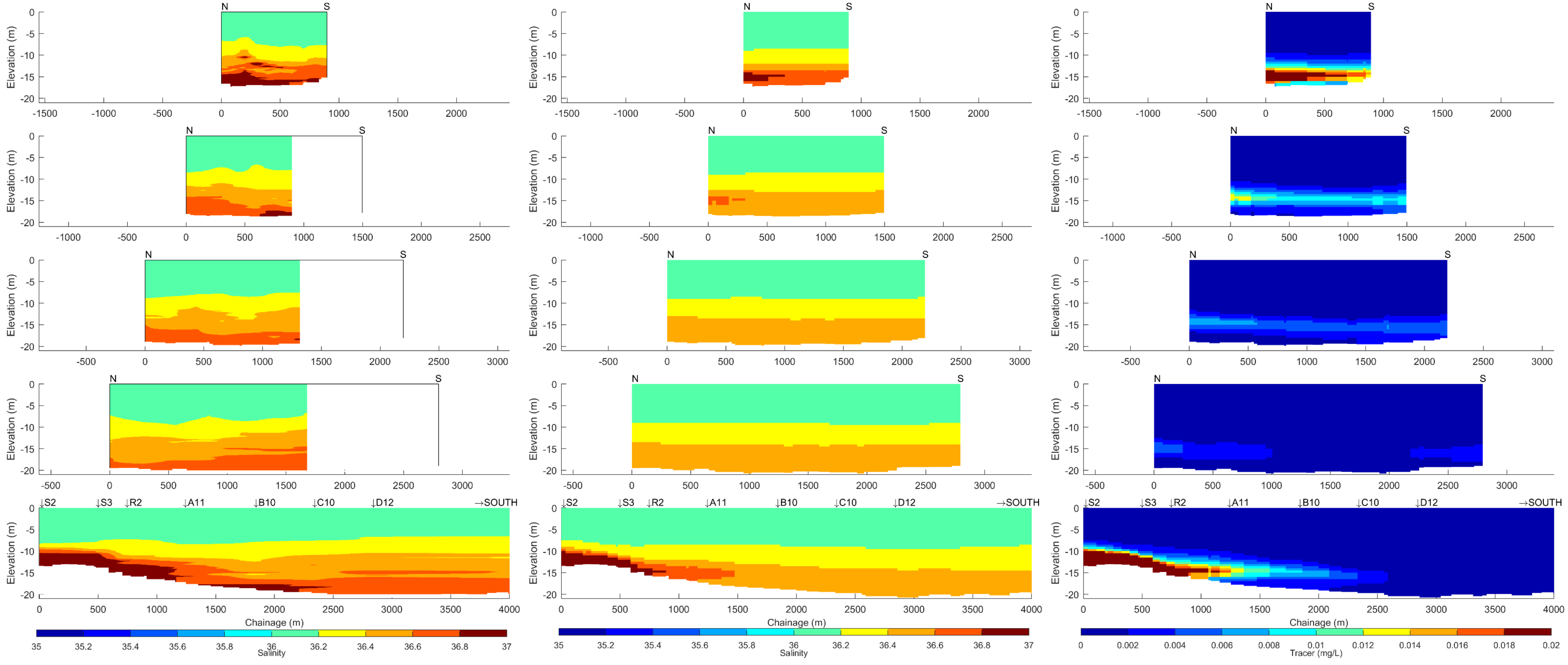

Figure 5-154 Salinity results – 18 April 2013 (field, model, tracer)

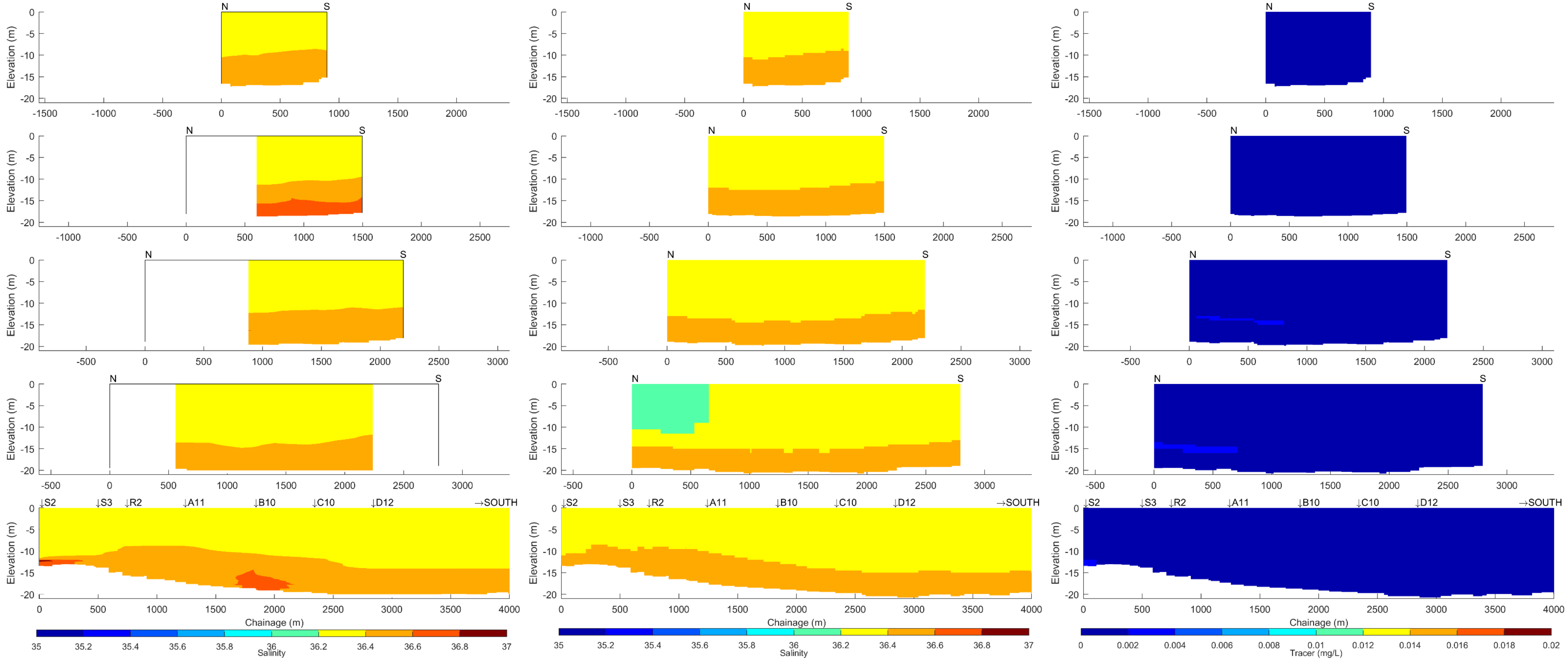

Figure 5-155 Salinity results – 20 April 2013 (field, model, tracer)

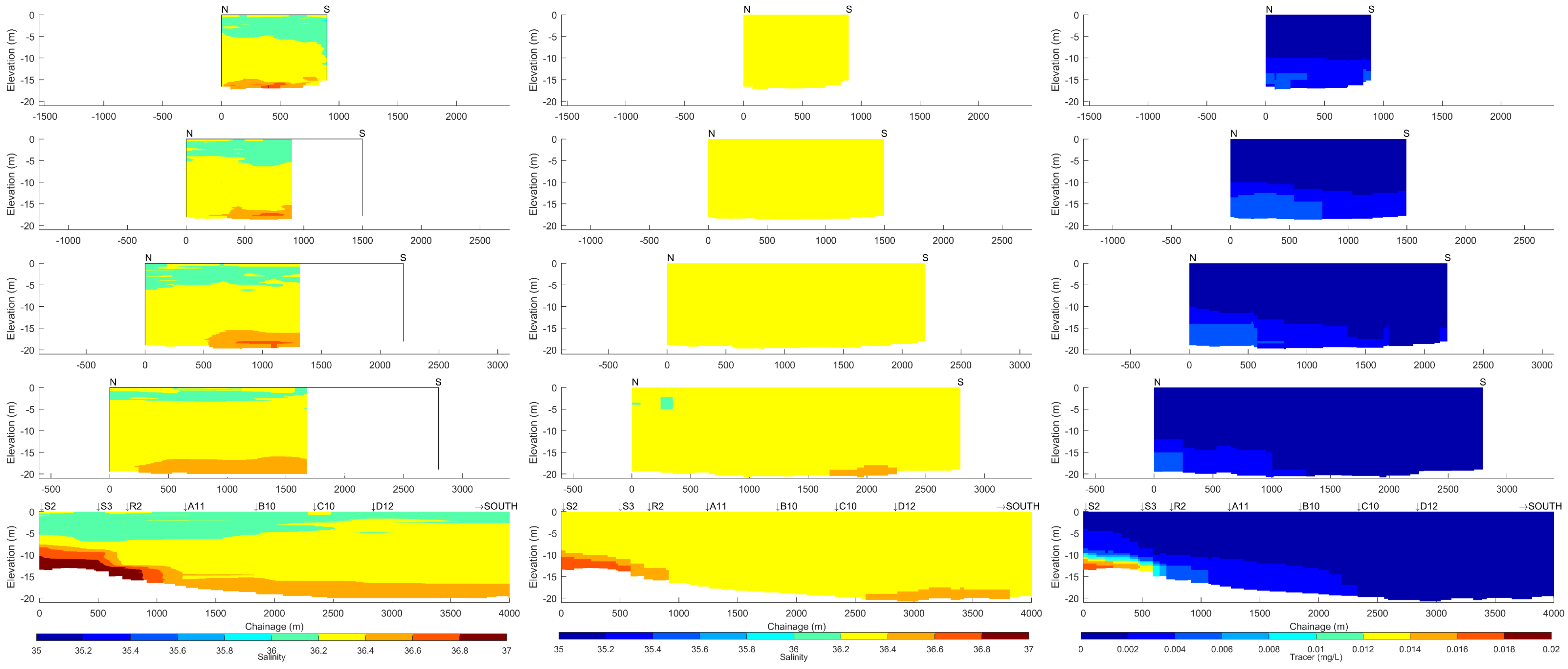

Figure 5-156 Salinity results – 22 April 2013 (field, model, tracer)

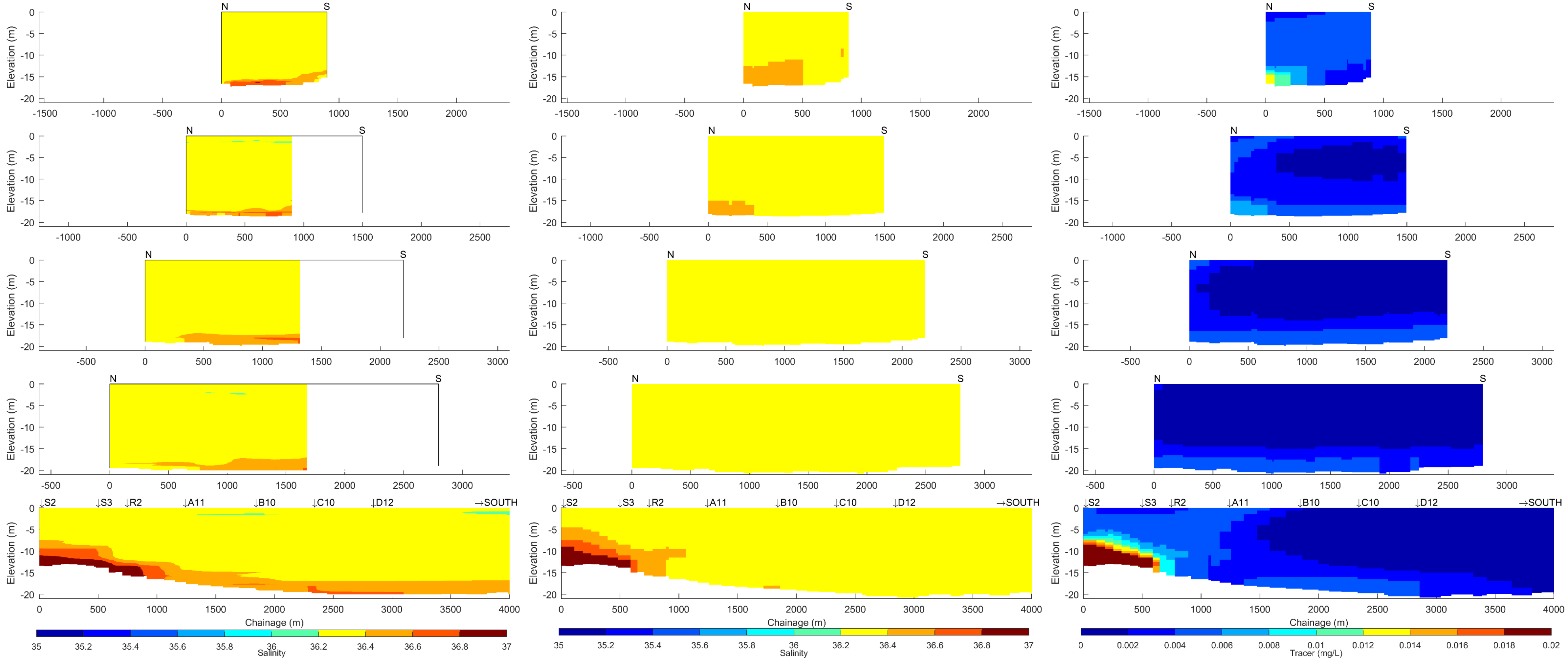

Figure 5-157 Salinity results – 23 April 2013 (field, model, tracer)

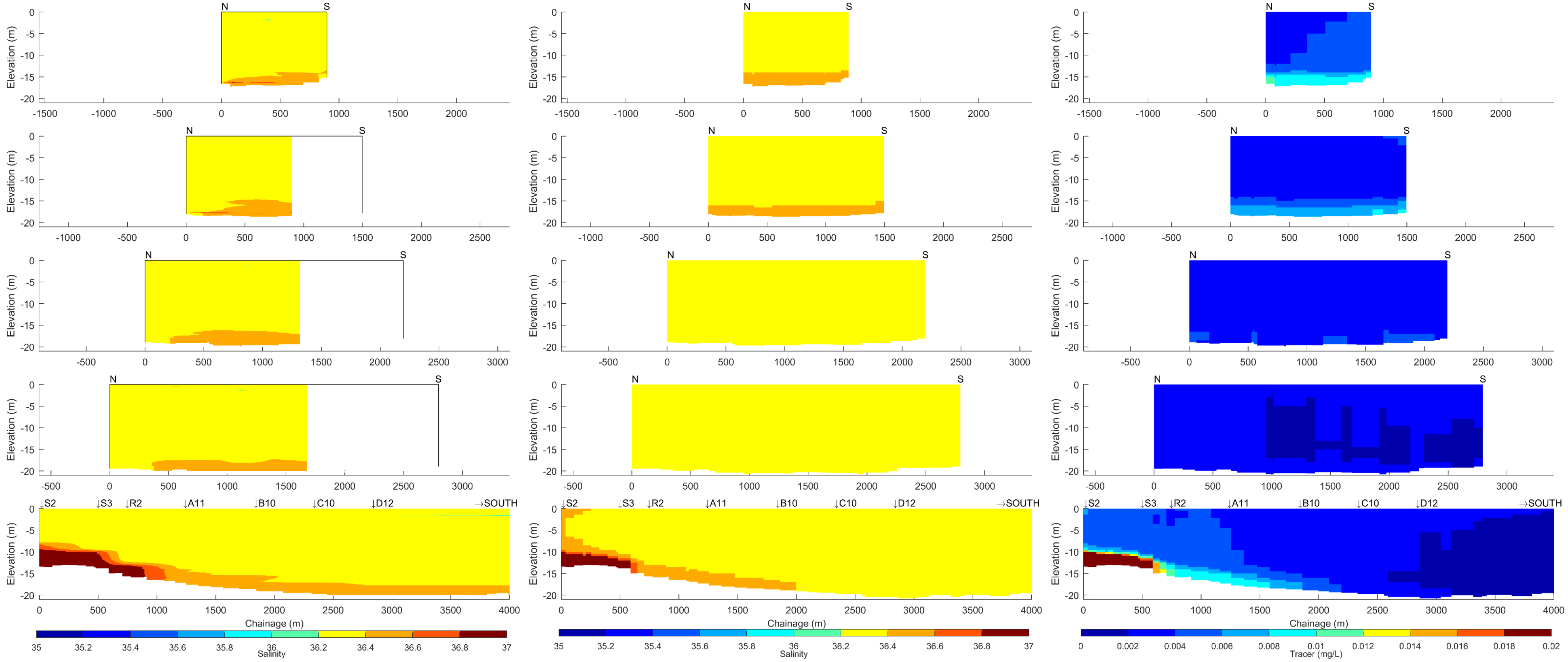

Figure 5-158 Salinity results – 24 April 2013 (field, model, tracer)

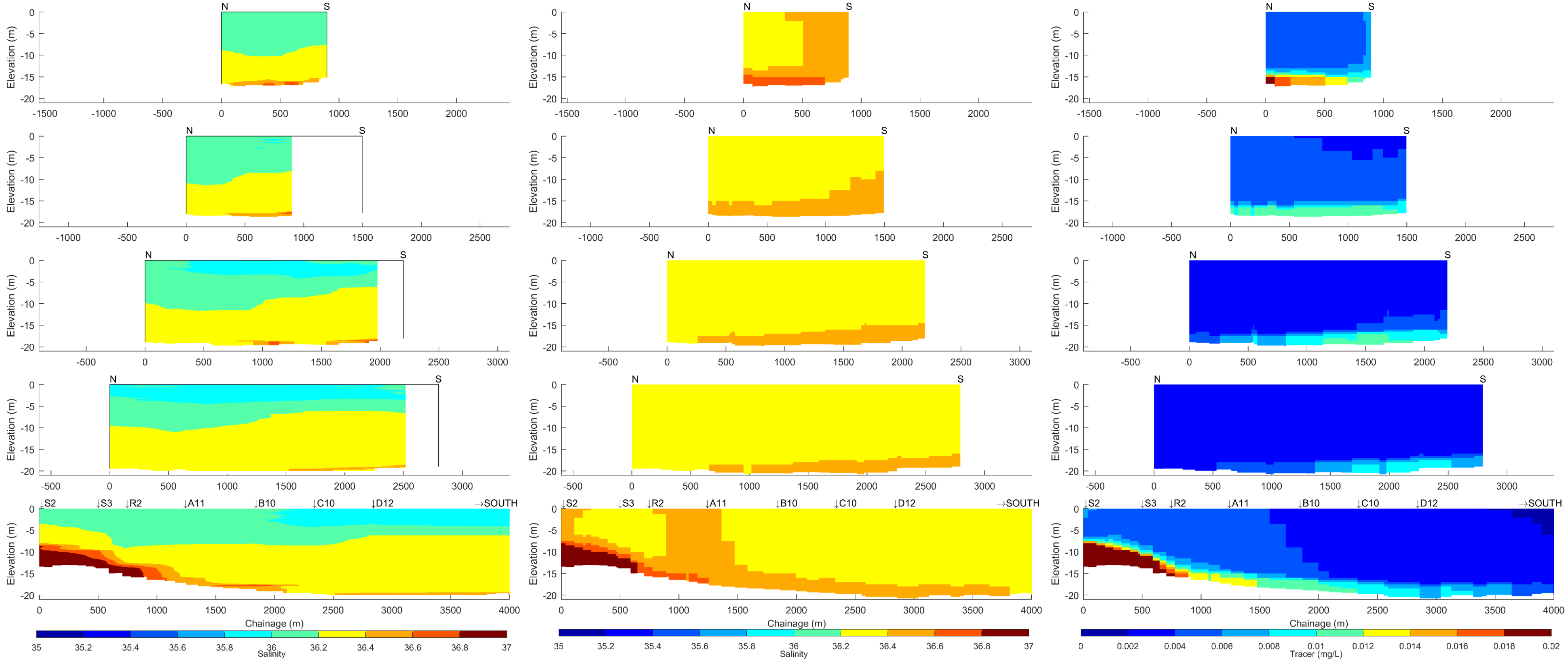

Figure 5-159 Salinity results – 26 April 2013 (field, model, tracer)

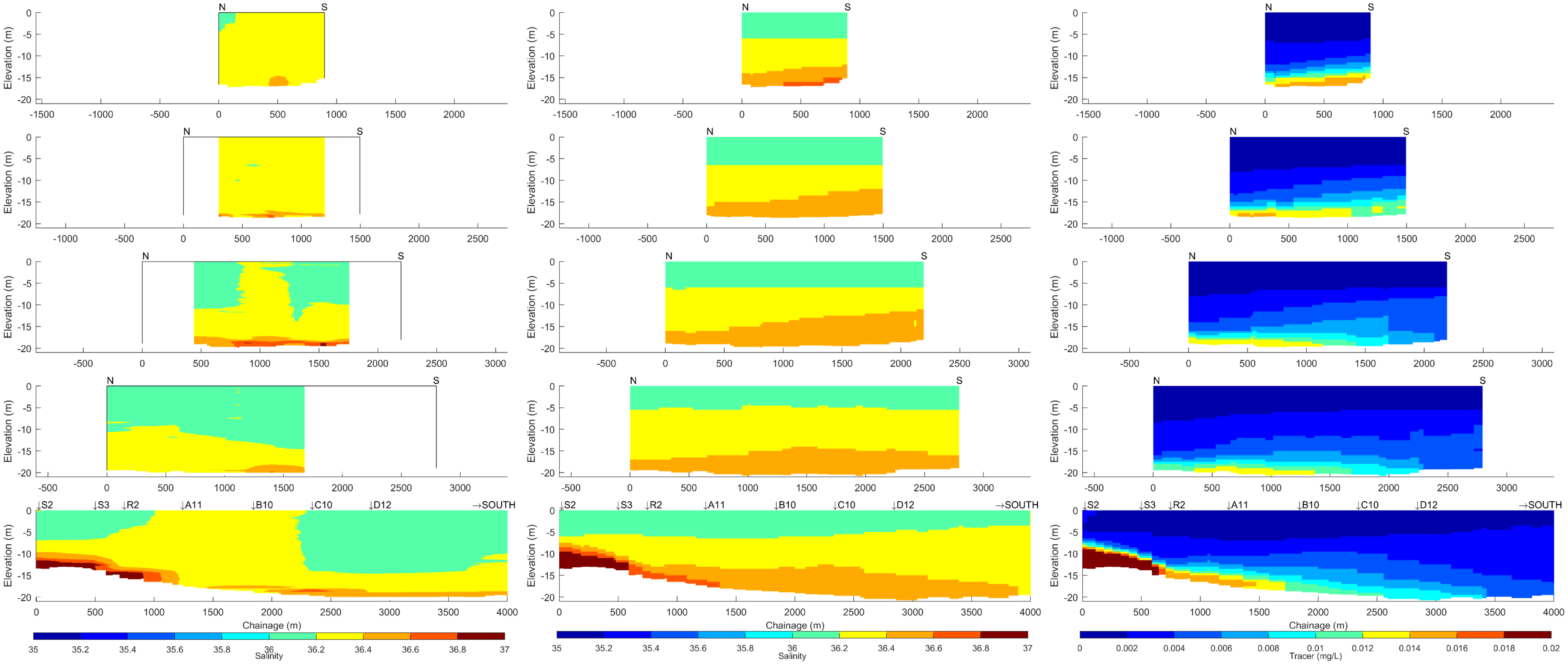

Figure 5-160 Salinity results – 28 April 2013 (field, model, tracer)

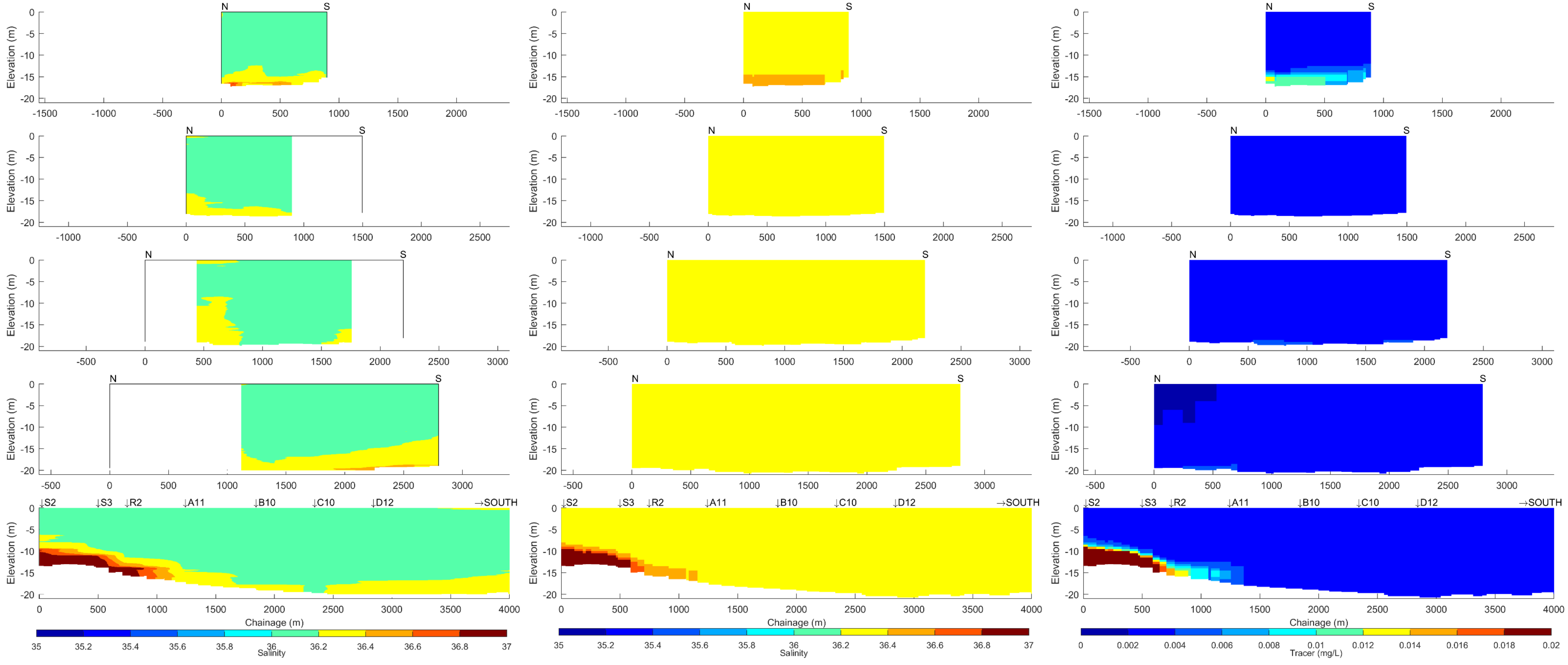

Figure 5-161 Salinity results – 30 April 2013 (field, model, tracer)

5.5.5.3.3 Dissolved Oxygen

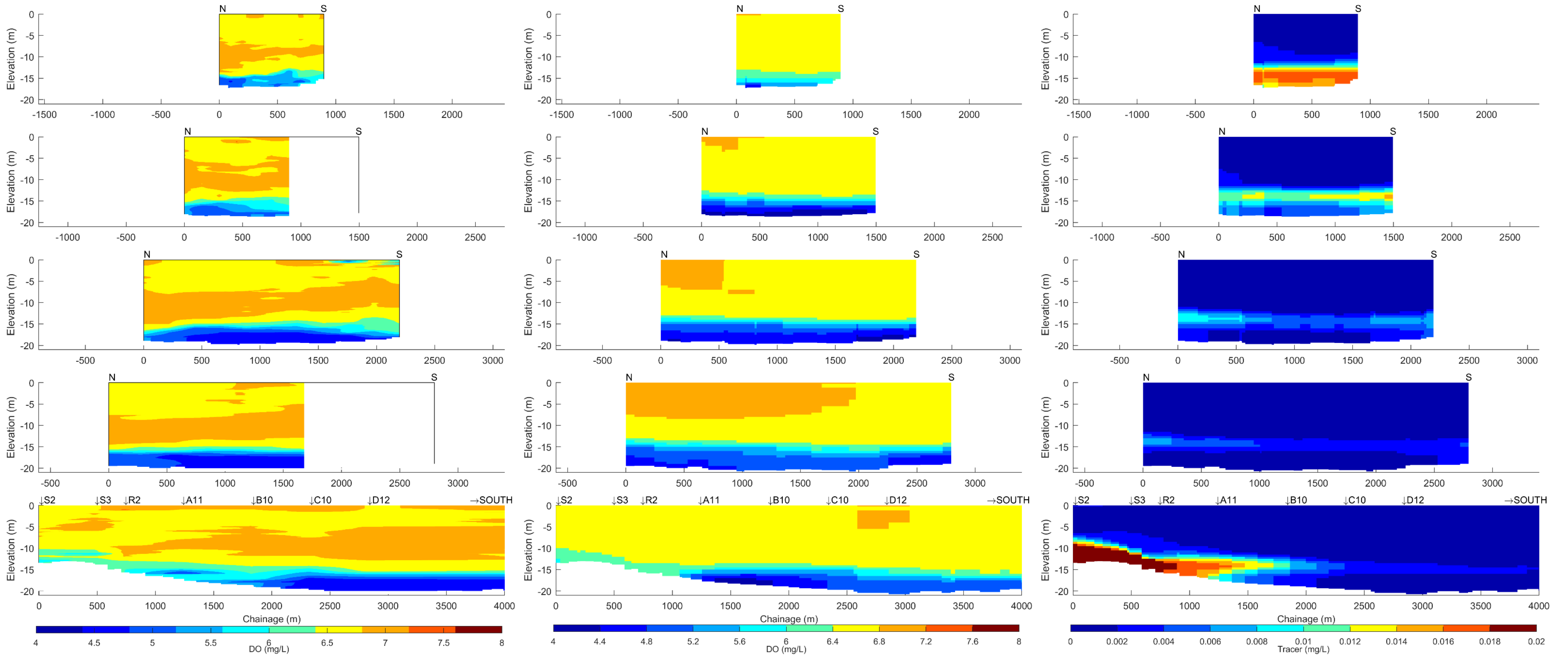

Figure 5-162 DO results – 16 April 2013 (field, model, tracer)

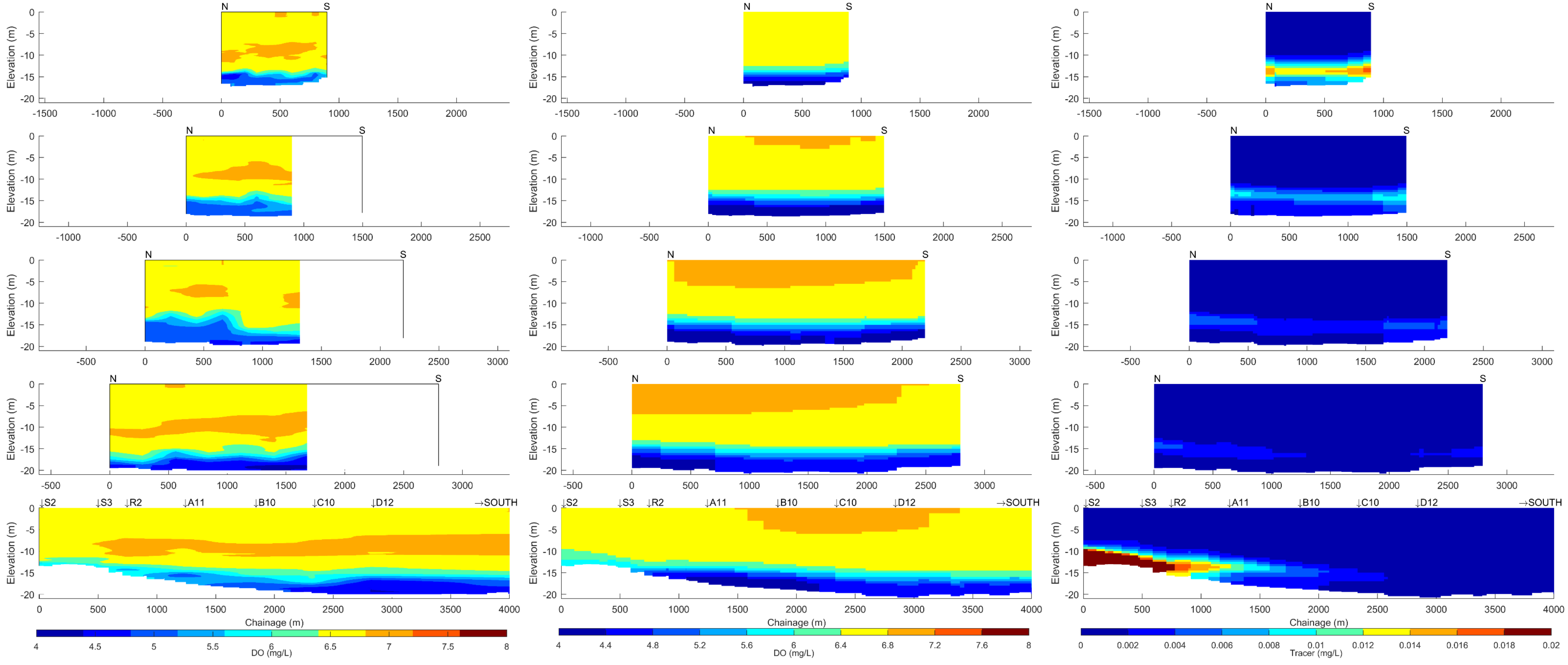

Figure 5-163 DO results – 17 April 2013 (field, model, tracer)

Model simulations

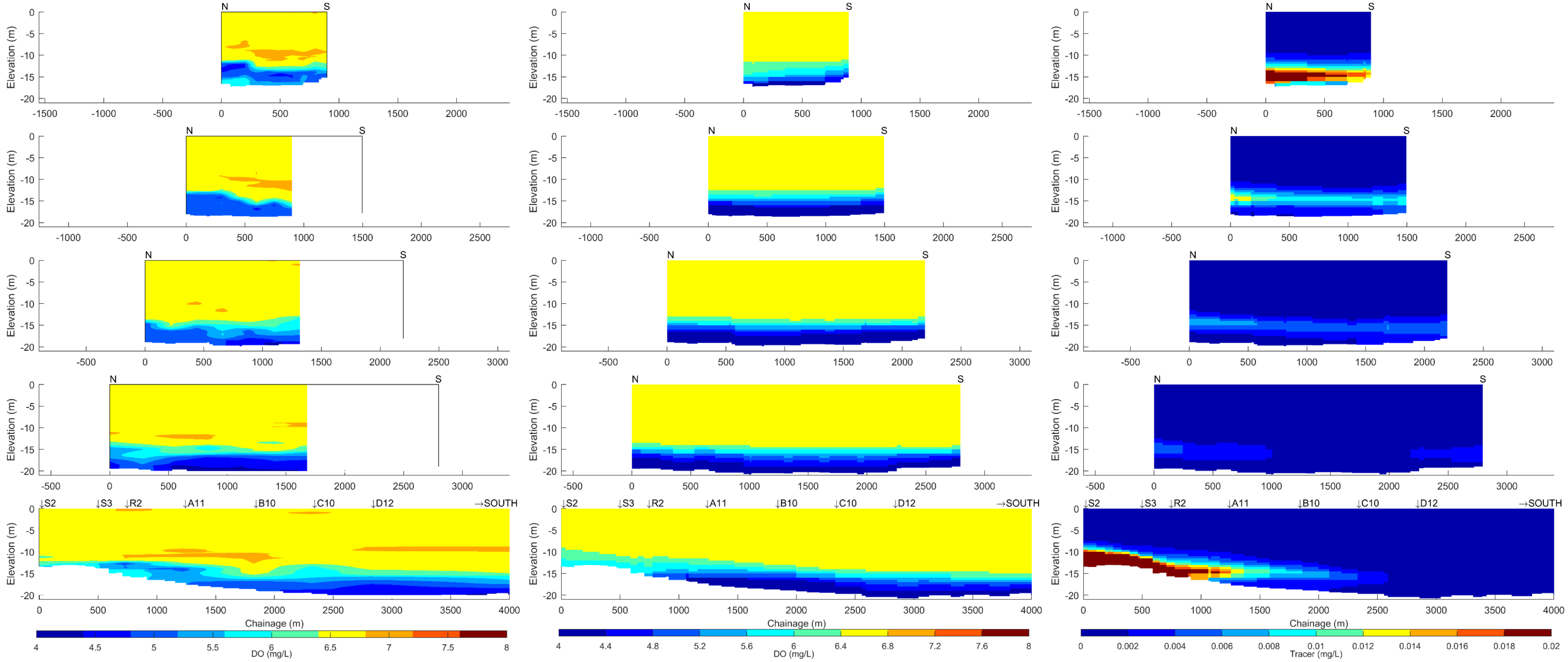

Figure 5-164 DO results – 18 April 2013 (field, model, tracer)

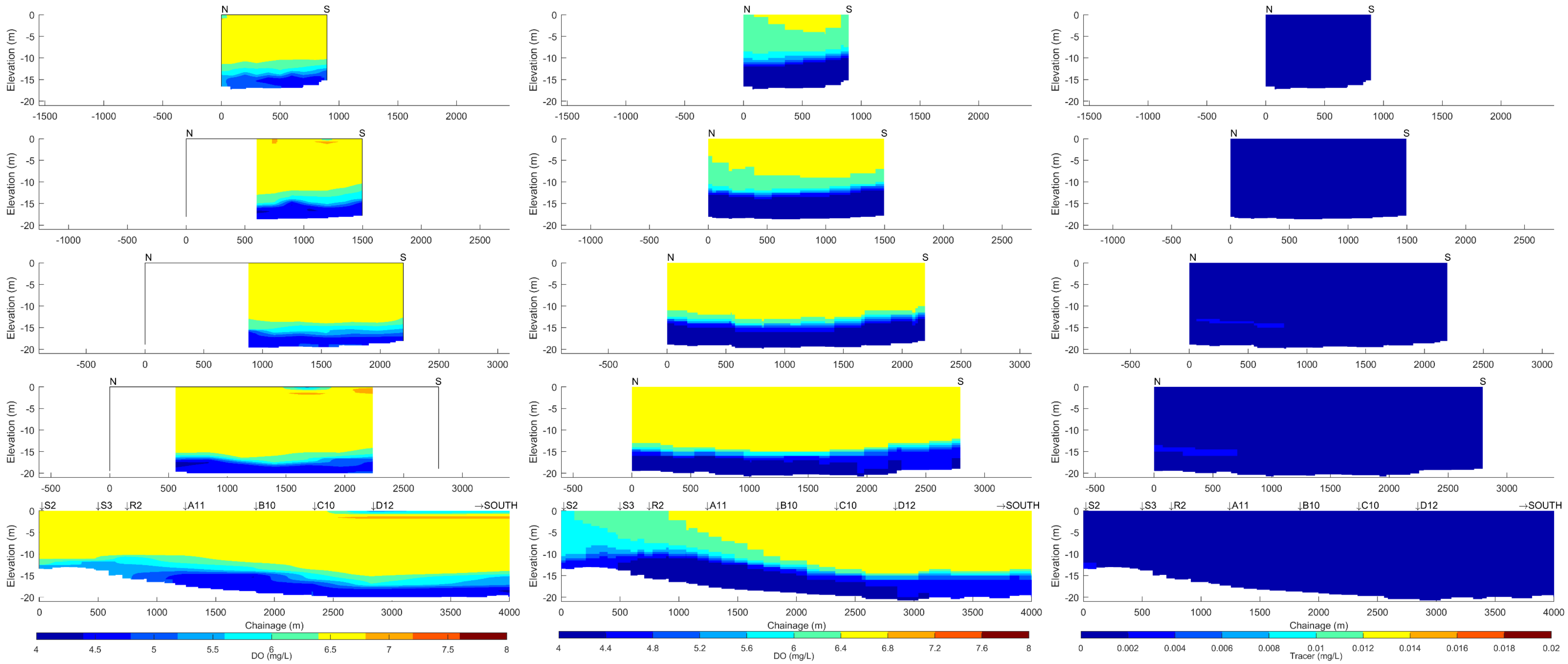

Figure 5-165 DO results – 20 April 2013 (field, model, tracer)

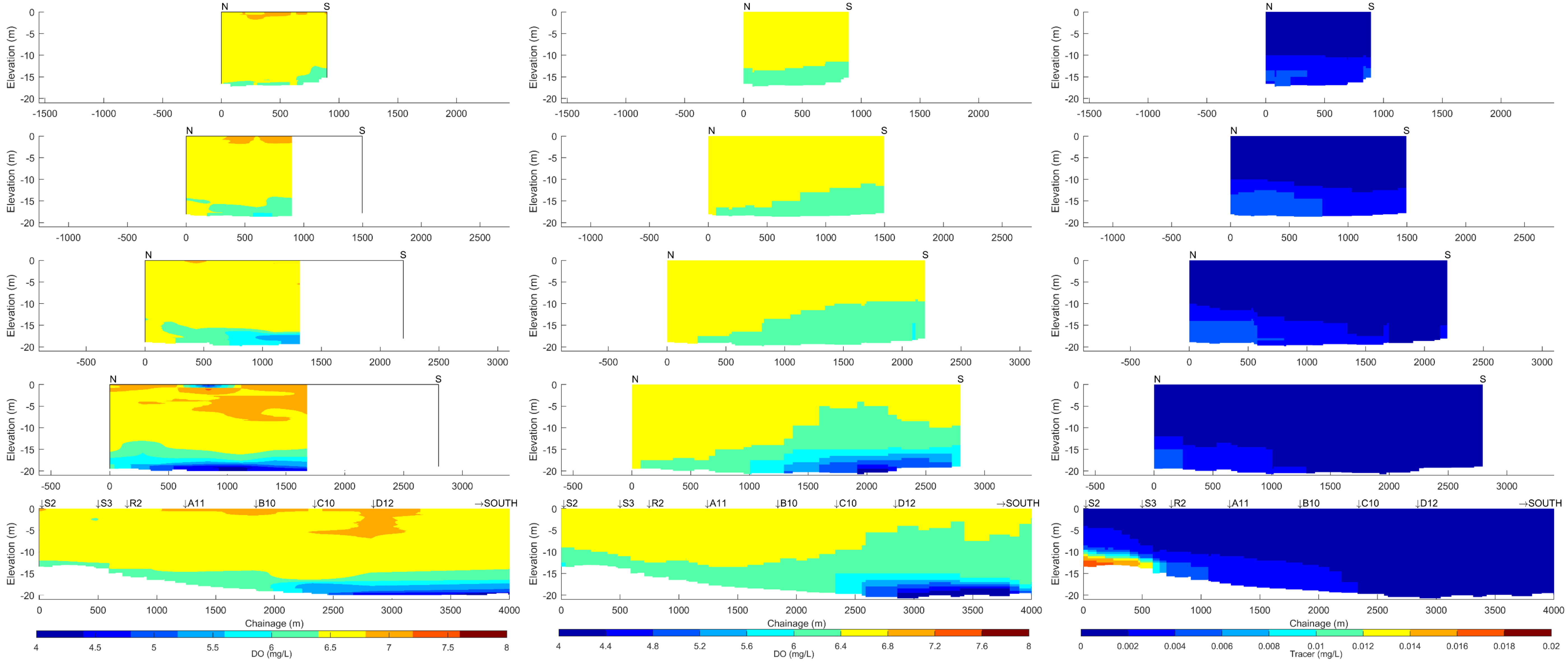

Figure 5-166 DO results – 22 April 2013 (field, model, tracer)

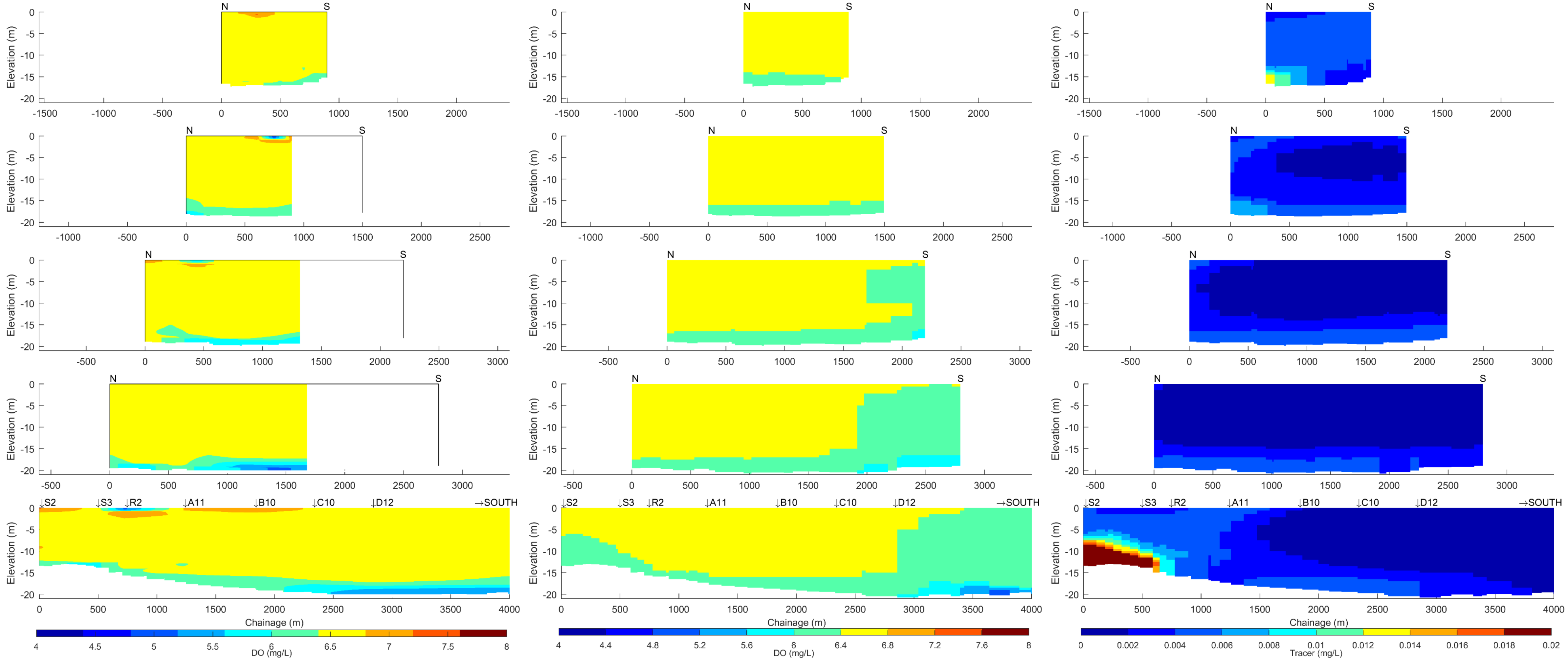

Figure 5-167 DO results – 23 April2013 (field, model, tracer)

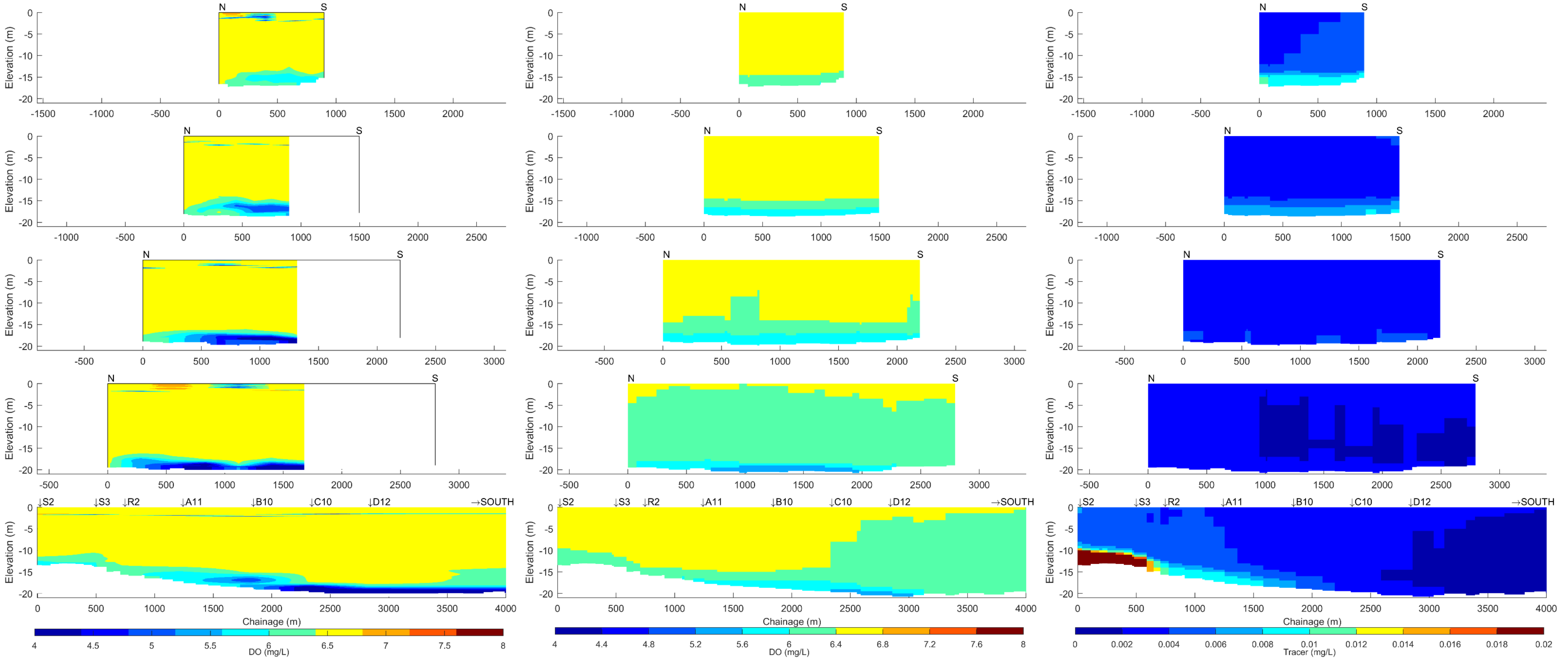

Figure 5-168 DO results – 24 April2013 (field, model, tracer)

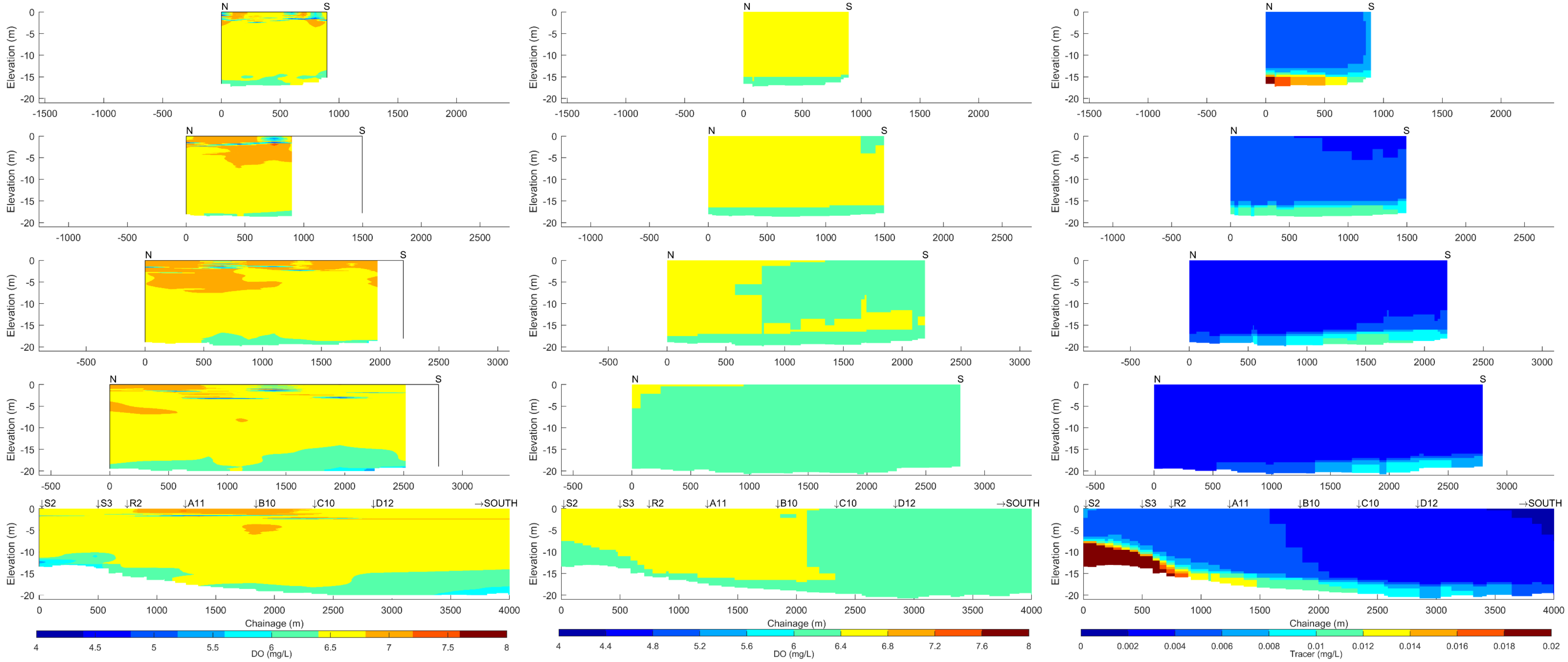

Figure 5-169 DO results – 26 April2013 (field, model, tracer)

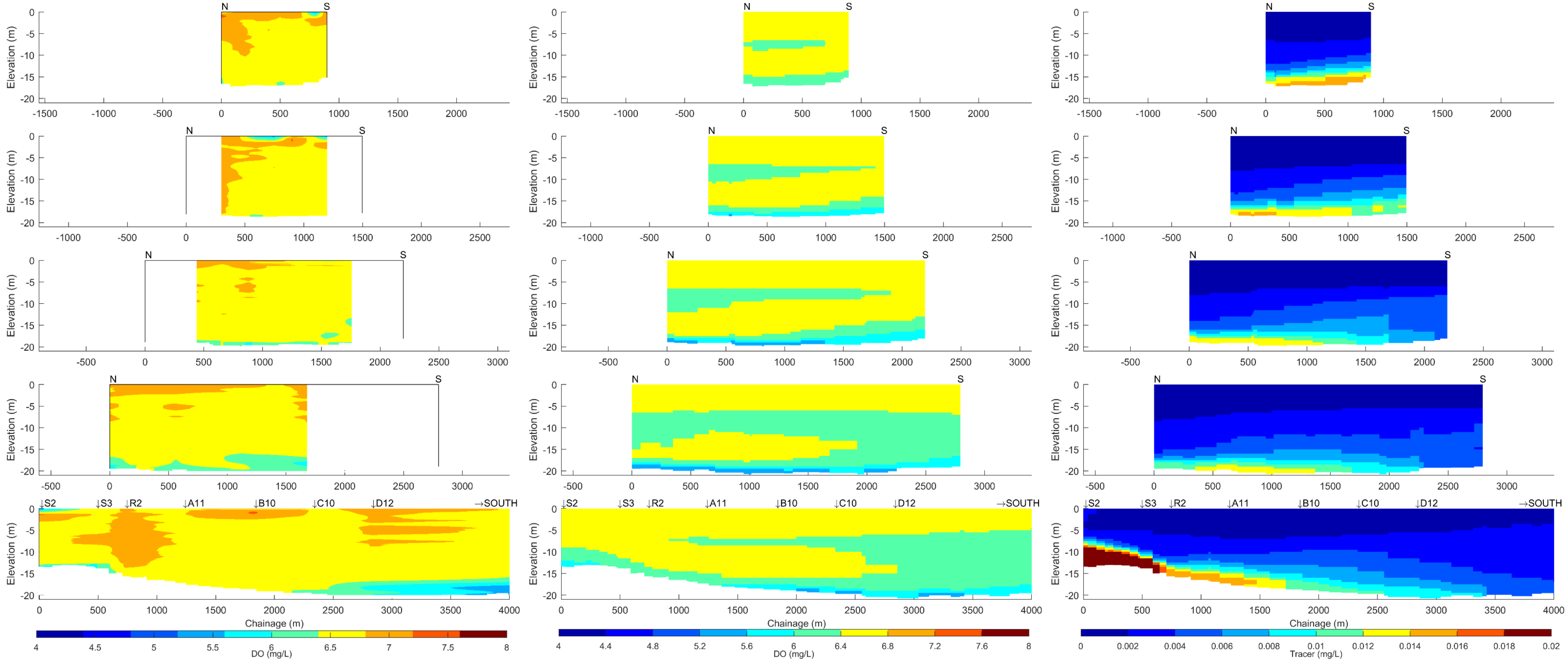

Figure 5-170 DO results – 28 April2013 (field, model, tracer)

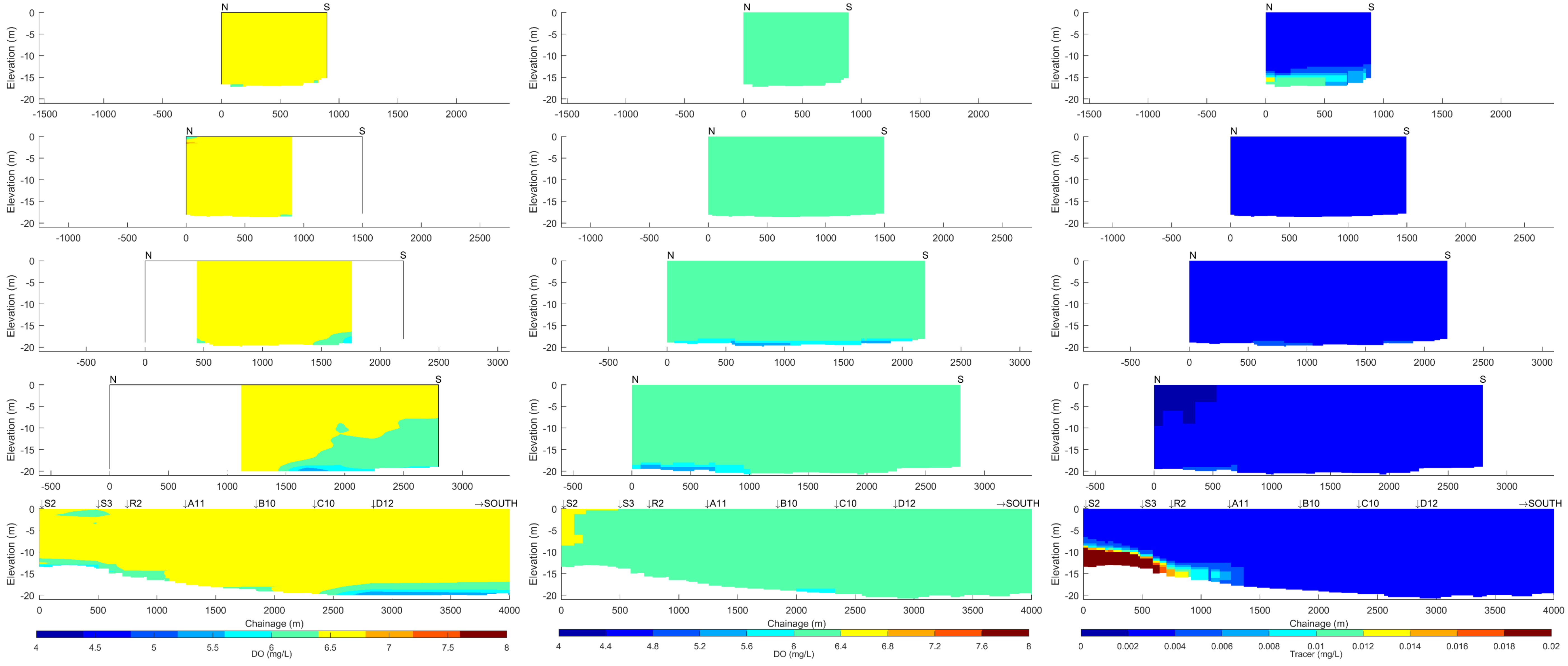

Figure 5-171 DO results – 30 April2013 (field, model, tracer)